CHEMICAL REVIEWS

Review

Cite This: *Chem. Rev.* XXXX, XXX, XXX–XXX

pubs.acs.org/CR

Well-Defined Nanoparticle Electrocatalysts for the Refinement of Theory

Jamie A. Trindell,[†] Zhiyao Duan,[†] Graeme Henkelman,*[] and Richard M. Crooks*[]

Department of Chemistry and Texas Materials Institute, The University of Texas at Austin, 105 East 24th Street, Stop A5300, Austin, Texas 78712-1224, United States

ABSTRACT: The relationship between experiment and theory in electrocatalysis is one of profound importance. Until fairly recently, the principal role of theory in this field was interpreting experimental results. Over the course of the past decade (roughly the period covered by this review), however, that has begun to change, with theory now frequently leading the design of electrocatalytic materials. Though rewarding, this has not been a particularly easy union. For one thing, experimentalists and theorists have to come to grips with the fact that they rely on different models. Theorists make predictions based on individual, perfect structural models, while experimentalists work with more complex and heterogeneous ensembles of electrocatalysts. As discussed in this review, computational capabilities have improved in recent years, so that theory is better represented by the structures that experimentalists are able to prepare. Likewise, synthetic chemists are able to make ever more complex electrocatalysts with high levels of control, which provide a more extensive palette of materials for testing theory. The goal of this review is to highlight research from the last ∼10 years that focuses on carefully controlled electrocatalytic experiments which, in combination with theoretical predictions, bring us closer to bridging the gap between real catalysts and computational models.

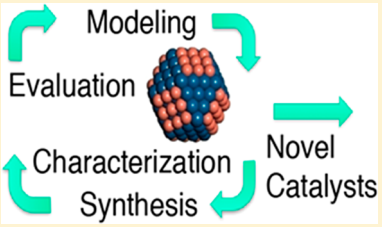

CONTENTS

Special Issue: Nanoparticles in Catalysis

Received: April 22, 2019

DOI: 10.1021/acs.chemrev.9b00246
Chem. Rev. XXXX, XXX, XXX–XXX

1. INTRODUCTION

This review provides a progress report on the fruitfulness of the theory/experiment marriage in the field of catalysis, and specifically electrocatalysis in nanoscale materials, since about 2008. The combined use of theoretical calculations and experimentally observed activity is now a partnership that is almost taken for granted in catalysis research (Figure 1).[1−4] In the field of electrocatalysis, theory and experiment have converged at nanocatalysts in the size range of ∼1−3 nm. In this range and assuming a high degree of structural uniformity, the full power of density functional theory (DFT) can be brought to bear.

From a theoretical perspective, computational power and tools continue to improve, leading to better accuracy and the ability to evaluate larger and more complex structures. With modern computers, DFT can regularly treat nanoparticles (NPs) having < ∼300 atoms within a reasonable time frame. Accordingly, NPs in this size range are particularly amenable for correlating theory and experiment, because DFT can treat all atoms in the system explicitly. This allows accurate first-principles assessment of the unique properties of small NPs. For electrocatalysis, site heterogeneity, geometric structures, surface tension, and the unique electronic structure arising from quantum confinement effects are particularly relevant.[5] Therefore, while this review is focused primarily on NPs in the <300 atom (< ∼2 nm) size range, larger sizes are also considered in some illustrative cases.

From an experimental perspective, constantly improving synthetic and materials characterization methods, particularly *operando* (i.e., in situ) methods, lead to more monodisperse and better-defined materials that are beginning to approach the (perfect) uniformity of theory. These factors allow theorists to refine their calculations, with the ultimate goal being computational design of electrocatalysts that are tailored for high activity and specificity.

In addition to the convergence of theory and experiment in the 1−3 nm size range, there are other reasons why such electrocatalysts are scientifically interesting and technologically important. First, the percentage of the total atoms present on the surface of NPs in this size range is much higher than that for bulk materials. For example, surface atoms account for 63% of the total atoms in a 1.6 nm cuboctahedral NP. In most cases, this results in higher per-atom catalytic activity compared to larger particles or bulk surfaces. Second, metal NPs having diameters of just a few nanometers often exhibit unique electrocatalytic properties due to finite size effects.[1] Compared to monometallic NPs, bimetallics offer even more avenues for optimizing electrocatalytic performance. For example, while Rh and Au are classically immiscible metals in the bulk phase, they can alloy at the nanoscale and exhibit composition-dependent activity.[6] The increased activity of bimetallic NP electrocatalysts is often explained in terms of geometric, ligand, and/or ensemble effects.[7]

DFT and DFT-derived theories facilitate the field of electrocatalysis in several ways. First, DFT can determine the atomic structures of NPs, including the elemental distribution in nanoalloys. This is an especially effective approach when theory and experiment are combined, because experiments can provide information about the atomic structures, which in turn allows for further refinement of theory for resolving structures.[6,8−10] Second, the energetics and kinetics of electrocatalytic reactions can be probed by DFT. Third, design principles and strategies derived from theoretical studies can be used to make predictions for experimental validation. In other words, theory can lead experiment as well as interpret experimental results. Finally, electrocatalysis is intrinsically complex due to the charged metal/electrolyte interface, but theoretical studies are moving toward more realistic models to provide fundamental insights about electrocatalyst stability and the effects of applied potential, pH, and solvation.[11−15]

In addition to theoretical challenges, there are also numerous experimental hurdles that must be crossed. Foremost in this regard is the difficulty associated with synthesizing highly active, well-defined, and stable metal NPs that are appropriate for DFT calculations. However, there are now wet synthetic techniques that make it possible to synthesize a wide variety of NPs having different compositions, shapes, and sizes.[16] This high level of synthetic control has led to the discovery of increasingly active catalysts, such as alloy and core@shell formulations, having controlled compositions and structures. For example, NPs having long-range order have been obtained by thermal annealing of random alloy NPs under reducing atmospheres. In some cases these ordered materials display improved electrocatalytic activity and stability,[16,17] but computational insight is necessary to fully understand these effects.

Accurate DFT analysis relies on a detailed understanding of NP structure. Therefore, the difficulty in thoroughly characterizing metal NPs, down to their exact atomic arrangements, still places a limitation on the correlation of theory and experiment. For adequate characterization of nanocatalysts, particularly those having sizes <3 nm, multiple characterization techniques are required to sufficiently elucidate the structure. High-resolution transmission electron microscopy (HR-TEM), X-ray absorption spectroscopy (XAS), X-ray diffraction (XRD), and cyclic voltammetry (CV) are often used in the analysis of nanoscale electrocatalysts, and therefore, a brief overview of these characterization techniques will be discussed later in this review.

Even when a high level of synthetic control is achieved and complete characterization of the catalyst is possible, a common shortcoming in many studies correlating structure to catalytic function is that the theoretical models rely on structural information determined prior to electrocatalysis. Unfortunately, however, extremely small metal NPs are often unstable under electrocatalytic conditions, meaning the active form of the catalyst may not be the same as the structure determined

DOI: 10.1021/acs.chemrev.9b00246
Chem. Rev. XXXX, XXX, XXX−XXX

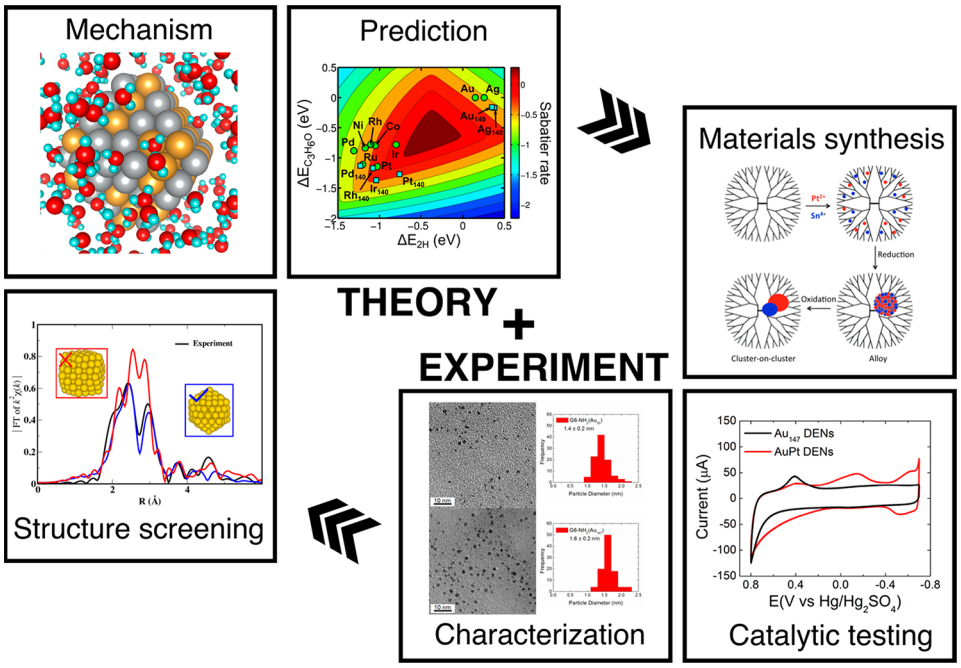

Figure 1. Iterating between theoretical predictions, synthesis, characterization, and electrochemical evaluation results in a design cycle to accelerate the discovery of novel catalysts.

prior to electrocatalytic experiments.[18−20] Examples of this include agglomeration or ripening of NP catalysts during electrocatalysis[21,22] and adsorbate-induced restructuring of the NP surface.[23,24] While these types of overall structural changes may be observed when ex situ characterization of the catalyst is performed both before and after electrocatalysis, this approach to characterization does not provide insight into the mechanism of instability. Advances in *operando* methods have proven valuable in this regard and will be discussed throughout this review.

To summarize, an improved understanding of the theory and experiment nexus will lead to the logical discovery of new nanomaterials for electrocatalytic applications. Accordingly, we first discuss how first-principles theory is coupled to synthesis, characterization, and electrocatalytic measurements. This is followed by a more in-depth analysis of specific case studies involving electrocatalytic reactions of particular intrinsic or technological importance, including the oxygen reduction reaction (ORR), carbon monoxide oxidation, and the carbon dioxide reduction reaction (CO_2RR). We conclude with some thoughts on future needs and how the field is likely to evolve in the coming years to achieve them.

2. TOOLS AND TECHNIQUES FOR COMPARING EXPERIMENT TO THEORY

2.1. Theoretical Methods for Interpreting and Predicting Electrocatalytic Behavior

Computational methods have been employed for decades to gain a molecular level understanding of experimental observations. For electrocatalytic studies, theoretical methods have been employed to predict atomic structures of NPs and nanoalloys,[1] facilitate structural characterization of catalysts,[25] elucidate reaction mechanisms,[26] and screen for new catalysts.[27]

2.1.1. Theoretical Methods for Determining NP Structures. Determining the surface structure of pure and alloy NPs is critical for understanding their function as electrocatalysts. The thermodynamically stable structures of NPs of a given size and composition can be determined independently by theoretical methods.[28] Calculations based on these atomic surface structures can then describe their electrocatalytic function.

Theoretical methods for determining structure usually couple methods that describe the energetics of the target system with those that can efficiently explore configuration space. DFT calculations can describe the energy of NPs with good accuracy, but they become prohibitively expensive when the system size reaches hundreds of atoms. Less accurate but more efficient model Hamiltonians, including bond-breaking models,[29] Ising models,[30] empirical force fields,[28,31] and most recently neural network potentials,[32] have been proposed for larger NPs. Various algorithms have also been developed to efficiently explore configuration space, including Monte Carlo methods with properly designed attempting movements[28,31] and global minimization methods including simulated annealing, basin hopping,[33,34] minima hopping,[35] genetic algorithms,[36,37] and machine-learning algorithms.[38]

Although thermodynamically stable structures can be readily obtained using the above-mentioned theoretical methods, real NP electrocatalysts are generally metastable, especially when the synthetic processes are kinetically controlled and no annealing treatment is applied. Unfortunately, the kinetics of the synthesis process is typically too complex to simulate directly. A different approach is to use computational methods to determine stable atomic structures of synthesized electrocatalysts that agree with structural characterization data from experiment. For example, the reverse Monte Carlo (RMC) method was developed to reconstruct atomic structures using X-ray scattering, neutron scattering, and extended X-ray absorption fine structure (EXAFS) spectroscopy by fitting experimental data using simulated spectra.[39−41]

RMC methods, however, often cannot unambiguously determine atomic structure and are biased toward structures

DOI: 10.1021/acs.chemrev.9b00246
Chem. Rev. XXXX, XXX, XXX−XXX

of maximum entropy. To circumvent this problem, DFT- or empirical-potential-based simulations can be used to constrain the atomic models to those that are reasonable.[42−44] A recent example of this approach used a supervised machine-learning method to discover relationships between NP geometries and corresponding simulated X-ray absorption near-edge structure (XANES) spectra (Figure 2).[45] The machine-learned model was subsequently able to determine the 3D geometry of Pt NPs based upon experimental XANES spectra.

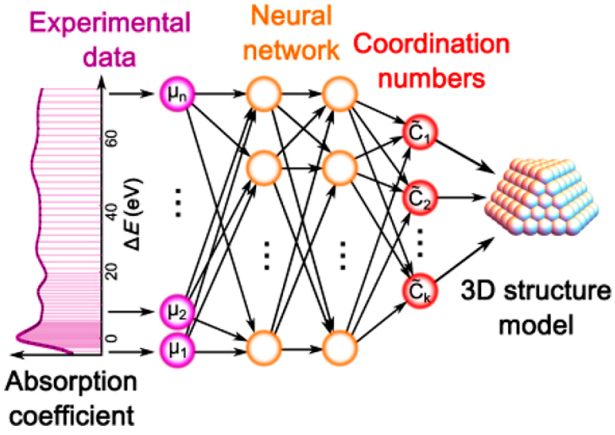

Figure 2. Example of supervised machine learning (SML) used in deconvoluting experimental in situ XANES data to obtain NP structures. Reproduced with permission from ref 45. Copyright 2017 American Chemical Society.

2.1.2. The Computational Hydrogen Electrode (CHE).

Once the structure of a NP has been determined, methods for probing the electrocatalytic properties are then required for the computational determination of structure−property relationships. One of the key factors for determining electrocatalytic activity is the overpotential, which is the additional potential beyond the equilibrium value required to drive electrocatalytic reactions. The overpotential of a specific electrocatalyst surface can be readily obtained using the computational hydrogen electrode (CHE) method developed by Nørskov and coworkers.[46] In this method, the energy of each ($H^+ + e^-$) pair in the elementary electrochemical steps is replaced by the energy of $^1/_2H_2$, as defined by the equilibrium of the normal hydrogen electrode (NHE). Thus, the reaction energies of elementary steps at different potentials can be calculated by simply raising or lowering the reaction energy in equilibrium with H_2 according to the change in potential relative to the standard hydrogen electrode (SHE, Figure 3). Using the CHE, the theoretical overpotential can be calculated as the limiting potential needed to render all elementary steps exothermic.

Although extremely useful, the CHE method is far from a complete description of the complex electrochemical interface, because it only treats the catalyst/adsorbate interaction explicitly with DFT. In electrocatalytic systems, solvation, surface charging effects, and specifically adsorbed ionic species can all play a role in influencing the kinetics of electrocatalytic reactions.

There are three primary models of the electric double layer: (1) introduction of an electric field with or without explicit solvent molecules;[47] (2) addition of explicit charge on the electrode with prescribed counter-charge distributions using an explicit or continuum solvent model;[48−53] and (3) explicit inclusion of both charges and ions with explicit solvent

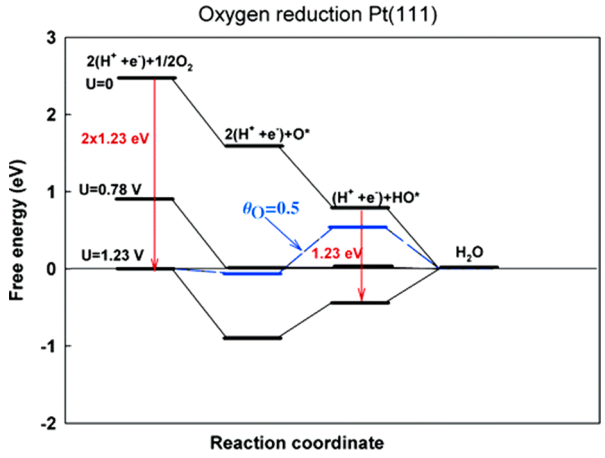

Figure 3. Example of a free-energy diagram for the ORR on Pt(111) surfaces constructed using the CHE method. The free-energy profile is examined at three different electrode potentials (U). Reproduced with permission from ref 46. Copyright 2004 American Chemical Society.

molecules.[11,54,55] Among the methods developed for simulating the electrochemical interface, it is worth mentioning grand canonical electronic DFT, in which the number of electrons and the balancing charge appearing in the continuum electrolyte can be automatically and continuously changed, as guided by the prescribed electrode potential. This method is a valuable tool for studying electrochemical interface and electrocatalysis under constant potential conditions.[52]

2.1.3. Scaling Relationships and Sabatier Analysis.

Accurate catalytic reaction kinetics calculated with DFT cannot typically be used directly for catalyst screening or design due to the computational cost and the large number of possible systems that can be screened. It is helpful, therefore, to identify a small set of microscopic descriptors that govern the reaction kinetics and use them to efficiently perform the catalyst screening/design.[27] This task is enabled by two important scaling relationships. The first, which is commonly known as the Brønsted−Evans−Polanyi (BEP) relationship, is that activation energies for elementary surface reactions are strongly correlated with reaction energies.[56,57] The second scaling relationship describes the linear relationships of adsorption energies of adsorbates across different transition metal surfaces. An example of this type of scaling relationship is that the binding energies of CH_x, OH_x, NH_x, or SH_x linearly correlate with the binding energies of C, O, N, and S for a series of transition metal surfaces (Figure 4).[58,59] Such correlations reduce the number of independent variables required to describe activity.

The catalytic activity as a function of selected descriptors can be evaluated by a Sabatier analysis[60] or by microkinetic modeling.[61] The resulting activity−descriptor relationship should follow the Sabatier principle of catalysis, which states that the adsorption strengths on the optimal catalyst should be neither too weak nor too strong. This principle can be expressed graphically with a 3D volcano plot, passing through a maximum activity at the optimal binding energies (Figure 5).[46] Once the volcano plot is derived from detailed mechanistic study, convenient adsorption energy calculations can be used to screen for catalysts having the desired optimal adsorption strength.

DOI: 10.1021/acs.chemrev.9b00246
Chem. Rev. XXXX, XXX, XXX−XXX

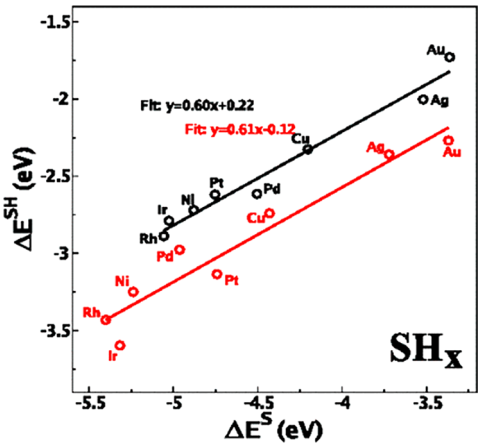

Figure 4. Scaling relationship of SH and S, on close-packed (black) and stepped (red) surfaces of face-centered cubic transition metals. Adsorption energies are referenced to the clean surface and the corresponding molecule in the gas phase. Reproduced with permission from ref 59. Copyright 2007 The American Physical Society.

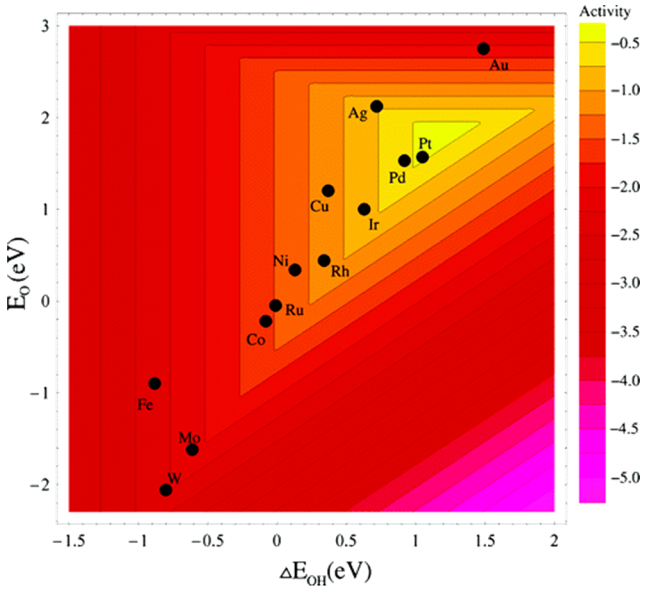

Figure 5. Representative volcano plot showing ORR activity as a function of both the *O and *OH binding energies on metal catalysts. Reproduced with permission from ref 46. Copyright 2004 American Chemical Society.

2.1.4. Summary of Theoretical Techniques for Analyzing NP Electrocatalysts. Theoretical calculations are vital for understanding the intricacies of electrocatalytic systems. Subtle information regarding nanocatalyst structure can be elucidated theoretically, using, for example the RMC method. CHE models are often used to analyze the energetics of electrochemical transformations over catalytic surfaces. The information gained from these studies continues to guide and inspire design strategies that encourage creative construction of active sites to overcome the often activity-limiting scaling relationships that exist between reactive species on a surface. It is now the job of theoretical chemists to continue pushing the limits of current computational methods beyond the simple CHE model by striving to simulate realistic electrocatalytic interfaces. As we continue to probe this space between tractable theoretical models and complicated experimental conditions, we can begin to refine the very questions we are asking about these systems, paving the way for clearer answers.

2.2. Techniques for Synthesizing Well-Defined, Nanoscale Electrocatalysts Relevant to Theory

2.2.1. Individual NPs as Model Electrocatalysts. One of the main limitations of correlating theory and experiment in electrocatalysis is that all ensembles of real electrocatalysts are, at least to some degree, structurally heterogeneous, while theory usually only considers a single, perfect structure. This means that the ideal system for coupling theory and experiment involves the study of a single, well-defined NP having a naked (or ligand-free) surface. There are two approaches for preparing single-particle electrocatalysts: in situ and ex situ synthesis.

In situ methods involve electrodeposition of a single NP onto an electrode surface.[62−66] However, the mechanisms of metal nucleation, deposition, and subsequent particle growth are still poorly understood and difficult to control.[67−70] Moreover, the presence of the electrode makes detailed structural characterization of individual NPs prepared in this way nearly impossible. There is one example in the literature in which individual, well-defined ∼400 nm NPs have been deposited and fairly well characterized (Figure 6).[62] At least for

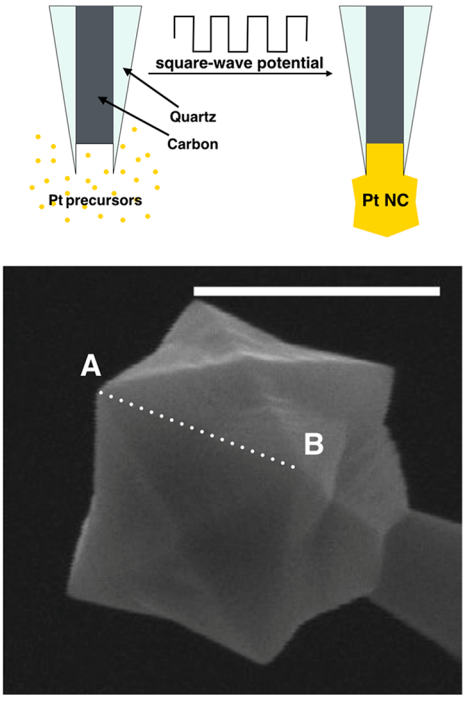

Figure 6. (top) Illustration of the use of square-wave voltammetry to electrodeposit single Pt nanocrystals on carbon nanoelectrodes. (bottom) Scanning electron microscopy (SEM) image of an electrodeposited Pt nanocrystal. The scale bar is 500 nm. Adapted with permission from ref 62. Copyright 2018 The Royal Society of Chemistry.

now, however, this approach is not directly applicable to quantitative correlation of theory and experiment for electrocatalysts smaller than ∼100 nm. In this size range, detailed characterization is very difficult. A possible exception may be when the NP electrocatalyst consists of a single atom, but even then, definitive characterization is not possible at this time.[71,72]

DOI: 10.1021/acs.chemrev.9b00246
Chem. Rev. XXXX, XXX, XXX−XXX

An alternative approach to the study of single-particle electrocatalysts involves ex situ synthesis and characterization, followed by immobilization of the NP onto an electrode surface.[73−75] Alternatively, in scanning electrochemical cell microscopy (SECCM),[76] nanoelectrodes are scanned over individual NPs in an ensemble to analyze their electrochemical behavior. SECCM is even more advantageous when combined with another imaging technique, such as optical imaging (Figure 7).[77] These ex situ approaches for studying single NPs

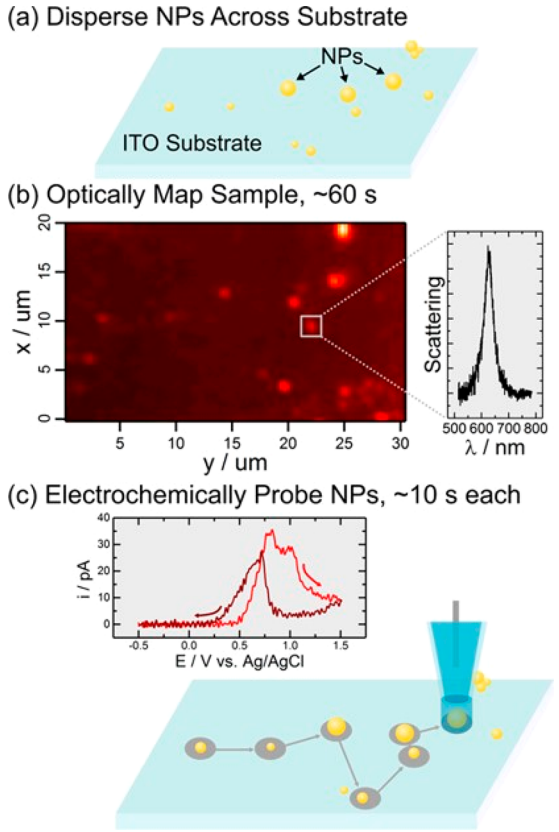

Figure 7. Generalized procedure for probing individual NPs via optically targeted electrochemical cell microscopy (OTECCM). (a) Au nanorods were first dispersed onto a noncatalytic substrate electrode at low coverages (<0.1 μm^{-2}) via drop coating. (b) The resulting samples are first characterized optically using a hyperspectral imaging protocol. (c) Targeted electrochemical measurements are then made via scanning electrochemical cell microscopy (SECCM) on optically identified NPs. The overall process is efficient, typically taking just a few minutes to characterize 5−10 NPs. Reproduced with permission from ref 77. Copyright 2018 American Chemical Society.

suffer from an inability to structurally characterize the single NP catalyst, especially after the electrochemical studies. Because single NPs most relevant to this review (<3 nm) cannot be sufficiently well characterized to yield meaningful correlation to theory, these approaches are not discussed further. Interested readers are referred to the relevant literature.[71,78−81]

2.2.2. Monometallic NP Ensembles. Because it is, at present, not possible to thoroughly characterize and evaluate individual NPs, we are often forced to study ensembles consisting of many NPs, which, as discussed earlier, are inherently heterogeneous in nature. The more structural and compositional heterogeneity that exists within an ensemble of electrocatalytic NPs, the more complicated predictive DFT calculations become. Thus, synthetic methods that yield a high degree of NP monodispersity are critical for comparison of theory and experiment. Even in these cases, however, it is important to realize that a small subpopulation of uncharacterized NPs can still contribute to observed electrocatalytic activity.[82]

Additionally, because small metal NPs are inherently unstable, they are usually covered with a monolayer or submonolayer of monomeric or polymeric ligands. In addition to providing stability, the ligands or capping agents used during NP synthesis can also be used to control the structure and composition of the resulting NP;[83−86] however, the ligands themselves can alter the electrocatalytic activity of the underlying metal NP.[87−92] Keeping these limitations in mind, a brief introduction to the principal synthetic techniques currently used for preparing metal nanoscale electrocatalysts with a high level of synthetic control is provided next.

The chemical reduction of metal salts in the presence of mediating/passivating ligands is still one of the most common synthetic techniques for preparing NPs.[84,93−96] The simplest reaction conditions often employ the reduction of metal precursors using BH_4^- or H_2 at room temperature.[95,97] Unfortunately, many metal precursors do not readily decompose at room temperature, and therefore, elevated temperatures are often required. Solution-based syntheses of metal NPs in organic solvents at high temperatures are broadly defined as solvothermal methods.[98] At elevated temperatures, the ligand or solvent itself can be employed as the reducing agent. An example of the latter is the polyol method, wherein high-boiling poly(glycol) solvents, such as ethylene glycol, serve a dual purpose as both solvent and reducing agent.[99−101]

Thermal decomposition, or thermolysis, methods are particularly useful for solvothermal preparation of nanoscale transition metal electrocatalysts.[102−105] For example, this synthetic method has been reported for the synthesis of Co and Ni NPs,[83,106] which have received increasing attention over the last several years as ORR electrocatalysts.[8,107−109] Thermolysis involves the decomposition of metal precursors with heating followed by subsequent nucleation and particle growth. There are two main synthetic methods for thermal decomposition: the heat-up method and the hot-injection method.[102,110] In the heat-up method, the metal precursors are slowly heated in the presence of solvent, reducing agent, and stabilizing ligand. In the hot-injection method, an organic solvent, commonly an alkylamine, is heated to several hundred degrees Celsius prior to the injection of the metal precursor solution into the reaction solution.[111]

The major difference between the heat-up and hot-injection methods is that the heat-up method allows thermodynamic control over metal nucleation and particle growth, while the hot-injection method may be governed by kinetically controlled processes.[102] Metal carbonyl compounds are often employed as metal precursors during thermolysis procedures, because they easily decompose with heating.[112] The addition of a stabilizing ligand to the synthesis can result in an even greater level of synthetic control. Poly(vinyl)pyrrolidone (PVP) is commonly employed for this purpose, because it is stable under the reaction conditions employed for thermolysis.[26] Additionally, oleylamine has been found to function as solvent, reducing agent, and surfactant at elevated temperatures in one-pot syntheses.[105,106,110,113]

Seed-mediated reduction has quickly become one of the standard methods for preparing well-defined electrocata-

DOI: 10.1021/acs.chemrev.9b00246
Chem. Rev. XXXX, XXX, XXX−XXX

lysts.[93,114,115] The advantage of this technique is that the presence of a metal seed results in preferential reduction of metal ions onto the seed particles. This ensures that NP growth only occurs on the pre-existing seeds, and hence, it affords a high level of control over the size and geometry of the resulting NPs. Importantly, ligands present during the synthesis can be used to favor metal deposition on desired facets of the metal seed, allowing for even greater shape control.[92,99,116] For monometallics, this method is mainly used to impart shape control for larger particles. The normal size range of the metal seeds employed in seed-mediated syntheses is 5−10 nm,[117] and that means this approach is usually not appropriate for preparing the smaller materials required for whole-particle comparison to first-principles theory.

Regardless of the synthetic method used, surface ligands are usually necessary to provide NP stability and increase synthetic control. The importance of ligands in colloidal systems continues to inspire investigation into the mechanisms of ligand-induced structural control during metal nucleation and particle growth.[83−86,99,118−120] For example, the use of different ligands to control the shape of resulting PtRu nanocrystals was recently reported by Dong and co-workers.[86] They showed that, by varying the ammonium complex used as the stabilizing ligand, the shape could be controlled from nanowires to nanorods to nanocubes (Figure 8).

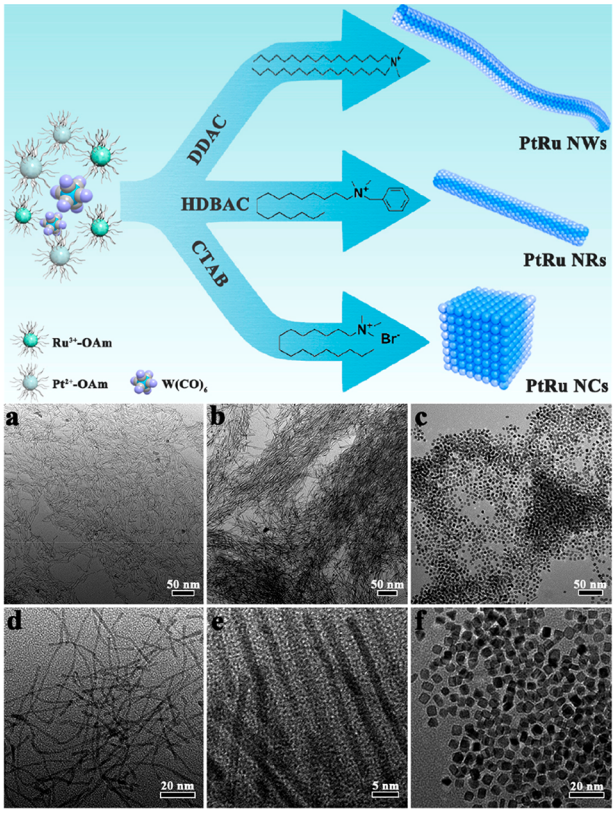

Figure 8. (top image) Synthetic scheme for obtaining multiple geometries of PtRu nanostructures using three different capping ligands. (bottom image) Synthetic morphological and structural characterizations of PtRu nanocrystals. Representative TEM images of (a, d) PtRu nanowires, (b, e) PtRu nanorods, and (c, f) PtRu nanocubes. Adapted with permission from ref 86. Copyright 2017 American Chemical Society.

One commonly used ligand is oleylamine, which, as previously mentioned, can act as the solvent, reducing agent, and stabilizing ligand at elevated temperatures.[106,110,121] A mixture of oleylamine and oleic acid is often employed in tandem during syntheses,[100,104,105,122] while other commonly used ligands include PVP[123−126] and citrate.[97,127] The synthetic flexibility of peptides as structure-controlling ligands is also having an important impact on the field of NP synthesis.[128] In some cases, polymers can act as the surfactant via inverse micelle encapsulation methods.[125,129] Control over NP structure can be modified depending on the chemical and physical properties of the polymer, such as the functional groups present and molecular weight.[130]

The strong interaction of thiol ligands with metal surfaces can poison catalytic reactivity.[131,132] However, Au NPs stabilized with thiol ligands are an active area of research in electrocatalysis.[133−135] Specifically, monolayer-protected Au clusters (MPCs, typically <2 nm) will be discussed in the CO_2RR section. A special case of these catalytic systems includes atomically precise thiolated Au nanoclusters. These types of cluster systems are excellent model electrocatalysts because their molecular composition can be known exactly.[136−138] However, the protecting ligands strongly modulate the electronic structure of the metal cluster, resulting in molecular-like properties. Accordingly, the previously discussed rules for tuning metal NP reactivities do not apply for these materials. Atomically precise clusters are, therefore, beyond the scope of this review, and interested readers are referred to a recent review article.[139]

2.2.3. Nanoalloy Ensembles. While monometallic NPs are still widely studied as promising electrocatalysts, bimetallics have begun to dominate the field. This switch in emphasis is driven by the potential to modify the binding energy of reactants and products on the NP surface due to interactions between the two metals. For example, random nanoalloys present different ensembles of atoms on their surface (Figure 9), and this can provide a means for tuning the number and types of active sites present on a metal NP for a given reaction.

For instance, a study of classically immiscible RhAu nanoalloys showed that the activity toward the ORR could be tuned using ensemble effects.[6] DFT calculations predicted that the Rh_1Au_2 triatomic ensemble possessed the most optimal binding energies for ORR reaction intermediates. This prediction was subsequently confirmed experimentally. The ensemble effect has also been shown to be responsible for the observed tunability of ORR activity in both AgPd and PdAu nanoalloys.[140,141] Thus, the type and level of mixing in nanoalloys is increasingly important in electrocatalysis, particularly in regard to correlation of theory and experiment.

To achieve more uniform nanoalloys, the synthetic techniques discussed previously for preparing monometallic NPs have also been successfully used to prepare a wide variety of unique bimetallic catalysts. For example, simple co-reduction can be used to form bimetallic NPs by introducing two different metal species to the reaction solution and reducing them simultaneously.[142,143] In contrast, sequential reduction of metals in a single reaction solution can lead to core@shell or alloy NPs, and in some cases a mixture of both.[144] Bimetallics can also be synthesized by thermolysis.[104,118,145]

During thermolysis, the exact temperature required for decomposition, as well as the rate of decomposition, is dependent on the metal species itself. These decomposition

DOI: 10.1021/acs.chemrev.9b00246
Chem. Rev. XXXX, XXX, XXX−XXX

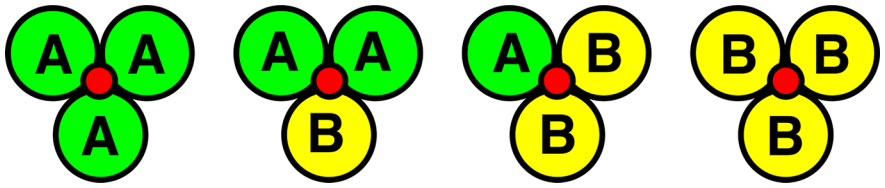

Figure 9. Illustration of oxygen (red circle) binding to four different triatomic surface ensembles where A and B are two different metals.

rates have an impact on the structure of bimetallics. For example, if both precursors decompose simultaneously, then alloy NPs may form.[28,104,113,121] If one precursor has a lower decomposition temperature, however, it will nucleate first, perhaps leading to the formation of core@shell NPs.[146] Additionally, both chemical reduction and thermolysis techniques can be used in tandem to attain otherwise hard-to-synthesize compositions and morphologies of NPs.[147]

Seed-mediated co-reduction (SMCR) can lead to the formation of alloys when two different metal salts are coreduced in the presence of small metal seeds.[148] A notable use of this synthetic method is the ability to prepare alloys of metals possessing large lattice mismatches, such as PdCu.[121] For example, the Skrabalak group showed that different geometries of PdCu NPs can be obtained by changing both the Pd:Cu precursor ratio and/or the pH, making the SMCR a versatile synthetic technique (Figure 10).[149] If the identities of

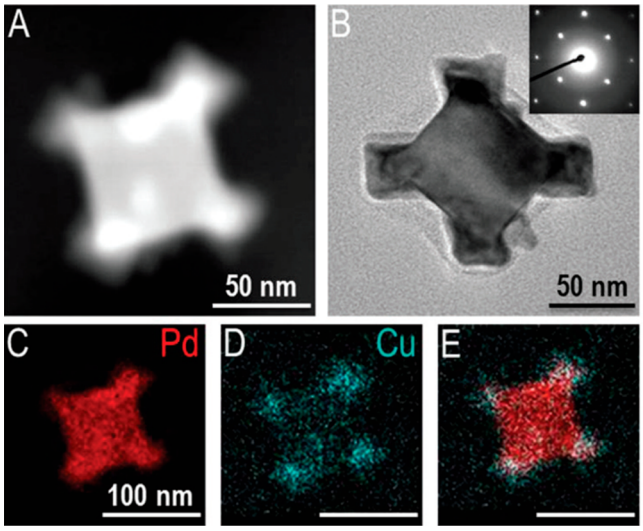

Figure 10. (A) STEM and (B) TEM and (inset) electron diffraction of an individual PdCu particle synthesized using seed-mediated co-reduction (SMCR). The nanocrystal was also characterized using STEM-EDS elemental mapping: (C) Pd only, (D) Cu only, and (E) an overlay of Cu and Pd signals. Adapted with permission from ref 149. Copyright 2017 The Royal Society of Chemistry.

the metal salt and the metal seed are different, however, then core@shell particles can result. Significantly, core@shell NPs of only a few nanometers have recently been reported using the SMCR synthetic method.[115,144]

SMCR has recently been used to transform random PdCu nanoalloys to monodisperse electrocatalysts having a highly ordered, intermetallic composition.[150] Intermetallic NPs have been reported to exhibit both increased activity and stability toward various electrocatalytic reactions.[150−152] In contrast to the SMCR synthetic method discussed in the previous paragraph, most intermetallic NPs are obtained via post-synthetic annealing of random nanoalloys in a reducing environment of forming gas (i.e., 5% H_2/N_2 gas).[150] Elevated temperature, however, can lead to NP instability via agglomeration and ripening.

Additionally, if the random alloy precursor NPs are not sufficiently uniform in size and composition, then the intermetallic NPs obtained during thermal processing will consist of different degrees of atomic ordering. This heterogeneity makes it difficult to determine the intrinsic catalytic reactivity of the ordered phase, thereby limiting the use of DFT calculations in predicting and understanding the true reactivity of intermetallic NPs as electrocatalysts. For this reason, as well as those previously stated, monodisperse, well-defined nanoalloys are vital for improved understanding and designing of novel electrocatalysts for practical applications.

2.2.4. Interactions between Electrocatalytic NPs and Supports. Regardless of the synthetic technique used or the resulting NP composition, electrocatalytic NPs are usually immobilized on a high-surface-area support, such as carbon black[101,121,153] or a metal oxide layer.[154−156] While the support itself can influence electrocatalytic performance,[141,157−160] immobilization may stabilize the NPs and thus make it possible to remove stabilizing ligands prior to electrocatalysis. Ligand removal is usually necessary to attain maximum activity of the catalytic surface and to simplify theory.

Ligand removal is commonly achieved by treating the catalyst at high temperature,[111,161,162] but electrochemical methods are also used to remove ligands and other contaminants from the surface of electrocatalysts.[123,161,163] Both methods can, however, lead to undesirable structural changes, including sintering, agglomeration, and dealloying.[164−166] Therefore, despite advances in synthetic methods that lead to well-defined NPs having desirable structures and compositions, difficulties during ligand removal and NP activation often cause an increase in polydispersity and heterogeneity of a given electrocatalyst ensemble. This may make it even more difficult to identify the catalytically active structures and hence frustrate comparison to theory. Overcoming this problem remains an open challenge in the field of electrocatalysis.

2.2.5. Dendrimer-Encapsulated Nanoparticles (DENs). One method that overcomes some of the synthetic limitations mentioned heretofore, especially those associated with ligand removal, is called dendrimer encapsulation. Dendrimer-encapsulated nanoparticles (DENs) are synthesized by taking advantage of highly dendritic polymers, or dendrimers, as synthetic templates for NP formation.[4,167,168] The typical size of DENs is in the range of just a few atoms to ~300 atoms, making them very well suited for comparison to theory.[10,167−169] Commercially available poly(amidoamine) (PAMAM) dendrimers are the most commonly employed for the synthesis of DENs; however, the use of other dendrimers,[170−175] such as poly(propyleneimine) (PPI), has been reported.[168]

DOI: 10.1021/acs.chemrev.9b00246
Chem. Rev. XXXX, XXX, XXX−XXX

In a basic synthesis of DENs, a metal salt precursor is added to a solution of dendrimers and subsequently reduced with BH_4^- at room temperature (Figure 11).[176] This synthetic method leads to one zerovalent NP per dendrimer while allowing for good synthetic control over both size and composition.[177,178] In addition to monometallic DENs, alloy and core@shell DENs can also be prepared.[179−181] For example, Au*M* (*M* = Pd, Pt, Rh) alloys,[169,176,182] as well as PdAu@Pt alloy-core@shell DENs,[10,158] have recently been successfully synthesized and employed as electrocatalysts. While a wide variety of DEN structures can be prepared, enhanced atomic diffusion in such small NPs can sometimes lead to structural and compositional rearrangements during, or even before, electrocatalysis.[183,184]

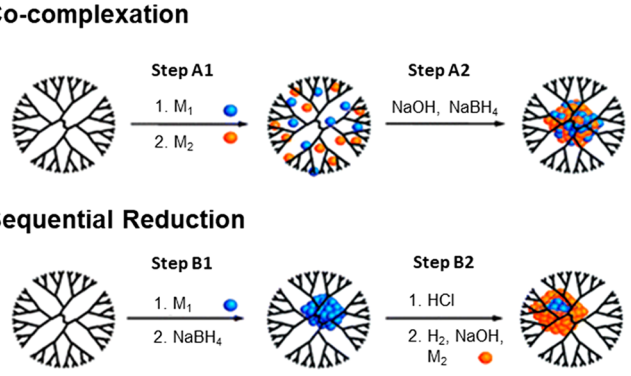

Figure 11. General synthetic routes for alloy (top) and core−shell (bottom) DENs. Adapted with permission from ref 176. Copyright 2009 American Chemical Society.

For electrocatalytic studies, DENs can be dispersed onto a Vulcan carbon support, drop-cast onto metal oxides, or electrochemically grafted to carbon electrodes via oxidation of the peripheral functional groups of the dendrimers.[185] Notably, in all of these cases, DENs have been shown to behave as ligand-free electrocatalysts and exhibit high catalytic activity.[168,175,186,187] In other words, even though the dendrimer is usually present during electrocatalysis and therefore able to stabilize the encapsulated NP, it does not impact electrochemical measurements.

2.2.6. Mass-Selected NPs. While a high level of synthetic control has been realized using the techniques mentioned thus far, there are still limits on the degree of control over the size and compositional monodispersity of nanoscale electrocatalysts. One recently developed technique that overcomes these limitations is the use of mass spectrometry to mass-select metal clusters synthesized in the gas phase, followed by soft-landing techniques to deposit very small, monodisperse metal clusters onto support materials for use as electrocatalysts (Figure 12).[188,189] Both the ligand-free nature and the extremely small size of mass-selected metal clusters (<2 nm) make this type of system ideal for comparison of electrocatalytic results to DFT calculations.[190−193]

The small size of metal clusters, in combination with the necessary deposition onto a solid support, makes mass-selected electrocatalysts very difficult to characterize using traditional techniques. One study overcame this limitation by using the mass-selection technique to deposit Pt clusters on carbon-coated TEM grids (Figure 13).[194] The use of TEM grids as the

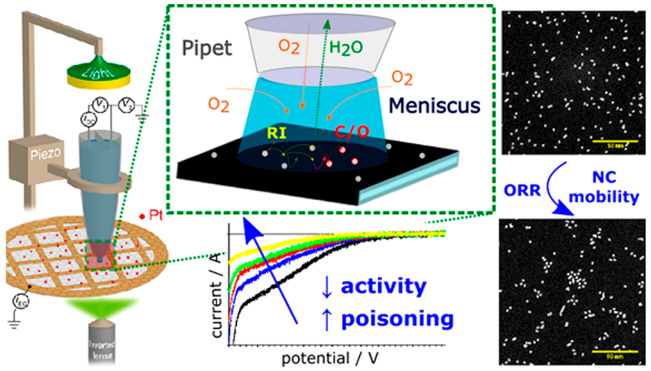

Figure 13. Combined use of dual-barrel scanning electrochemical cell microscopy (SECCM) and an inverted optical microscope to characterize Pt NP stability during the ORR. Reproduced with permission from ref 194. Copyright 2018 American Chemical Society.

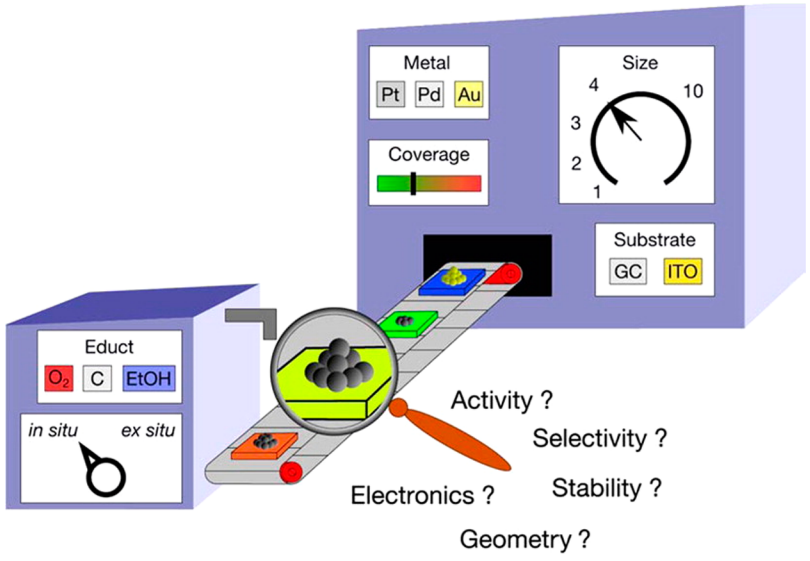

Figure 12. Illustration showing a model system for studying cluster size effects toward electrocatalysis using the mass-selected synthetic template. Reproduced with permission from ref 189. Copyright 2016 American Chemical Society.

DOI: 10.1021/acs.chemrev.9b00246
Chem. Rev. XXXX, XXX, XXX−XXX

cluster support allowed for subsequent microscopic analysis prior to evaluation of their properties as ORR electrocatalysts. While use of this recently developed technique works best for studying monometallic clusters, larger, bimetallic NPs have also been reported.[195,196] The many advantages of using mass-selected electrocatalysts are discussed in a recent review.[191]

2.2.7. Summary of NP Synthetic Methods for Electrocatalysis. Great progress has been made in developing precision synthetic methods for synthesizing electrocatalysts having properties that are appropriate for correlating theory and experiment. Nevertheless, there is a long way to go before this field matures. The ideal model electrocatalytic system is a single, stable, structurally well-defined NP attached to an inert electrode surface. For now, however, that goal is unattainable, and therefore, we are forced to deal with simultaneous evaluation of large numbers (ensembles) of particles with the assumption that their average electrocatalytic response can be represented by a single theoretical model. While this approach works fairly well for monometallic electrocatalysts, the situation is more complicated for bimetallics due to ligand and ensemble effects that are difficult to control experimentally. Intermetallic NPs that exhibit well-defined arrangements of atoms on their surfaces are beginning to emerge, and they will likely be able to address this problem. Currently, these materials still suffer from some limitations, however, as they tend to be rather large and hence not fully compatible with whole-particle, first-principles theory. They also suffer from problems associated with sample heterogeneity in regard to atomic arrangement.

2.3. Characterization Techniques for Electrocatalysts

Once synthesized, thorough characterization of electrocatalysts is vital to ensure accurate correlation of theory and experiment. Characterization of metal NPs having sizes in the <3 nm range is especially difficult and requires a combination of techniques to elucidate structure and composition. Given adequate experimental characterization data, theoretical calculations and simulations can help determine the final structure as well as predict the catalytic activity of NP electrocatalysts.[197]

While knowing the initial composition and structure of a metal nanocatalyst is important, a second factor that needs to be considered when studying nanoscale electrocatalysts is their stability under catalytic, or *operando*, conditions.[166,198] As mentioned earlier, the structure of very small NPs is often inherently unstable and degradation of electrocatalysts can occur within seconds under the influence of electrochemical reactions.[21] In this section, we will provide a brief overview of the characterization techniques that are particularly effective for obtaining the type of structural information that is required for ensuring accurate correlation of theory and experiment. These techniques include those based on X-ray diffraction and absorption, electron microscopy and related methods, and electrochemical characterization methods.

2.3.1. X-ray Diffraction (XRD). In XRD, X-rays scatter from a crystalline material, resulting in a unique diffraction pattern that can provide valuable structural information. XRD techniques are widely used to analyze the lattice spacing of NPs, thereby providing insight into their crystalline structure as well as qualitative compositional information such as the degree of atomic mixing.[199,200] Because traditional XRD techniques require crystalline materials, samples can be analyzed while supported on amorphous substrates such as carbon.[201] This is especially advantageous for studying electrocatalysts because they are often prepared as carbon inks. The small size of the crystalline facets of NPs creates peak-broadening, which can be used to estimate their size in accordance with the Scherrer equation.[200] Synchrotron-based high-energy X-ray diffraction (HE-XRD) is especially useful for analyzing metal NPs due to the capability to achieve surface-sensitivy.[199,202] Unfortunately, for NPs <3 nm in diameter, the Bragg diffraction peaks become so broad that most structural information is lost.

The limitation of sample crystallinity required for XRD can be overcome by coupling HE-XRD with atomic pair distribution function (PDF) analysis. PDF analysis takes into consideration the total scattering of the sample, including both traditional Bragg peaks as well as those from diffuse scattering centers, and therefore, it is useful for characterizing disordered nanomaterials.[203,204] Experimental atomic PDF spectra can be fit using simulated structural models to yield quantitative information about NP structure and atomic environment.[205−207] HE-XRD also enables *operando* characterization and can be used to closely probe structural and phase transformations of nanocatalysts under a range of conditions.[109,208,209] For example, dissolution of Ni from ∼3 nm PtNi nanoalloys has been analyzed during electrochemical cycling using in situ HE-XRD.[210] Structural changes have also been observed in PtNi and PtNiCo nanocatalysts during *operando* HE-XRD/PDF studies during the ORR (Figure 14).[207] As accessibility to synchrotron facilities continues to increase, these types of *operando* studies will continue to advance our understanding of dynamic structural and compositional changes of electrocatalysts. Such information is vital for improving their durability and activity.

Small-angle X-ray scattering (SAXS) complements XRD and has emerged as a useful tool for nanocatalyst characterization.[211] While XRD analyzes X-rays scattered at wide angles relative to the incident beam, SAXS relies on the energy of X-rays scattered at angles of just 0.5−10°. XRD results in Angstrom-scale resolution, while SAXS is limited to a lower resolution of ±0.1 nm.[211] Therefore, SAXS analysis provides information about NP size distributions and structural features on the scale of 1−100 nm, and XRD is necessary to obtain atomic-scale information such as the extent of alloying in a sample.

There are two main advantages of SAXS that make it an increasingly important technique for nanocatalyst characterization. First, noncrystalline materials, including liquids and powders, can be analyzed with minimal sample preparation. Second, SAXS has the ability to monitor catalyst changes in situ during electrochemical measurements.[212,213] However, catalyst supports (e.g., Vulcan carbon or metal oxides) utilized in electrochemical studies can interfere with SAXS analysis.[214] A technique known as anomalous SAXS (ASAXS) utilizes a synchrotron energy source to overcome this limitation of background interference from the support. ASAXS probes the metal of interest at different X-ray energies, allowing the signal from the support to be distinguished from the sample.[214] In one report, for example, ASAXS was used to monitor both the average size and the composition of PtCu nanoalloys during electrochemical leaching experiments.[215] A recent review provides additional information about the relationship between theory and NP characterization by SAXS.[211]

2.3.2. X-ray Photoelectron Spectroscopy (XPS). In contrast to the high-energy X-rays discussed for XRD, XPS is a surface-sensitive technique that traditionally utilizes "soft" X-

DOI: 10.1021/acs.chemrev.9b00246
Chem. Rev. XXXX, XXX, XXX−XXX

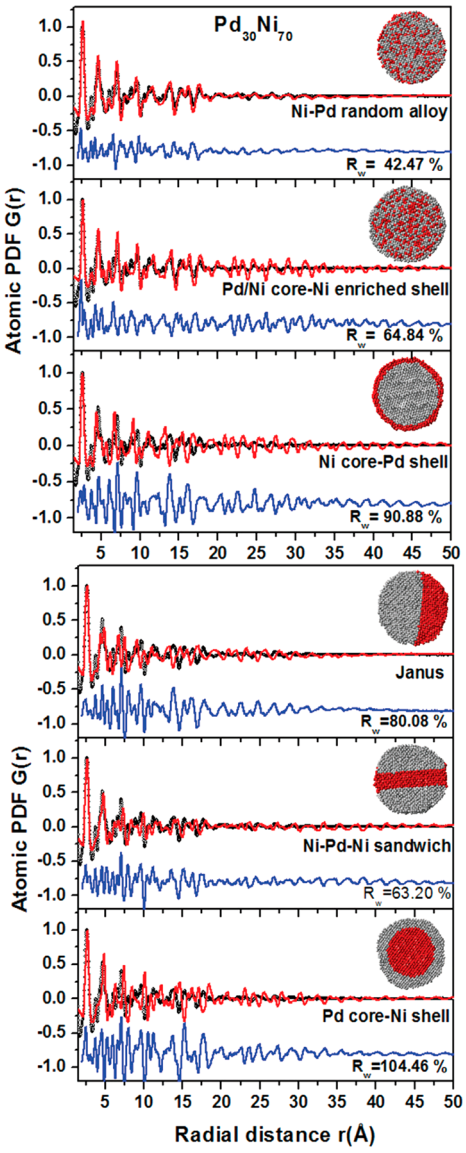

Figure 14. Example of HE-XRD/PDF analysis of different structures of PdNi bimetallic NPs. Reproduced with permission from ref 207. Copyright 2016 The Royal Society of Chemistry.

rays with energies in the range 200−2000 eV. The absorption of these lower energy X-rays enables examination of the binding energies of core-level electrons as they are ejected from approximately the first ∼10 nm of a conductive sample.[216] Because the binding energies of core electrons are sensitive to the atomic number of the element, the identity of the elements in the sample can be determined by referencing the experimentally collected XPS spectra to known binding energies of particular elements. For the same reason, XPS is sensitive to the oxidation state of elements present in NPs.

The atomic percentage of each element near a NP surface can also be determined by XPS. One important caveat, however, is that this review article is primarily concerned with NPs in the <3 nm size range and, therefore, the escape depth of the electrons exceeds the diameter of the NPs. This means that, for this class of NPs, XPS is really a bulk analysis tool. The use of synchrotron radiation allows for surface-sensitive measurements, even for small NPs.[217−220] However, the detection limit of XPS is only in the parts per thousand range, and the measurements are usually performed in ultrahigh vacuum. This latter requirement has severely limited in situ applications of XPS to electrocatalysis, but that is changing with the development of an ambient pressure version of the methodology.[221−226]

2.3.3. X-ray Absorption Spectroscopy (XAS). Another important tool in the field of electrocatalysis is X-ray absorption spectroscopy (XAS).[25] In this technique, the incident photon energy is scanned through a range where the excitation of the core electrons of metals to unoccupied states above their Fermi level can be observed. Near the absorption site, multiple scattering resonances result from the interaction of the excited photoelectron with neighboring atoms, producing absorption peaks that provide information about the local electronic and geometric structure. Element-specific studies can be conducted by probing a sample with X-rays that are equal to or just above the specific binding energy for a core electron of a known atomic species. This type of analysis is known as X-ray absorption fine structure (XAFS) and encompasses two main spectral regions of interest: X-ray absorption near-edge structure (XANES) and extended X-ray absorption fine structure (EXAFS).[17]

Although there is no well-defined cutoff between the XANES and EXAFS regions of an absorption spectrum, XANES is generally associated with energies extending from the pre-edge region to energies ∼30−50 eV above the absorption edge. The EXAFS region extends to energies ∼1000 eV above the absorption edge. The XANES region is sensitive to oxidation state and the coordination chemistry of the absorbing atom, while EXAFS is used to determine interatomic distances, coordination numbers, and the identity of nearby neighbors of the absorbing atom.[17,227] Therefore, these techniques provide highly useful information about electrocatalyst structure; for example, they can distinguish between alloy or core@shell structure of a nanocatalyst. For nanomaterials in which surface and core atoms are present in roughly equal numbers, EXAFS can also provide specific surface information (though for particles larger than several nanometers in diameter, XAS spectra are dominated by the core atoms). Other advantages of XAS include the ability to easily study both amorphous and crystalline electrocatalysts *operando*.[182,228−230] Finally, XAS is an averaging technique, so it is highly complementary to electron microscopy.[195,209]

2.3.4. Electron Microscopy (EM). Transmission electron microscopy (TEM) is another important method used for the analysis of electrocatalytic materials. It involves passing a beam of electrons through a sufficiently thin, conductive sample and then monitoring the images formed. A marked advantage of EM is its ability to provide atomically resolved structural information about individual NPs. When coupled with energy dispersive X-ray (EDX) spectroscopy, TEM can also provide elemental analysis of NPs.

Scanning transmission electron microscopy (STEM) involves rastering the electron beam across the surface of the sample. By detecting scattered electrons outside of the path of the transmitted electrons, use of *Z*-contrast microscopy (also known as high-angle annular dark-field imaging, HAADF) allows for straightforward interpretation of atomic configurations. HAADF-STEM is especially good for studying bimetallic NPs that have similar lattice spacings but different atomic numbers due to the relative scattering efficiencies of low- and high-*Z* elements, and therefore different resulting intensities (Figure 15).[231] Additionally, compared to TEM,

DOI: 10.1021/acs.chemrev.9b00246
Chem. Rev. XXXX, XXX, XXX−XXX

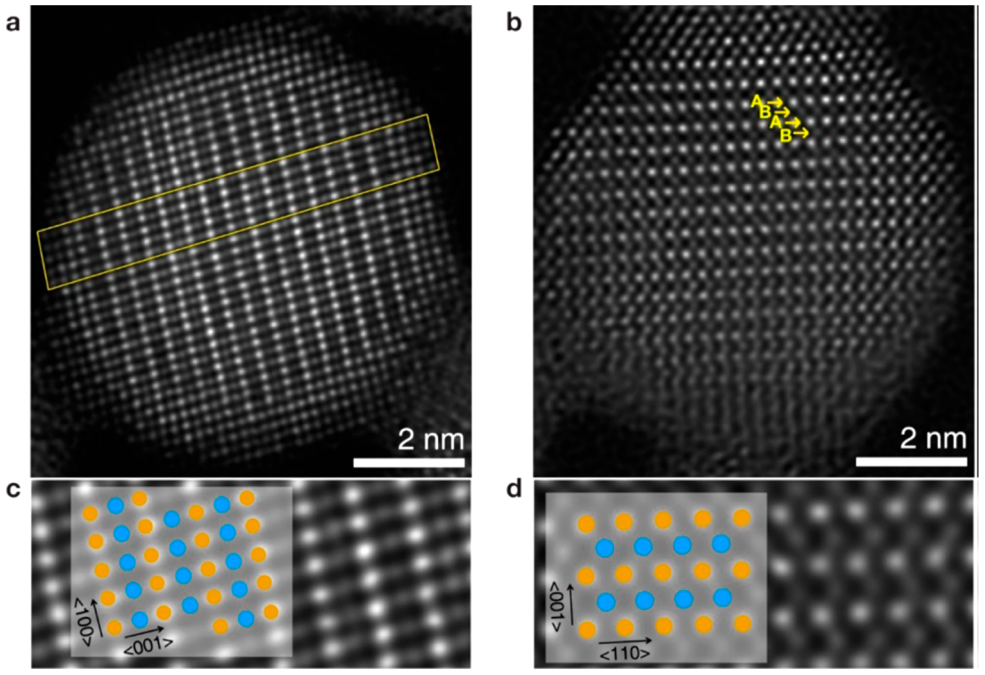

Figure 15. Structural investigation of an atomically ordered-AuCu NP with high resolution. Aberration-corrected HAADF-STEM images of an ordered-AuCu NP (a, b) and magnified STEM images of the center of the particle together with overlapping schematics of structural projections (c, d). Atoms in orange and blue color represent gold and copper, respectively. Adapted with permission from ref 231. Copyright 2017 American Chemical Society.

STEM improves the resolution of EDX spectroscopy for elemental analysis.

Because EM is not an averaging method, it is highly complementary to XAS and diffraction methods. The importance of correlating structural information obtained from multiple characterization techniques is highlighted by the limitation of TEM in identifying sub-nanometer atomic species. This is significant, as few-atom clusters, and even single metal atoms, can be active electrocatalysts.[232−235] For example, a recent report by Henkelman and co-workers demonstrated that pure Rh clusters in this size range were present in a RhAu alloy sample and that they contributed to the observed electrochemical ORR activity.[6] While these Rh clusters were not initially visible using TEM, EXAFS measurements suggested their presence. This motivated the authors to search for and identify them using HAADF-STEM. This example highlights the shortcomings of standard TEM while simultaneously demonstrating the importance of using advanced EM techniques to observe all catalytic species present in an ensemble sample.

From the perspective of electrocatalysis, the principal use of EM is analysis of catalysts before and, in some cases, after a reaction. However, even when post-mortem catalyst analysis is undertaken, one usually compares different particles in the ensemble. Because of this spatial limitation, information regarding the time scale and mechanism of changes in electrocatalyst structure is not available. One approach for addressing this problem is a technique known as identical-location TEM (IL-TEM), which provides a means for analyzing the same NPs before and after electrocatalytic reactions.[236−239] Additionally, IL-TEM has been used to gain atomic-level insight into the nucleation and growth of electrodeposited Au NPs during synthesis (Figure 16).[68] Studies appropriate for IL-TEM analysis are conducted using "finder grids", which feature distinct markings that facilitate navigation on the grid. For electrocatalytic experiments, this method usually requires that a TEM grid be used as the working electrode. This challenge in experimental design and the fact that analysis still must be carried out under a vacuum have limited the adoption of this method.

The very exciting method of in situ electrochemical EM is just now beginning to be available.[70,240,241] While the thin SiN windows used with in situ cells minimize loss of resolution, most of the limitations of this technique stem from the products of water hydrolysis created by the interaction of the beam with the aqueous solvent. Therefore, while this type of analysis is not yet commonplace, cells for in situ EM are now commercially available,[70] and it is an area of active research that will be transformative for the study of electrocatalysis as the technology advances and becomes more accessible.

2.3.5. Electrochemical Methods. The final characterization technique we discuss is electrochemical methods. Determination of the electrochemically active surface area (ECSA) of a catalyst is important for correctly evaluating current densities and therefore specific activity. There are several methods for obtaining an ECSA measurement for metal NPs, most of which involve cyclic voltammetry in acidic media. Four commonly cited methods are the integration of the reduction peak of metal oxides,[233,242−245] integration of hydrogen adsorption and desorption peaks,[108,141,246−251] integration of CO oxidation peaks,[71,252] and underpotential deposition (UPD) of (usually) Cu or Pb followed by integration of the subsequent oxidation peak.[230,253−258] Note, however, that addition of any ligand, whether it be hydrogen atoms, molecules like CO, or a metal, to the surface of a <2−3 nm NP can result in substantial structural changes.[24,259]

The UPD potentials of Cu (or Pb) are sensitive to the identity of the underlying metal,[169,174,260] NP size,[261,262] and surface facets.[263,264] These sensitivities in deposition potential make UPD a useful technique for surface-sensitive nanocatalyst

DOI: 10.1021/acs.chemrev.9b00246
Chem. Rev. XXXX, XXX, XXX−XXX

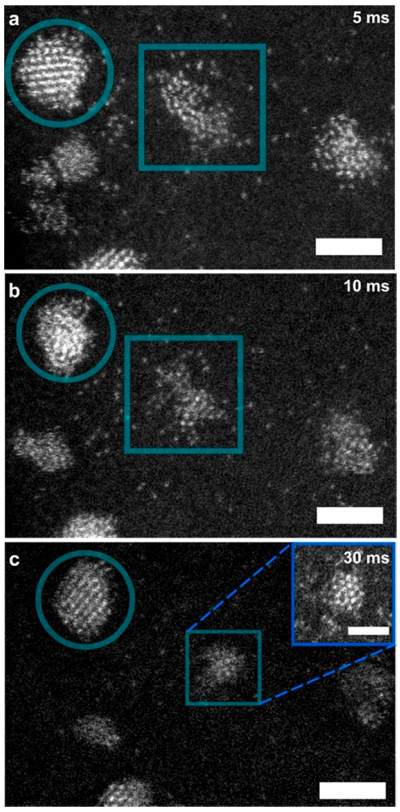

Figure 16. Identical-location STEM (in annular dark-field mode) still images of early stage electronucleation and growth focusing on isolated atoms, atomic clusters, and NPs. (a–c) One example of how a NP forms from an atomic cluster over a 30 ms electrodeposition time period. The scale bar is 2 nm. Electrodeposition was carried out by applying −0.5 V vs SCE for (a) 5 ms, (b) 10 ms, and (c) 30 ms. Reproduced with permission from ref 68. Copyright 2018 American Chemical Society.

characterization.[263,265] Notably, the presence of discrete UPD potentials for Cu deposition on different Pt NP facets could be successfully predicted using DFT, even on NPs <2 nm (Figure 17).[266] Interestingly, this study demonstrated that Cu does not deposit on corner and edge atoms, thereby leading to an incomplete shell. A concern with performing UPD prior to catalytic studies, however, is that some reactive Cu or Pb atoms might remain and participate in the observed catalytic activity.[267]

2.3.6. Summary of NP Characterization Techniques for Electrocatalysis. As demonstrated in this section, characterization methods appropriate for evaluation of electrocatalysts have improved markedly over the past decade or so. Despite these advances, however, surprisingly few studies of electrocatalysts provide post-mortem information. This is particularly problematic for studies that correlate theory and experiment, because evolution of catalyst structure during electrocatalytic experiments renders the initial structural characterization useless. Even when post-mortem data are provided, they may or may not be relevant to the electrocatalytically active species. Fortunately, in situ and *operando* methods are becoming accessible, if not routine. At present, in situ electrochemical methods are widely available, *operando* XAS measurements are becoming more commonplace, and the recent remarkable advances in EM hold out the promise of real-time structural analysis of single NPs under reaction conditions.

3. CORRELATING CATALYTIC STRUCTURE TO ACTIVITY FOR WELL-DEFINED ELECTROCATALYTIC SYSTEMS

3.1. The Oxygen Reduction Reaction (ORR)

The oxygen reduction reaction (ORR) is the cathode reaction that occurs in low-temperature proton-exchange-membrane fuel cells (PEMFCs), which electrochemically convert the chemical energy stored in hydrogen fuel into electrical power.[268] PEMFCs are the key technology for using hydrogen fuel in the transportation sector and are predicted to play an important role in alternative energy schemes. However, the slow kinetics of the ORR, even on Pt, results in a significant overpotential for oxygen reduction.[269]

To make PEMFCs economically feasible, significant research efforts have been devoted to developing active, low-cost, and durable ORR electrocatalysts. These research efforts can be roughly divided into four categories: (i) understanding the reaction mechanism of the ORR and identifying active sites on Pt surfaces; (ii) optimizing the activity and selectivity of Pt ORR catalysts; (iii) discovering non-Pt ORR electrocatalysts; and (iv) improving the stability of ORR catalysts under reaction conditions. In this section, we summarize some key developments in each of these areas by emphasizing recent

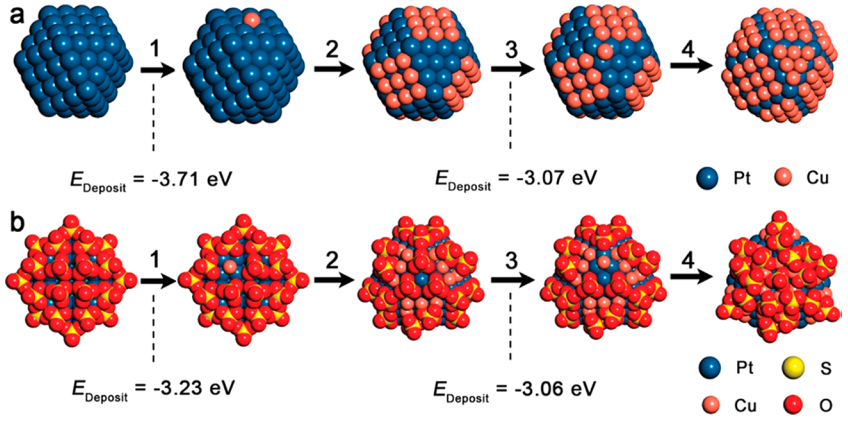

Figure 17. Cu deposition process shown with (a) Pt_{147}^{DFT} and (b) $(SO_4)Pt_{147}^{DFT\text{-}half}$ models. Reproduced with permission from ref 266. Copyright 2012 American Chemical Society.

DOI: 10.1021/acs.chemrev.9b00246
Chem. Rev. XXXX, XXX, XXX−XXX

research that demonstrates synergy between theory and experiment.

3.1.1. Mechanism of the ORR on Pt Catalysts. The ORR can proceed via either a two-electron or a four-electron reaction pathway. In the two-electron pathway, the O_2 molecule is partially reduced to yield H_2O_2 (eq 1). For PEMFCs, however, the energy-efficient four-electron pathway to water is preferred (eq 2).

$$O_2 + 2H^+ + 2e^- \rightarrow H_2O_2 \qquad \{E_0 = 0.70\ V\} \tag{1}$$

$$O_2 + 4H^+ + 4e^- \rightarrow 2H_2O \qquad \{E_0 = 1.23\ V\} \tag{2}$$

Depending on whether or not the O−O bond dissociates before the reduction step, the four-electron pathway can adopt the dissociative pathway (eqs 3−5)

$$O_2 + 2* \rightarrow 2O* \tag{3}$$

$$2O* + 2H^+ + 2e^- \rightarrow 2OH* \tag{4}$$

$$2OH* + 2H^+ + 2e^- \rightarrow 2H_2O + 2* \tag{5}$$

or the associative pathway (eqs 6−10)

$$O_2 + * \rightarrow *O_2 \tag{6}$$

$$*O_2 + H^+ + e^- \rightarrow *OOH \tag{7}$$

$$*OOH + H^+ + e^- \rightarrow *O + H_2O \tag{8}$$

$$*O + H^+ + e^- \rightarrow *OH \tag{9}$$

$$*OH + H^+ + e^- \rightarrow H_2O + * \tag{10}$$

The chemical intermediates on the catalyst surface that are involved in the electron-transfer steps are *O, *OH, and *OOH.

Using DFT to calculate the adsorption free energies of the intermediates, Nørskov proposed a simple computational hydrogen electrode (CHE) model to evaluate the reactivity of different transition metals (TMs) toward the four-electron ORR pathway.[46] On TM surfaces, the rate-limiting potentials (U_{rlp}) are defined as the lowest applied potential required to render every reduction step downhill in free energy.

The 2D volcano plot shown in Figure 18 was constructed using the Sabatier analysis method and calculated U_{rlp} values.[46] This plot shows the activity trend of TMs toward the ORR as a function of oxygen binding energies. Catalysts located on the left side of the volcano bind oxygen too strongly, and therefore, the activity of the ORR is limited by the desorption of OH*. In contrast, for catalysts on the right side of the volcano that weakly adsorb oxygenated species, adsorption of *OOH on the surface is hindered, retarding the ORR activity. Pt lies closest to the top of the volcano due to its intermediate oxygen binding strength, which is consistent with experimentally observed trends. This volcano plot also suggests that the most efficient ORR catalyst would have an oxygen binding energy ~0.1 eV lower than Pt.[56] This simple model, which is based solely on thermodynamics, beautifully explains the high ORR activity of Pt and provides a guideline for further optimizing ORR catalysts. Therefore, recent research has gone into lowering the oxygen binding energy on Pt surfaces using the techniques discussed throughout the next several sections.

3.1.2. Optimizing ORR Activity on Pt Surfaces. Inspired by the foregoing theoretical insights, a number of experimental strategies have been explored to weaken the

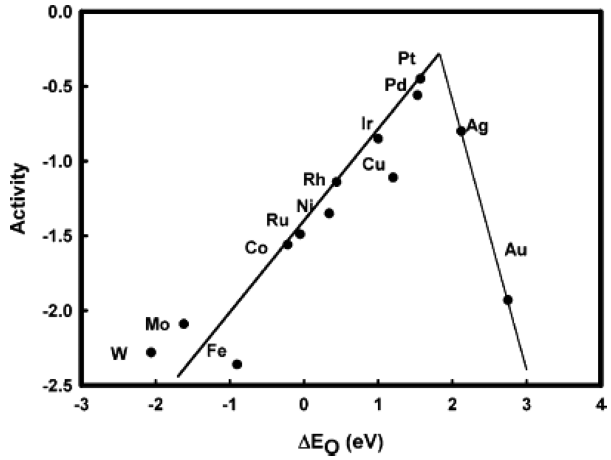

Figure 18. Representative volcano plot showing ORR activity as a function of oxygen binding energy on different metal catalysts. Reproduced with permission from ref 46. Copyright 2004 American Chemical Society.

binding energies of oxygenated species on the Pt surface. These include compressing the surface-Pt lattice spacing (strain effect) and alloying Pt with other TMs (ligand effect). These approaches can shift the d-band center of surface Pt atoms downward in energy, leading to weaker binding of intermediates and therefore increased ORR activity.[270,271]

The use of the strain effect to tune the oxygen binding energy of a catalyst has previously been demonstrated by depositing a Pt monolayer on different planar, macroscopic metal substrates.[272−274] For example, a Pt monolayer supported on Pd(111) exhibited improved ORR activity compared to a Pt(111) single crystal. This increase in activity was attributed to compressive strain of the Pt overlayer, as was later confirmed theoretically by Mavrikakis.[274] The use of the strain effect to modulate the ORR activity of a Pt shell has also been reported for NPs.[275−278] The synthesis of these electrocatalysts typically involves UPD of Cu onto a metal NP, followed by galvanic replacement of the Cu shell with Pt. This approach makes it possible to deposit a single monolayer of a noble metal shell, thereby improving ORR activity.[279]

Sometimes the compressive strain exerted on a Pt shell can be too strong, leading to degraded ORR activity. In such cases, the strain on the Pt overlayer can be reduced by forming either thicker (i.e., multilayer) Pt shells or Pt islands.[278,280,281] Thicker Pt shells can be synthesized using multiple, sequential UPD-galvanic replacement cycles. For example, Adzic et al. reported using this method to deposit multiple Pt overlayers on ~3 nm Ru NPs.[278] They observed optimal ORR activity for Pt shells that were two monolayers thick. DFT calculations for these materials show that two monolayers of Pt optimized the binding energies of O and OH on the surface and therefore supported the experimental findings.

Modulating the compressive strain of a metal shell to increase ORR activity has been theoretically and experimentally explored for many other systems. For example, this design strategy has proven to be effective even for alloy shells that are Pt rich (rather than exclusively Pt).[273,282] Strain in Pt shells can also be tuned by varying the composition of an alloy core.[10,283,284] For example, as the percentage of Cu in a PtCu random alloy core increases in PtCu@Pt_{2ML} NPs, the ORR activity also increases.[282] The surface binding energies of alloy-core@Pt systems have been screened theoretically to

DOI: 10.1021/acs.chemrev.9b00246
Chem. Rev. XXXX, XXX, XXX−XXX

evaluate optimal alloy compositions for increased ORR activity.[285] One promising structure that was predicted is $Pd_{0.72}Au_{0.28}$@Pt, which was subsequently validated experimentally.[10]

While this type of PdAu@Pt catalyst was shown to have high ORR activity, there is a strong drive in the field to develop increasingly active electrocatalysts while simultaneously decreasing the amount of expensive, noble metals. Therefore, alloying Pt with 3d TMs, including Ni, Co, Fe, and Cu, is now a widely employed strategy to boost ORR activity.[107,272,286−288] A successful example of this approach includes FePt@Pt core@shell NPs, as demonstrated by the Sun group.[249] Both the structure and composition of the FePt alloy core act to modulate the surface strain of the Pt shell. Specifically, face-centered tetragonal (fct) FePt@Pt NPs exhibited higher ORR activity compared to a face-centered cubic (fcc) structure, which has an overstrained Pt shell. Substitution of some of the Fe for Cu in the core resulted in FeCuPt@Pt NPs having superior ORR activity, a finding that was predicted by DFT calculations and hybrid quantum mechanics/molecular mechanics (QM/MM) simulations.[249] This provides a good example of how a high level of synthetic control can be used in conjunction with theory to develop increasingly active electrocatalysts.

Sometimes fundamental studies of macroscale surfaces point NP research in productive directions. For example, geometric effects on the activity of macroscopic Pt_3Ni crystals for the ORR were explored by the Marković group.[289] The order of catalytic activity for the different low-index surfaces was found to be $Pt_3Ni(100) < Pt_3Ni(110) \ll Pt_3Ni(111)$. Specifically, $Pt_3Ni(111)$ surfaces, synthesized under ultrahigh vacuum (UHV) conditions, were found to have 90-fold higher ORR activity compared to a commercial Pt/C catalyst. To understand the increased ORR activities observed, Monte Carlo simulations predicted that the NP structure should undergo Pt surface segregation, which induced the formation of a Pt skin with a Ni-rich underlayer.[290,291] This structure leads to substantial destabilization of the oxygenated adsorbates due to a d-band shift as a result of the ligand effect from the underlying Ni.[271,272]

Clearly, macroscale single crystals are not appropriate for use in PEMFCs, but the foregoing findings challenged the field to create nanoscopic electrocatalysts having similar properties. This resulted in the synthesis of shaped PtNi NPs exposing (111) facets on the surface. The specific shapes that have been investigated include nanoframes,[292] icosahedra,[293] and octahedra.[294−299] An example of highly active octahedral PtNi NPs was reported by Strasser in 2012.[300] By utilizing low-temperature solvothermal methods, monodisperse, surfactant-free, 9.5 nm PtNi alloy octahedra were prepared. These materials exhibited a 10-fold increase in Pt mass activity, reaching 1.45 A/mg_{Pt}.

Additionally, it was recently reported that the ORR activity of PtNi NPs can be further enhanced by substituting other d-metals, such as Cr,[301] Co,[302−304] and Mo.[305,306] Specifically, compared with commercial Pt/C catalysts, Mo-doped Pt_3Ni octahedral NPs were found to be more active than commercial Pt/C catalysts, exhibiting a 73-fold enhancement in mass activity toward ORR.[307] DFT calculations suggested that the high ORR activity of this Mo−Pt_3Ni/C catalyst stems from segregation of Mo atoms to edge and vertex sites of the octahedral NPs, thereby modifying the binding strengths of reactive intermediates. It should be noted, however, that no direct experimental evidence was reported to confirm the preferential segregation of Mo to the edges and vertices. The difficulty of achieving this level of structural characterization highlights one of the principal difficulties of correlating theory and experiment.

In addition to 3d TMs, other metals combined with Pt have also been explored for the ORR.[273,308−310] For example, in a theoretical study by Nørskov, computational screening was performed on Pt alloyed with early TMs.[311] PtSc and PtY were identified as the most stable Pt binary alloys, with their ORR activity predicted to be better than that of pure Pt. Electrochemical measurements showed that the activities of bulk, polycrystalline Pt_3Sc and Pt_3Y electrodes were enhanced, relative to pure Pt, by factors of 1.5−1.8 and 6−10, respectively. Although the activity of these electrocatalysts is quite promising, synthetic methods for preparing well-defined PtSc or PtY alloy NPs having controlled compositions are currently unavailable.

3.1.3. Non-Pt ORR Electrocatalysts. In addition to reducing Pt-loading in ORR electrocatalysts, an even more desirable and ambitious goal is development of catalysts that do not contain precious metals (or at least not Pt). The design principles discussed thus far translate well, for example, to Pd. As shown in Figure 18, Pd binds oxygenated species just a little stronger than Pt.[109,312−317] For instance, Sun and co-workers have shown that fct-FePd/Pd NPs are active and stable ORR catalysts.[318] The synthesis of these well-defined nanocatalysts (~8.5 nm dia.) involved forming highly ordered fct-FePd NPs, using chemical reduction and thermal decomposition techniques, followed by reductive annealing. To further increase the activity of the resulting intermetallic compounds, a Pd-shell was formed on the fct-FePd NPs via thermal etching of surface Fe in acetic acid. A fct FePd@Pd electrocatalyst having a shell thickness of 0.65 nm displayed activity and stability similar to that of Pt/C. As discussed previously, the results are interpreted in terms of the strain effect of the Pd shell: a 0.65 nm-thick Pd shell possesses the ideal lattice compression for maximal ORR activity. In contrast, thicker shells destabilize the catalyst, while thinner shells are too thin to prevent leaching of Fe. The high level of synthetic control reported in this work is particularly well-suited for comparison with theory.

Another design strategy available for preparing Pt-free bimetallic electrocatalysts for the ORR is to combine one oxyphilic and one oxyphobic metal on the NP surface to utilize the ensemble effect to tune the oxygen binding energy.[141,144,315] Recently, the Henkelman group performed computational screening of Au and Ag alloys as ORR electrocatalysts.[6] The RhAu alloy emerged as a material having an oxygen binding strength comparable to pure Pt on the Rh_1Au_2 ensemble site (Figure 19). This finding was validated experimentally by synthesizing RhAu NPs via a microwave-assisted polyol-based synthesis in ethylene glycol and then testing their ORR activity. Rotating ring-disk voltammetry (RRDV)[6] showed that the theoretical prediction was correct: the $Rh_{33}Au_{67}$ electrocatalyst was found to have the highest ORR activity due to the higher concentration of Rh_1Au_2 active sites on the surface. This system is especially interesting because Rh and Au are immiscible in the bulk phase. This example again shows that theory can be used to predict the composition and structure of effective electrocatalysts and that, when coupled with clever synthetic design, promising new nanomaterials can emerge.

DOI: 10.1021/acs.chemrev.9b00246
Chem. Rev. XXXX, XXX, XXX−XXX

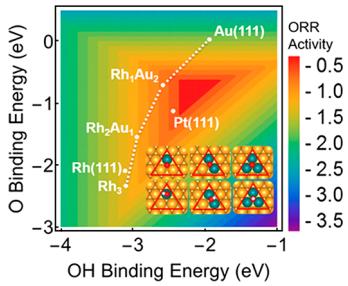

Figure 19. Oxygen and hydroxyl binding energies calculated at Rh-triatomic ensembles on Au(111). The inset shows the optimal binding configurations of oxygen and hydroxyl at different triatomic ensembles. The gold, teal, red, and white spheres represent Au, Rh, O, and H atoms, respectively. Adapted with permission from ref 6. Copyright 2018 American Chemical Society.

3.1.4. Limitations in Catalyst Design: Scaling Relationships. Although significant advances have been achieved in the design of better ORR catalysts under the guidance of the theoretical CHE model, the intrinsic activity of ORR catalysts has not been notably improved despite substantial effort. This difficulty originates from the scaling relations of the binding energies of intermediates.[58,59] For the ORR, the optimal difference between *OOH and *OH should be close to 2 eV (Figure 20).[319] However, the binding energies of *OOH and

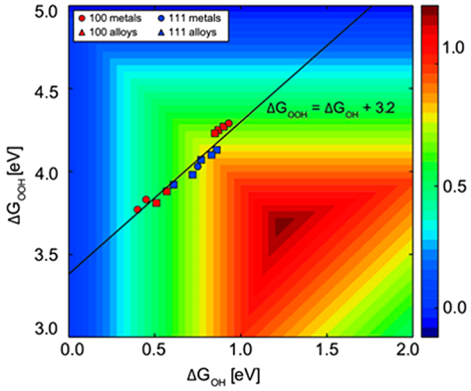

Figure 20. Calculated potentials where an overall electrocatalytic reaction for ORR becomes endergonic (i.e., limiting potentials). Adapted with permission from ref 319. Copyright 2015 Oxford University Press.

*OH cannot be tuned independently; instead, there is a pervasive linear relationship between the two found on most metal surfaces, including alloys.[56] To break the scaling relation, the catalyst surface must bind *OH and *OOH differently, by having, for example, bifunctional sites that bind *OH and *OOH independently. A number of strategies have been proposed for this purpose,[268,319] including the incorporation of molecular catalysts that permit more flexibility in tuning binding energies. While these organometallic complexes are promising for the future, they are beyond the scope of this review and will not be discussed further.[268] Recently, surface-bound sulfide species on Pt were found to destabilize OH adsorption relative to OOH, leading to an enhancement in the ORR activity of Pt.[310] This work presents a promising method to break the linear scaling relation between *OH and *OOH on a surface by introducing ligands at controlled surface coverages. Note, however, that this report focuses on a Pt film substrate and similar studies on NP surfaces would be desirable.

3.1.5. Summary of NP Optimization for ORR Electrocatalysts. This section has discussed the strong interplay between theory and experiment that has aided in the discovery of electrocatalysts for the ORR. DFT calculations have shone a bright light on the fundamental tunability of nanometer-scale materials in terms of strain, ligand, geometric, and ensemble effects. Specifically, modulation of the binding energies of O and OH onto an electrocatalyst can be used to drive synthetic design. However, despite the high ORR activity that has been obtained through thoughtful structural control, the stability of such small NPs under electrocatalytic conditions remains a serious problem. Indeed, the factors that control stability are just beginning to be understood by theorists.

3.2. Carbon Monoxide (CO) Electro-Oxidation

CO oxidation is one of the most important model electrochemical reactions, and not surprisingly, it has been studied for many years.[320,321] One reason for this is that the relative simplicity of this reaction makes it conducive for theoretical studies. From the perspective of technological applications, CO is important because it adsorbs strongly onto both bulk and nanoscale metal surfaces, often poisoning electrocatalytic activity.[321−323] For example, trace amounts of CO in a H_2 fuel stream will render Pt fuel cell catalysts inactive due to formation of a CO adlayer on the Pt surface.[324,325] Accordingly, many studies have been devoted to developing CO tolerant fuel cell anode catalysts,[126,326−328] and two main design strategies have emerged. The first involves discovery of catalysts that have low affinities for CO binding. The second strategy is to design catalysts that oxidize CO at a low overpotential, thereby converting CO to CO_2 and eliminating the adsorbed CO adlayer. In this section, we review some of the key features of CO oxidation catalysts with particular emphasis on those evaluated using theoretical models.

3.2.1. Pt as a Model Catalyst for CO Oxidation. The reaction mechanism of CO electro-oxidation on Pt is generally believed to follow the Langmuir−Hinshelwood (LH) mechanism (eqs 11 and 12).[267,329]

$$* + H_2O \rightarrow *OH + H^+ + e^- \quad (11)$$

$$*OH + *CO \rightarrow 2* + CO_2 + H^+ + e^- \quad (12)$$

Regarding the detailed kinetics of the CO oxidation reaction on Pt NPs, there are two principal issues that are still highly contested areas of active research.[330,331] The first issue is related to the identity of the appropriate kinetic model for CO oxidation. Some authors report that the reaction kinetics can be treated within the mean-field approximation.[332−336] This method assumes that CO and OH diffuse rapidly on the catalyst surface, so that the reaction rate can be expressed simply in terms of the coverages of *CO and *OH. In contrast, if *CO is assumed to be immobile on the Pt surface, then the reaction probably follows a nucleation and growth mechanism, with *CO and *OH reacting only at the interface of the adsorbed species.[337,338]

The second area of debate regarding the kinetics of CO oxidation is related to an observed preoxidation peak in CO stripping voltammograms (Figure 21).[339] There are conflicting explanations for this prepeak on Pt catalysts.[340−344]

Significantly, a recent study combining kinetic Monte Carlo simulations and differential electrochemical mass spectrometry

DOI: 10.1021/acs.chemrev.9b00246
Chem. Rev. XXXX, XXX, XXX−XXX

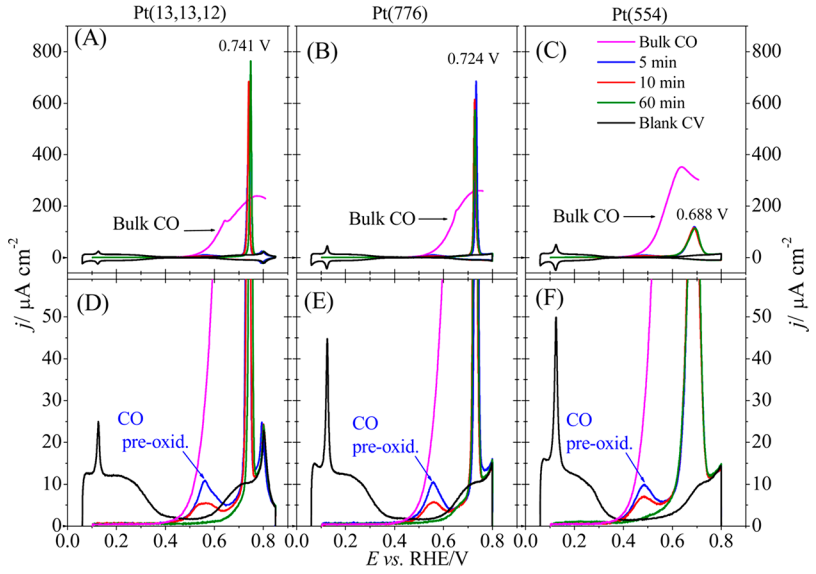

Figure 21. Effect of dissolved CO on its preoxidation on Pt stepped surfaces in 0.1 M $HClO_4$: (A) Pt(13,13,12); (B) Pt(776); (C) Pt(554). Parts D, E, and F are scaled up images of parts A, B, and C, respectively, to show the time dependence of CO oxidation peaks on Pt step-sites. Reproduced with permission from ref 339. Copyright 2015 American Chemical Society.

(DEMS) suggested a detailed kinetic model consistent with both experimental and simulated chronoamperometric transients (Figure 22).[334] The proposed model features three different stages as a function of increasing applied potential. First, oxygenated species form at defects, such as step-sites, and readily react with weakly bound *CO to produce CO_2. Next, *CO on terrace sites can diffuse to the defect sites and react with the oxygenated species present. Finally, following the oxidation of a few percent of the total *CO coverage at defect sites via surface diffusion, oxygenated species can form on terraces, creating more active sites and enabling complete CO oxidation on the surface.

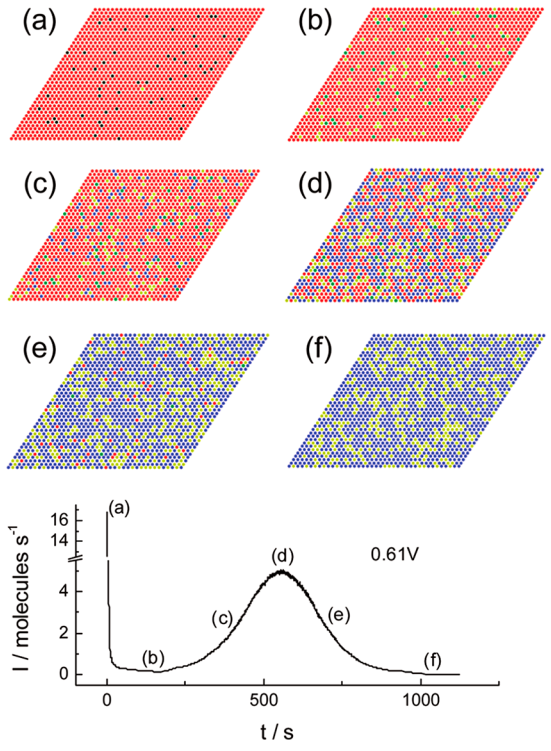

Figure 22. Snapshots of the oxidation of a weakly bound CO adlayer ($CO_{ad,w}$) on defect sites of Pt(111) at 0.61 V (initial 0.03% surface coverage of CO after adsorption at 0.1 V). $CO_{ad,s}$ on terraces (red dots), $CO_{ad,w}$ next to defects (black), oxygen-containing ad-species (blue dots), free Pt(111) sites (yellow dots), and $CO_{ad,s}$ next to defects (green dots). The CO hopping rate: 0.1 s^{-1}. Reproduced with permission from ref 334. Copyright 2012 American Chemical Society.

While the above study focused only on polycrystalline surfaces, a recent study by McPherson et al. provided a different perspective of the CO oxidation mechanism on NPs.[345] In situ infrared (IR) spectroelectrochemistry experiments indicated the facile oxidation of *CO on terraces of the larger agglomerated Pt particles, relative to *CO on step-sites. This observation is consistent with previous model studies by Feliu and co-workers.[339] However, information from the smaller ∼2 nm Pt NPs was only observed as a minor contribution in both the IR spectra and CO stripping voltammograms. The challenges of studying the kinetics on NPs of this scale are an important area of ongoing research in the field of PEMFCs.[346]

3.2.2. Au as an Efficient Electrocatalyst for CO Oxidation. CO electro-oxidation on Au exhibits several special characteristics. First, adsorbed CO on a Au surface cooperatively enhances adsorption of an oxidant (i.e., *OH), leading to the oxidation of CO. This cycle is referred to as self-promoted CO oxidation.[347−349] Second, the effect of solution pH is very important to the activity of Au electrocatalysts.[348,350] In a recent theoretical study,[408] CO binding strength was predicted to increase with increasing pH. In alkaline solution, the onset potential for CO electro-oxidation was found to be 0.5 V (vs RHE) more negative than that in acidic media, confirming that stronger CO adsorption leads to better CO electro-oxidation activity on Au(111). This pH-dependent activity of Au electrocatalysts has been interpreted in terms of the stronger chemisorption of CO under alkaline conditions, which then promotes the formation of *OH at low potentials. In contrast, in acidic solutions, *CO does not remain chemisorbed on the Au surface when CO is not present

DOI: 10.1021/acs.chemrev.9b00246
Chem. Rev. XXXX, XXX, XXX−XXX

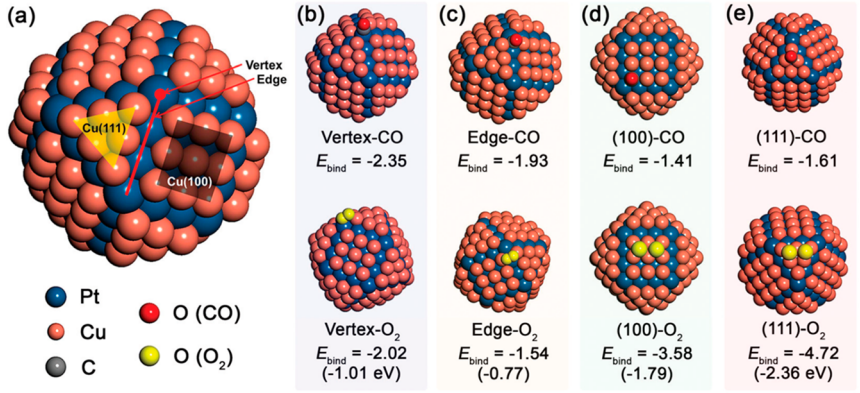

Figure 23. Adsorption chemistry of Pt@Cu_{Face} NPs toward CO and O_2. (a) Four binding site categories: Cu(100), Cu(111), edge, and vertex. (b–e) The strongest CO and O_2 binding geometry on each site. Reproduced with permission from ref 354. Copyright 2017 The Royal Society of Chemistry.

in solution. Accordingly, *OH adsorption occurs at much higher potentials in acidic solution.

The CO electro-oxidation activity of Au in alkaline solution can be further enhanced by decreasing the size of Au NPs. It was demonstrated that Au NPs of 4.2 nm in size have the highest catalytic activity.[351] However, the origin of this size effect continues to be debated and requires further theoretical investigations.[352] In addition to NP size effects, the activity of Au NPs in acidic media was reportedly enhanced via electronic interactions between the Au nanocatalysts and a TiO_x support.[244] Specifically, the TiO_x substrate induced a negative charge on the Au NP surfaces, generating an anionic Au species. This reactive surface site favored the coadsorption of CO and OH and promoted CO oxidation, as previously explained by the self-promotion mechanism.[361] More recently, 3–5 nm PdAu nanoalloys with different compositions were synthesized and analyzed for CO oxidation.[353] Characterization of these NPs demonstrated a Pd-rich surface and a Au-rich core. Nanoalloys with low % Au contents of 20–30% demonstrated increased CO oxidation activity relative to pure Pd NPs. The observed activity trends were attributed to both ensemble and electronic effects.

While Au NPs for CO electro-oxidation are an ongoing area of research, it is important to note that the metric used for calculating CO binding energies (i.e., constant electric field present in the double layer) is not a good descriptor for experimental systems, which are instead maintained at constant electrode potential. Experimentally, CO adsorbates could significantly modify the surface charge of Au catalysts, complicating binding energy calculations. Therefore, an improved understanding of the chemical environment of catalytic surfaces under experimentally relevant electrocatalytic conditions may prove invaluable for increasing the accuracy of theoretical calculations for CO oxidation.

3.2.3. Bifunctional Mechanism for CO Oxidation. It is now well established that the electrochemical oxidation of CO on bimetallic Pt-based catalysts occurs via a bifunctional mechanism.[251,354−356] In this mechanism, *OH can form at a reduced overpotential on the more oxophilic metal and then react with adjacent *CO species. For Pt-based alloys, the second metal can induce an electronic effect on neighboring Pt atoms, weakening the Pt−CO bond. A weaker bond between CO and Pt tends to reduce overall *CO coverage.[357−360] The surface-coverage of *CO plays an important role in modulating the reactivity of a CO oxidation catalyst. However, for a bifunctional catalyst, the surface coverage of the reactive *OH species also affects CO oxidation, making it more difficult to control the system experimentally or to model it theoretically.

Despite these experimental and theoretical limitations, bimetallic NPs have successfully been utilized for CO oxidation.[361] For example, the bifunctional mechanism has been predicted by theory to be responsible for electro-oxidation of CO over Pt@Cu NP electrocatalysts (Figure 23).[354] DFT calculations suggested that the presence of an incomplete Cu shell allowed the exposed Pt to bind CO, which could interact with *OH on nearby Cu atoms to yield CO_2. Notably, this proposed theoretical hypothesis for the enhanced activity observed over Pt@$Cu_{partial}$ was carefully explored experimentally using ∼2 nm Pt DENs modified via Cu UPD.[267] The Pt@$Cu_{partial}$ catalyst was initially shown to be substantially more active in alkaline solution than pure Pt DENs. After 5 min of CO electro-oxidation, however, the resulting CV of Pt@$Cu_{partial}$ was similar to pure Pt DENs, indicating dissolution of the partial Cu shell. Surprisingly, the onset potential of CO electro-oxidation was still ∼300 mV more negative than that of pure Pt DENs. The active sites on this Cu-dissolved Pt@$Cu_{partial}$ catalyst were proposed to be isolated Cu atoms left on the surface. DFT calculations confirmed that these isolated Cu sites can specifically adsorb OH, thereby facilitating reaction with CO adsorbed to the Pt surface.

A recent study explored the electrocatalytic activity of ∼3.5 nm PtFe bimetallic NPs toward CO oxidation by controlling the atomic arrangement of the two metals (Figure 24).[362] In this report, PtFe random alloys, as well as Pt_3Fe@Pt and Pt@Fe_xO_y core@shell structures, exhibited enhanced CO tolerance compared to Pt. Specifically, low *CO surface coverages on PtFe alloys increased the number of Pt sites free for H_2 oxidation, indicating a high tolerance against CO poisoning. In contrast, the Pt surface sites of the core@shell NPs promoted the facile oxidation of adsorbed CO. Surprisingly, the Pt_3Fe intermetallic catalyst was not as active toward CO oxidation as alloy or core@shell NPs. The decrease in activity observed for the intermetallic catalyst was attributed to a heterogeneous composition with an Fe-rich surface, likely resulting from the conditions used for annealing (i.e., 650 °C, Ar−H_2). In a similar study, PtSn@Pt alloy-core@shell NPs were shown to have superior CO tolerance compared to the PtSn alloy and intermetallic architectures.[363] While DFT calculations were not performed in these studies, they serve as a good example of

DOI: 10.1021/acs.chemrev.9b00246
Chem. Rev. XXXX, XXX, XXX−XXX

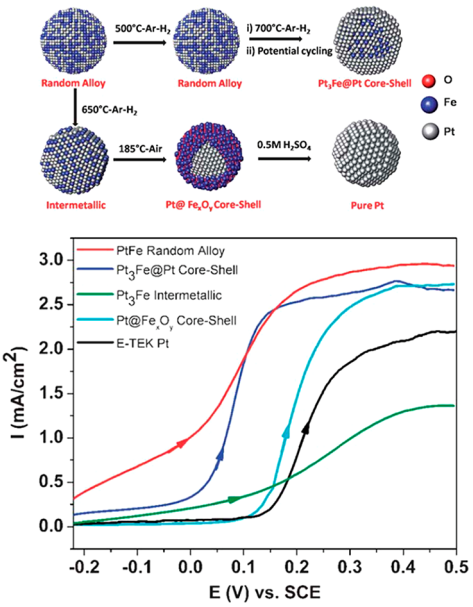

Figure 24. (top) Synthetic scheme for generating different PtFe bimetallic nanostructures. (bottom) Rotating disk polarization curves for electrooxidation of CO/H_2 mixtures (1000 ppm of CO, balance H_2) on different PtFe catalysts with comparison to E-TEK Pt catalysts (all catalysts contain 30% total metal loading). Curves were recorded at 25 °C with 1 mV s^{-1} scan rates and 1600 rpm rotation rates. Electrolyte: 0.5 M H_2SO_4 solution. Reproduced with permission from ref 362. Copyright 2011 The Royal Society of Chemistry.

how sophisticated synthetic procedures can drive ongoing theoretical studies on the structure-dependent activities of NP systems.[364]

The use of alloy cores to tune the CO oxidation activity of Pt shells has also been investigated. For example, DFT calculations and microkinetic analysis predicted enhanced CO oxidation activity over $Pd_{1-x}Au_x$@Pt alloy-core@Pt NPs.[365] In contrast to the bifunctional effect previously discussed, the AuPd core tunes the relative stability of adsorbed CO and O on the Pt shell via the ligand effect. The stabilization of reactive adsorbates was predicted to increase the CO oxidation activity relative to pure Pt NPs. This activity enhancement was subsequently confirmed experimentally using Pd_xAu_{140-x}@Pt DENs.[176] Notably, DFT calculations suggest that the koppa-shaped trend for activity versus alloy core composition is driven primarily by structural changes. Specifically, a pure Au core leads to deformation of the Pt shell and a compression of the Pt lattice, decreasing activity. In contrast, Pd tends to segregate on the NP surface, forming an inverted configuration. A small addition of Au, however, stabilizes the alloy PdAu core, preventing Au and Pd from diffusing to the NP surface.

In a recent report by Chen et al., the concept of the bifunctional effect in CO electro-oxidation has been extended.[366] In addition to the introduction of more oxyphilic surface sites via alloying, two additional strategies to increase the number of *CO and *OH reactant pairs on the surface should be mentioned here. First, strongly adsorbed molecular species in the inner Helmholtz plane can serve as promoters for OH adsorption. As mentioned previously, strongly adsorbed CO on Au surfaces can enhance OH adsorption in alkaline solutions, leading to a self-promoting reaction mechanism.

Second, solvated species located in the outer Helmholtz plane, such as OH or metal cations, can also promote CO electro-oxidation through a bifunctional mechanism. Generally, Pt has higher activity for CO electro-oxidation in alkaline media rather than in acidic media due to the abundant presence of OH in the electrolyte, facilitating OH adsorption.[367] However, the adsorption energy of OH has also been found to be pH-dependent, as suggested by recent theoretical studies.[368,369] Additionally, Li^+ and Be^{2+} cations have been reported to enhance the bifunctional effect on a surface through noncovalent interactions with adsorbed *OH.[370] Casting light on these electrochemical factors in the general framework of bifunctional electrocatalysis will stimulate new design strategies for electrocatalysts.

3.2.4. Summary of CO Electro-Oxidation. This section presented a brief overview of the computational tools and experimental methods that have been used to gain better insight into the reactivity of CO electro-oxidation on both macro and NP electrocatalysts. A notable characteristic of CO oxidation catalysts is that the presence of *OH can facilitate CO oxidation at reduced potentials. This is known as preoxidation. Using both theory and experiment, a strong relationship between *CO and *OH surface coverages and catalyst activity has been uncovered. By controlling the presence of these two competing adsorbates on the surface, increasingly efficient CO oxidation catalysts can be realized. To this end, the effort to better understand the bifunctional mechanism of CO oxidation over bimetallic catalysts is an ongoing area of research.

The fundamental design concept for bifunctional catalysts involves use of an oxophilic metal to preferably bind *OH and an oxophobic metal to bind CO. However, if a catalyst binds adsorbates too strongly, surface diffusion of the reactive species can be inhibited, limiting catalytic activity. Therefore, compositional control can lead to improvements in CO oxidation catalysts by intentional mixing of *CO and *OH. In situ characterization techniques, such as DEMS, have allowed a deeper understanding of the subtle reactivities of the surface during electrocatalysis. The interplay of improved experimental and theoretical methods will lead to a better understanding of CO electro-oxidation and, hence, more CO-tolerant electrocatalysts.

3.3. The Electrochemical CO_2 Reduction Reaction (CO_2RR)

3.3.1. Brief Introduction to the Reaction Mechanism of the CO_2RR. Electrochemical reduction of CO_2 is an important reaction in alternative energy schemes. Accordingly, a large amount of literature is published on this reaction every year.[287,371−374] The reaction pathway for the reduction of CO_2 to CO (E^0_{CO} = −0.11 V vs RHE) is given in eqs 13−15.[375]

$$CO_{2(g)} + H^+ + e^- + * \rightarrow *COOH \quad (13)$$

$$*COOH + H^+ + e^- \rightarrow *CO + H_2O_{(l)} \quad (14)$$

$$*CO \rightarrow CO_{(g)} + * \quad (15)$$

The rate of formation of CO is driven by both the adsorption of CO_2 to form *COOH on the catalytic surface and the desorption of the CO product. Electrochemically driven formation of *COOH is the rate-limiting step on many electrocatalysts, leading to the large overpotentials observed experimentally. The final step, eq 15, involves desorption of CO from the active site, which is not influenced by the

DOI: 10.1021/acs.chemrev.9b00246
Chem. Rev. XXXX, XXX, XXX−XXX

electrochemical potential. Rather, desorption of CO from a catalytic surface depends on the nature of the metal and the binding energy of CO at the active site. Another major limitation of the CO_2 reduction activity of an electrocatalyst is the competing hydrogen evolution reaction (HER, eqs 16 and 17).[375]

$$H^+ + e^- + * \rightarrow H^* \quad (16)$$

$$H^* + H^+ + e^- \rightarrow H_2 + * \quad (17)$$

An alternative pathway is given in eq 18.

$$H^* + H^* \rightarrow H_2 + 2^* \quad (18)$$

The binding of H^+ onto most metal surfaces (eq 16) is facile compared to CO_2, and competition for active sites between these two species significantly impedes CO_2 reduction (E^0_{HER} = 0 V vs RHE). However, *H is necessary on catalytic surfaces to drive the formation of desirable hydrocarbon products. Therefore, modulation of the binding energies of *COOH, *CO, and *H provides a useful tool for tuning CO_2RR activity. Unfortunately, consistent with the types of scaling relationships previously discussed, the binding energies of *COOH and *CO scale together and cannot readily be tuned individually. That is, while increasing the binding strength of *COOH on a surface can increase the CO_2 reduction activity, the *CO binding strength will also increase, thereby potentially poisoning the surface and offsetting any improvement in activity. For example, while there are recent reports of Pt-based nanocatalysts for the CO_2RR,[376] the strong binding of CO on Pt can poison the catalytic surface. Creating Pt nanostructures having weaker CO binding affinity may reduce poisoning, but it will also weaken COOH binding which may decrease activity.

Decreasing the binding energy of *H on active sites for CO production is another strategy for increasing the CO_2RR activity. While *H is, overall, less sensitive to shifts in binding energy, H^+ adsorption still scales with *COOH binding (Figure 25).[375] These scaling relationships between adsorbates on an electrocatalytic surface are a challenging aspect of increasing CO_2 reduction activity. While there are recent reports of catalytic systems capable of breaking the COOH–CO scaling relationship, most of these consider 2D,[377] molecular,[378,379] or porous catalysts[380] which are outside the scope of this review and will not be considered further. The use of surface ligands to preferentially stabilize *COOH and *CO reaction intermediates over *H has also been reported and will be discussed in detail in section 3.3.3.

In contrast to the strong binding of CO on Pt surfaces, bulk Au and Ag electrocatalysts are known to bind CO too weakly, releasing it almost instantly from the surface once formed. The weak binding of CO limits formation of further reduction products so that Au and Ag electrocatalytic surfaces are known to produce almost exclusively CO and H_2 (via the competing HER).[375,381] In contrast, Cu exhibits optimal CO binding energy (i.e., not too strong nor too weak) that can facilitate further reduction to hydrocarbons such as methane (E_0 = 0.17 V vs RHE, eq 19) and ethylene (E^0 = 0.06 V vs RHE, eq 20).[382−384]

$$CO_2 + 8H^+ + 8e^- \rightarrow CH_4 + 2H_2O_{(l)} \quad (19)$$

$$2CO_2 + 12H^+ + 12e^- \rightarrow C_2H_4 + 4H_2O_{(l)} \quad (20)$$

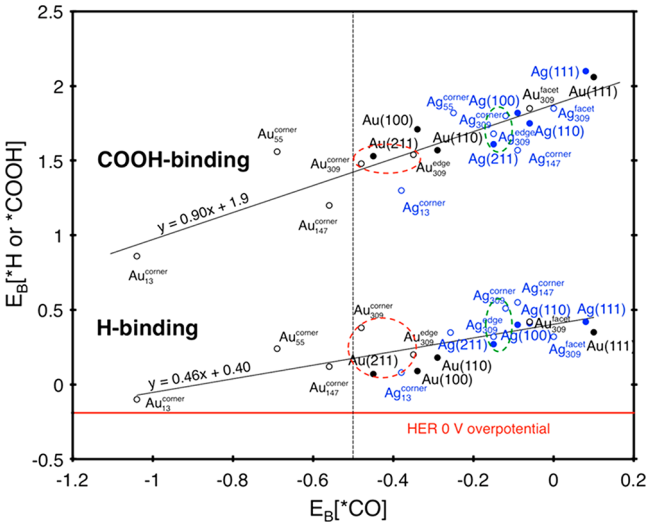

Figure 25. Scaling relation between E_B[*COOH] (upper part) and E_B[*H] (lower part) versus E_B[*CO]. Open circles represent binding energies at nanoparticles, whereas full circles represent binding energies at the bulk surfaces for Ag (blue) and Au (black). The vertical dashed line indicates a threshold E_B[*CO] between adsorbed *CO on the catalysts and released CO(g). The horizontal red line indicates E_B[*H] at which the overpotential of HER is 0 V. Reproduced with permission from ref 375. Copyright 2015 American Chemical Society.

Mechanistically, *CO is acknowledged to be an important intermediate for the formation of hydrocarbon products from CO_2RR (Figure 26).[385] Specifically, in the case of ethylene, one reaction pathway considered is the dimerization of two *CO adducts.[386] Despite being highly active for CO_2RR, Cu suffers from poor product selectivity control and yields many different products (albeit with low efficiencies).

Soluble reduction products further complicate both experimental characterization and theoretical modeling of some CO_2RR catalysts. For example, in addition to hydrocarbons, Cu is also active for the production of soluble species, such as methanol.[193,383,387] Notably, Pd is known to reduce CO_2 to formic acid with zero overpotential.[388−390] Therefore, an important challenge for theory is predicting the overall selectivity of a catalyst when competing reaction mechanisms are possible, as is the case for the CO_2RR. For example, corner sites of Au NPs are predicted by theory to have high activity for CO production,[375] but experimentally, it has been found that the competing HER greatly decreases CO selectivity.[130] This example underscores the importance and utility of using both theory and experiment to solve problems in electrocatalysis. Specifically, in this particular case, theorists are able to predict how the size, shape, and composition of NPs affect the binding energy of intermediates, and then, these predictions can be tested experimentally (if NPs matching the theoretical constructs can be synthesized). We will expand on these points in the next several sections.

3.3.2. The Effect of Electrocatalyst Size and Surface Structure on the CO_2RR. Different sizes and surface structures change the binding energies of COOH and CO to electrocatalyst surfaces, and this in turn can alter reactivity. For example, Au,[20,130,381,391] Ag,[256,375] Cu,[129,193,392] and Pd[393] NP electrocatalysts all exhibit size-dependent CO_2 reduction activity. This experimentally observed size dependence for the CO_2RR has been attributed to the binding energies of

DOI: 10.1021/acs.chemrev.9b00246
Chem. Rev. XXXX, XXX, XXX−XXX

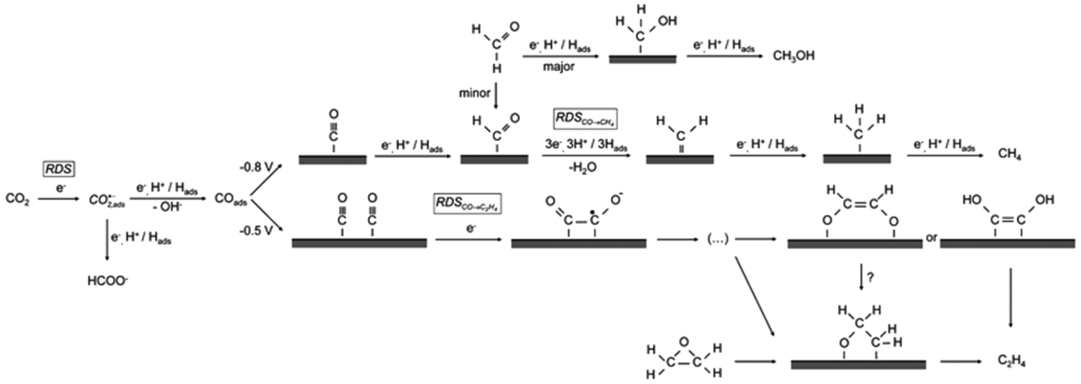

Figure 26. Proposed mechanism for the electrochemical reduction of carbon dioxide on copper. Reproduced with permission from ref 385. Copyright 2011 The Royal Society of Chemistry.

COOH, CO, and H on undercoordinated surface atoms, such as edge, corner, and face sites (Figure 27).[256] In contrast and

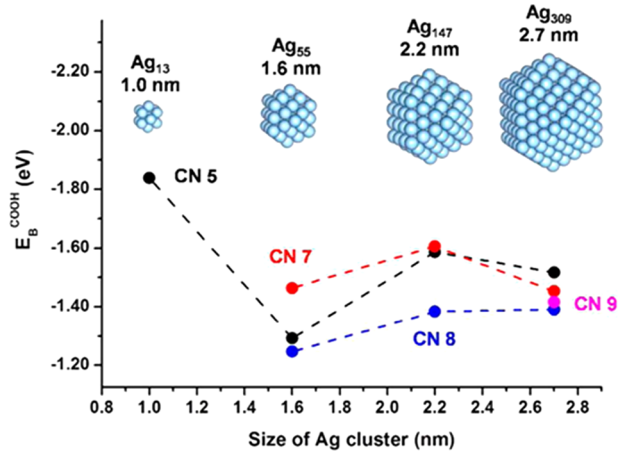

Figure 27. DFT results on the binding energies of the COOH intermediate (ΔE_B^{COOH}) as a function of Ag nanoparticle size. Ag_{13} (1.0 nm), Ag_{55} (1.6 nm), Ag_{147} (2.2 nm), and Ag_{309} (2.7 nm) models with cuboctahedral geometry were examined. Adapted with permission from ref 256. Copyright 2015 American Chemical Society.

as mentioned earlier, adsorption of H^+ is facile on most metal surfaces, and therefore, the binding energy of H is relatively independent of coordination number and hence not easily tunable.[393]

While it is generally agreed that H binds favorably on all active sites, there has been debate in the literature as to which sites are most active for the CO_2RR.[375] In 2013, Sun and co-workers studied the size- dependence of 4−8 nm Au NPs for CO_2 reduction and reported maximum CO production for ∼8 nm Au NPs.[394] They performed DFT studies and concluded that the increased activity of the 8 nm NPs was due to the higher number of edge sites present on the surface. It must be noted, however, that the larger size of the NPs (i.e., >3 nm) made it impossible to model the entire NP using DFT. Due to this limitation, Au(111) and Au(211) slab models were used to represent the NP face and edge sites, respectively, while a Au_{13} cluster was used to model corner sites.

There have been claims that models of the type described in the previous paragraph are not appropriate for NPs and that the entire NP should be used in calculations. For example, theoretical work by Back et al. disputed the claim that edge sites of Au NPs are more active for CO production than corner sites.[375] Specifically, by incorporating all of the atoms of an icosahedral Au_{309} NP in first-principles DFT calculations, they concluded that the corner sites of ∼2 nm Au NPs are actually the most active for CO production. Additionally, while active on all sites, the HER was determined to be most favorable over edge sites. The low CO selectivity observed over ∼2 nm Au NPs has been explained by the favorable HER over all of the active sites, outcompeting HER. These examples demonstrate the advantage of including all of the atoms in theoretical models of nanoscale electrocatalysts.

In contrast to the higher CO_2RR activity of corner sites predicted for Au NPs, the edge sites of Ag NPs were predicted to possess the optimal binding energy for COOH. That is, DFT predicted that the stable geometry of 5 nm Ag NPs had an optimal number of edge sites for COOH binding.[375] These results were used to rationalize previously observed experimental observations, which demonstrated the highest CO production efficiency for 5 nm Ag NPs.[256] Specifically, these Ag NPs were active for CO production with a reduced overpotential of ∼300 mV vs polycrystalline Ag.

The synthesis of well-defined, monodisperse Ag NPs is hindered by the low solubility of certain Ag species in solution during synthesis, as well as by facile oxidation of Ag NPs once synthesized. These factors can lead to instability and subsequent particle growth, and therefore, nanostructured, macroscopic Ag surfaces are more commonly studied.[395−398] Specifically, electrochemical oxidative−reductive etching of Ag foils in $KHCO_3$ has recently been reported to produce Ag nanostructures (i.e., Ag nanocorals) that are highly active for CO_2 reduction, while simultaneously suppressing the HER.[399−402] Unfortunately, the morphologies of these nanostructured catalysts are large and difficult to prepare with uniform features, and therefore, they are not conducive to first-principles calculations.

In another study, Pd-based NPs ranging in size from 2.4 to 10.3 nm were examined for CO production.[393] These NPs were synthesized using reduction of a $PdCl_2$ precursor with $NaBH_4$ in the presence of citrate ligands. Maximum CO production was observed for the 3.7 nm NPs, reaching a Faradaic efficiency of 91%. The decrease in activity observed for Pd NPs <3.7 nm was thought to arise from CO binding too strongly on the Pd surface, resulting in poisoning and deactivation of the electrocatalytic surface. DFT calculations suggested that the stabilization of the *COOH reaction intermediate is most favorable on the corner and edge sites of Pd NPs, leading to higher CO activity on those sites. A

DOI: 10.1021/acs.chemrev.9b00246
Chem. Rev. XXXX, XXX, XXX−XXX

volcano-shaped plot of turnover frequency (TOF) vs Pd NP size reveals a clear modulation of CO production with changing numbers of edge and corner active sites (Figure 28).

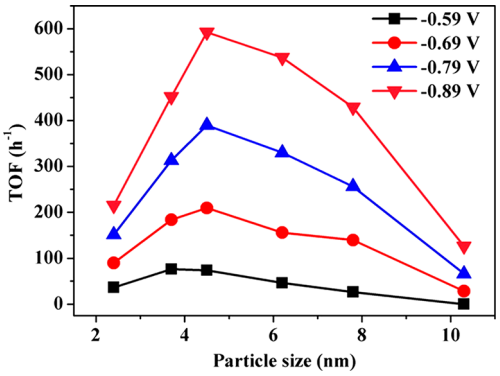

Figure 28. Size dependence of TOF for CO production on Pd NPs at various potentials. Reproduced with permission from ref 393. Copyright 2015 American Chemical Society.

Finally, Strasser and co-workers conducted an experimental and theoretical analysis of the effect of Cu NP size (2−15 nm) on CO_2RR activity.[129] These Cu NPs were synthesized using inverse micelle encapsulation and subsequent treatment with O_2 plasma etching to remove polymers from the NP surface. They found that, for Cu NPs having sizes of <5 nm, CO and H_2 production was increased compared to that of the more reduced hydrocarbons observed on bulk Cu electrodes. They used theoretical models to attribute this to the high binding energy of CO on undercoordinated surface sites. While these sites are active for both CO and H_2 production, the strong binding is hypothesized to decrease the surface mobility of *H and *CO intermediates, preventing the formation of more reduced hydrocarbons.

CO_2RR activity has been observed using carbon-based electrodes, such as graphene oxide and carbon nanotubes.[384,403−405] However, it has recently been reported that the observed activities in these systems actually result from trace metal impurities, which are common in these types of materials.[406,407] For example, Ager and co-workers demonstrated that Cu impurities in commercial graphene oxide can catalyze CO_2 reduction to methane.[408] These results are particularly significant, because carbon supports are frequently used in CO_2RR studies and they may host unidentified but electrocatalytically active impurities. Clearly, this kind of situation is particularly problematic for correlating experimental results to theory. In other words, even trace impurities can lead to erroneous conclusions in electrocatalysis.

3.3.3. The Effect of Ligands on the Selectivity of the CO_2RR. In addition to size effects, the presence of stabilizing surface ligands can affect the CO_2RR. For example, the use of thiol ligands for stabilizing CO_2RR electrocatalysts is typically avoided due to the strong binding affinity of thiols on metals, which can poison catalytic surfaces. One well-studied exception is monolayer-protected Au clusters (Au MPCs).[391,409−411] Specifically, $Au_{25}(SR)_{18}$ clusters have been reported to exhibit high catalytic activity for the CO_2RR.[392,412,413] The high stability and activity of this catalyst has been attributed to the unique structure of surface staples of individual Au atoms bound to thiol ligands (Figure 29a).[20,412]

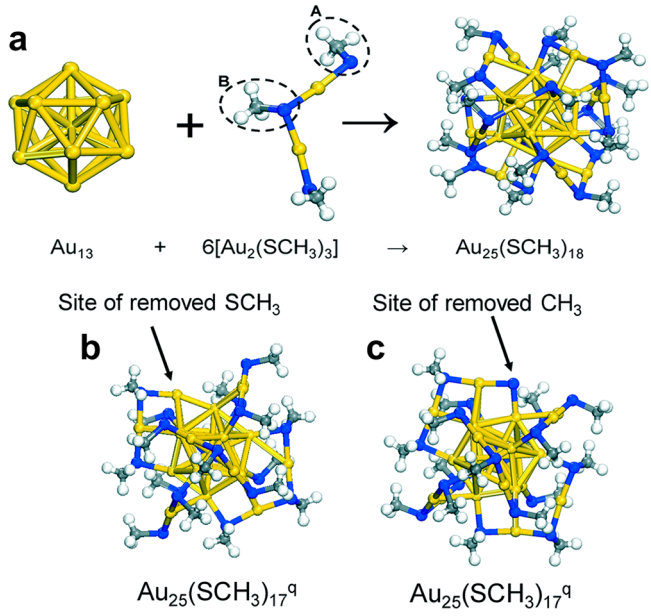

Figure 29. (a) Schematic of the fully ligand-protected $Au_{25}(SCH_3)_{18}$ nanocluster. The system is composed of a Au_{13} icosahedral core protected by a shell network of six $Au_2(SR)_3$ units. The Au, S, C, and H atoms are colored yellow, blue, gray, and white, respectively. The labels "A" and "B" on the $Au_2(SCH_3)_3$ shell network represent the two distinct types of coordinated sulfur in the NC shell. (b) Active structure after loss of a thiol ligand. (c) Active predicted structure after loss of an alkyl ligand from the thiol. Adapted with permission from ref 20. Copyright 2018 The Royal Society of Chemistry.

DFT calculations have been used to study the CO_2RR on model $Au_{25}(SCH_3)_{18}^q$ catalysts having different charge states (i.e., q = −1, 0, +1).[20] Significantly, these calculations determined that, regardless of the initial charge state, CO production was only thermodynamically favorable upon electrochemically driven loss of a ligand (i.e., −SR or −R). Removal of a thiol ligand (−SR) created an exposed Au surface atom as an electroactive site for CO formation (Figure 29b). However, this site was also found to be active for the parasitic HER. In contrast, selective removal of only the alkyl group (−R) from the ligand created a unique −Au−S−Au− surface site (Figure 29c), where the S atom, rather than Au, served as the active site for the CO_2RR (and competing HER). The electronic properties of the S active site (after loss of an −R ligand), compared to that of an Au active site (after loss of a −SR ligand), increased both the activity and the CO selectivity of the catalyst. This was explained by noting that DFT results predicted increased stabilization of *COOH and reduced *H binding on the S active site. While these theoretical findings are consistent with experimental results[412,413] for $Au_{25}(SCH_3)_{18}$ catalysts, the identity of the proposed active site has not been independently confirmed experimentally. This study is another good illustration of the difficulties involved in definitively identifying theoretically predicted active sites on catalysts in the <2 nm size range.

Another thiol ligand used for modulating CO_2RR activity is cysteamine ($HS−CH_2−CH_2−NH_2$).[256,258,410,414] For example, it has been used on carbon black supports as an anchoring ligand for Ag NPs during the CO_2RR.[256] DFT studies suggested that the Ag−S bond promotes stabilization of the *COOH intermediate via localization of unpaired electrons. In situ attenuated total reflectance infrared (ATR-IR) spectros-

DOI: 10.1021/acs.chemrev.9b00246
Chem. Rev. XXXX, XXX, XXX−XXX

copy, combined with quantum-mechanical-based molecular dynamics simulations, demonstrated that the terminal $-NH_2$ group of cysteamine increases electrocatalytic activity by hydrogen bonding with CO_2.[258,414] Specifically, the sulfur atom binds to the metal surface, while the free amine coordinates with incoming CO_2 molecules (Figure 30A,B), thereby increasing the local concentration of CO_2 at the surface while preferentially stabilizing the formation of *COOH intermediates over *H.

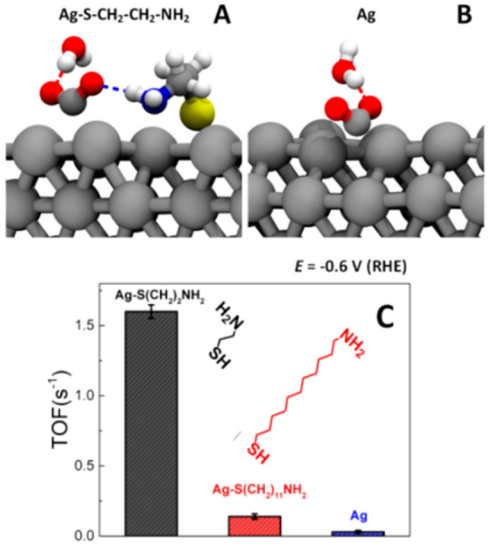

Figure 30. (A) Chemisorbed CO_2 on the cysteamine-functionalized Ag(111) surface. This illustrates H-bond between $-NH_2$ and CO_2. (B) Chemisorbed CO_2 on the Ag(111) surface in the absence of a stabilizing H-bond. (C) Comparison of turnover frequencies (TOFs) for CO at −0.6 V (RHE) on functionalized Ag NPs. Adapted with permission from ref 258. Copyright 2018 American Chemical Society.

While cysteamine has been shown to increase the electrocatalytic activity of Au and Ag NPs for CO formation, a dependence on carbon-chain length has been observed for related thiol ligands. For example, while 11-amino-1-undecanethiol has both a thiol group and a terminal amine, similar to cysteamine, CO_2RR activity was greatly decreased relative to cysteamine (Figure 30C).[258] This was attributed to the amine group being too far from the catalyst surface to participate in the electrocatalytic reaction. Replacement of the primary amine of cysteamine with a pyridinyl group was reported to induce a change in catalytic selectivity from CO to formate due to a change in mechanism.[410]

In a more recent study by Kim et al., the effects of amine-, thiol-, and carboxyl-functionalized ligands on the CO selectivity of Ag NPs were analyzed using gas chromatography.[415] The results showed that the oleylamine ligand induced the highest CO production efficiency by destabilizing H binding and the overall suppression of the HER. In contrast, the thiol ligand resulted in increased overall activity but decreased selectivity for CO. DFT calculations supported the claim that amine-capped Ag NPs break the scaling relationship by stabilizing *COOH and destabilizing *H.

More recently, N-heterocycles (NHC) have attracted attention as modifying ligands for CO_2RR electrocatalysts.[416−420] For example, ∼7 nm NHC carbene-functionalized Au NPs exhibited a 30% increase in Faradaic efficiency toward CO_2RR relative to oleylamine-capped Au NPs.[421] Tafel analysis of the CO_2RR kinetics of the NHC carbene-functionalized Au NPs indicated a change in reaction mechanism. However, computational studies of these types of complex ligand interactions are difficult to model, making it hard to elucidate the source of increased activity.

3.3.4. Bimetallic Nanocatalysts for the CO_2RR. Bimetallic electrocatalysts afford another opportunity to modify the binding energies, and hence activity and selectivity, of reactive adsorbates on the surface of CO_2RR electrocatalysts. Au-based electrocatalysts, such as AuPd[422−424] and AuCu,[255,425−428] have been extensively reported. For example, the product selectivity over Au@Pd NPs can be tuned by modulating the Pd shell thickness over the range 1−10 nm,

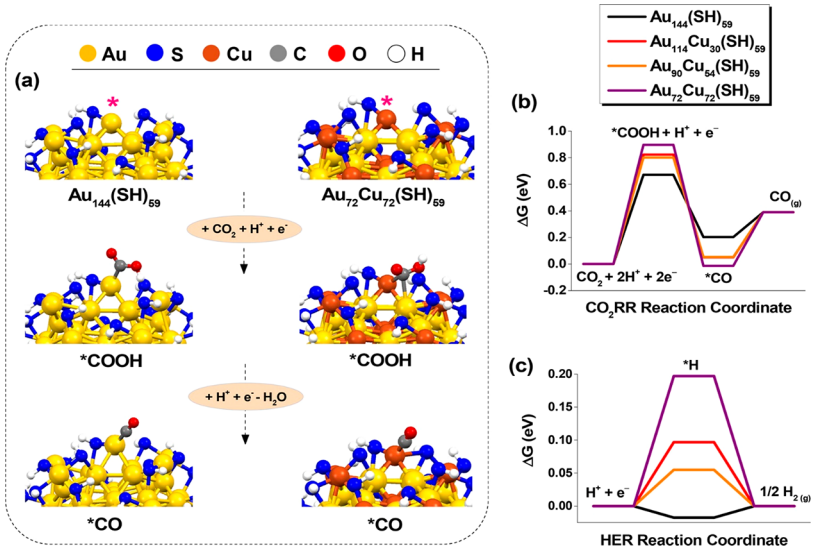

Figure 31. (a) Atomic-level reaction pathways and (b) free-energy diagram for CO_2RR at singly dethiolated $Au_{144}(SH)_{59}$, $Au_{114}Cu_{30}(SH)_{59}$, $Au_{90}Cu_{54}(SH)_{59}$, and $Au_{72}Cu_{72}(SH)_{59}$ nanoclusters. One −SH unit was removed from each structure to create an accessible active site (marked with a pink asterisk). (c) H_2 evolution reaction (HER) free-energy diagram at singly dethiolated nanocluster models. Reproduced with permission from ref 432. Copyright 2018 American Chemical Society.

DOI: 10.1021/acs.chemrev.9b00246
Chem. Rev. XXXX, XXX, XXX−XXX

with the C_5 product being observed on 10 nm-thick shells.[429−431] In contrast to the hydrocarbon products obtained using Au@Pd electrocatalysts, alloying Au with Cu has been reported to increase the selectivity of the catalyst for CO relative to Au-only NPs.[392,428] The size of these AuCu alloys was also found to be an important factor in their electrocatalytic performance. Specifically, AuCu NPs having sizes of < ∼5 nm actually exhibited a lower CO:H_2 ratio than Au-only NPs.[231] DFT calculations suggested that CO binds too strongly on AuCu alloys having sizes <2 nm, thereby poisoning active sites for the CO_2RR.[432]

Kauffman et al. reported that the strong binding of CO on AuCu could be reduced by using ∼2 nm, thiol-capped $Au_xCu_{(100-x)}(SH)_{59}$ nanoalloys.[432] Specifically, they observed that 2-phenylethanethiol ligands increased the CO:H_2 ratio relative to ligand-free AuCu NPs. DFT studies suggested that the ligand stabilized the *COOH intermediate and destabilized *H, thereby increasing CO selectivity. As previously observed for $Au_{25}(SCH_3)_{18}$ NPs,[20,412] the fully thiolated $Au_xCu_{(100-x)}(SR)_{59}$ NPs are not predicted to be electrocatalytically active. Instead, in situ electrochemical removal of a thiol ligand is necessary to form Cu−S surface staples, which are predicted to be highly active for CO production. It was suggested that the increased stability of *COOH is due to favorable interactions on adjacent Cu and Au surface atoms at the active site (Figure 31a). This mechanism of stabilization was supported by observed composition-dependent activity (Figure 31b,c), with the highest Faradaic efficiency for CO observed for alloys composed of ∼50% Cu.

Another promising method for enhancing the activity of AuCu nanoalloys involves transforming the NPs from an atomically random (disordered) to an intermetallic (ordered) state.[231] The seed-mediated reduction of Cu^{2+} onto Au NP seeds was used to synthesize AuCu NPs, while different heating conditions during synthesis induced atomic mixing between Cu and Au. Intermetallic AuCu NPs having a size of ∼7 nm displayed CO mass activities (A/g_{Au}) 2.6 times higher than Au-only NPs, but their selectivity toward CO decreased by ∼10%. DFT calculations attributed the increase in activity to the compressive strain of a three-atom-thick Au shell on the surface of the intermetallic core, leading to more favorable *COOH binding. The formation of the Au shell was the result of the high processing temperature required to induce complete atomic ordering to the intermetallic state. Unfortunately, these Au overlayers were also associated with NP instability and suspected to leach Au, leading to an activity decrease of ∼15% over 12 h. This study illustrates the need for better synthetic techniques that will lead to both order and stability.

In addition to AuCu, other Cu nanoalloys, including CuAg[433−435] and CuPd,[100,121,436,437] have been examined as electrocatalysts for the CO_2RR. Due to the minimal miscibility of Ag with Cu, CuAg alloys with a Cu-rich surface are usually obtained.[433] Due to the limited structural and compositional control available for CuAg nanostructures, most reports focus on surface and thin film alloys rather than NPs.[438−440] For example, Jaramillo and co-workers prepared CuAg thin films using vapor deposition techniques to overcome miscibility limitations.[439] This catalyst was reported to favor the formation of soluble CO_2 reduction products, such as acetaldehyde and acetate, compared to Cu-only films. The lack of hydrocarbon formation was determined to result from both destabilization of oxygenated intermediates (i.e., *COOH) and reduced *H surface coverage. These results demonstrated that effectively increasing the miscibility or extent of atomic mixing of a system is a promising synthetic tool for modifying catalytic activity. More recently, "nanodimer" structures exhibiting a Ag/Cu interface were reported to increase both overall CO_2 reduction activity and selectivity for ethylene.[440]

3.3.5. Summary of Synergy between NP Structural Design and CO_2RR Activity. Despite the vast amount of research relating to the CO_2RR, its full potential is far from being realized. There are some general guidelines for moving forward, however. First, the binding energies of *COOH, *CO, and *H on the surface of CO_2RR electrocatalysts are vital for controlling overall catalytic activity. Second, unlike reactions like CO electro-oxidation and the ORR, control over selectivity is an important factor for the CO_2RR. Minimizing H_2 production and maximizing hydrocarbon formation is of foremost importance in this regard. Both activity and selectivity are controlled by numerous factors, including (for NPs) the electrocatalyst size, composition, and stability; the presence and type of surface ligands; the nature of the electrolyte solution; and the applied potential. This parameter space is far too large to be probed experimentally, and therefore, guidance from theory is of special importance. *Operando* characterization of the evolution of NP electrocatalysts is also key to the development of this field.

4. CONCLUSIONS AND FUTURE OUTLOOKS

The need for structurally diverse electrocatalysts having high activity and controlled selectivity for technologically relevant electrochemical transformations is surging well beyond current capabilities. The key to making progress is the marriage between experiment and theory and particularly experimental model systems against which the efficacy of theory can be benchmarked. Iterations between experiment and theory combined with constantly increasing computational power will eventually lead to a point where theory can define efficient catalytic structures. To achieve this goal, experimentalists must strive for discovery of new synthetic NP models that can be directly compared to first-principles theory. This means fairly small numbers of atoms per NP; a high degree of homogeneity in size, composition, and structure; atomic-level characterization; and good stability under *operando* conditions. Single-particle and single-atom electrocatalyst studies are perhaps the best models for comparison with theory, but huge challenges must be overcome before these types of systems become viable.

Theorists, on the other hand, must design more efficient computational methods. They must also develop methods that are able to incorporate some degree of NP heterogeneity. Experimentalists need practical guidance from theorists for breaking the kinds of scaling relationships discussed in this article and for predicting electrocatalysts having structures and compositions that can be synthesized. Finally, an especially important frontier that has barely been addressed at this point is the ability to predict the stability of effective electrocatalysts.

The needs described in these final two paragraphs are huge, and they are sufficient to keep the community of electrocatalyst scientists and engineers busy for a long time. The clock is ticking, however, and time is of the essence for finding efficient electrocatalysts to power transportation and to close the carbon cycle.

DOI: 10.1021/acs.chemrev.9b00246
Chem. Rev. XXXX, XXX, XXX−XXX

AUTHOR INFORMATION

Corresponding Authors

*E-mail: henkelman@utexas.edu. Phone: 512-471-4179.
*E-mail: crooks@cm.utexas.edu. Phone: 512-475-8674.

ORCID

Graeme Henkelman: 0000-0002-0336-7153
Richard M. Crooks: 0000-0001-5186-4878

Author Contributions

†J.A.T., Z.D.: These authors contributed equally.

Notes

The authors declare no competing financial interest.

Biographies

Jamie A. Trindell graduated with a B.Sc. in Chemistry/Biochemistry from the University of West Florida in 2014, where she synthesized fluorescent polycyclic azaborine chromophores under the guidance of Dr. Michael Huggins. She is now in the final year of her Ph.D. studies in the lab of Prof. Richard Crooks at The University of Texas at Austin, where her research focuses on understanding the fundamental properties of electrocatalytic metal nanoparticles.

Zhiyao Duan received his Ph.D. diploma in 2013 from the University of Pittsburgh with a thesis on multiscale simulation of the electrochemical oxygen reduction reaction on Pt-3d transition metal alloys. Currently, he is doing a postdoc under the supervision of Prof. Graeme Henkelman at The University of Texas at Austin. His research focuses on studying catalysis and electrocatalysis on metal/oxide interfaces and electrochemical interfaces under constant potential conditions.

Graeme Henkelman obtained his Ph.D. in Chemistry at the University of Washington at Seattle. After postdoctoral studies at Los Alamos National Laboratory, he joined The University of Texas at Austin where he is currently the George W. Watt Centennial Professor of Chemistry. His research group focuses on the development of new computational algorithms for finding chemical reaction pathways and extending the time scale of simulations beyond what can be simulated directly with molecular dynamics. These methods allow for the investigation of reactions at surfaces, novel catalysts, defect dynamics in materials, and new battery materials.

Richard M. Crooks received a B.S. degree in chemistry from the University of Illinois and a Ph.D. in electrochemistry from The University of Texas at Austin in 1987. Following a two-year postdoctoral appointment at MIT, he moved to the University of New Mexico in 1989 and then to Texas A&M University in 1993. In 2005, he returned to UT-Austin, where he is presently the Robert A. Welch Chair in Materials Chemistry. His research interests are in the fields of electrocatalysis, separations, and chemical sensing.

ACKNOWLEDGMENTS

We gratefully acknowledge support from the Chemical Sciences, Geosciences, and Biosciences Division, Office of Basic Energy Sciences, Office of Science, U.S. Department of Energy (Contract: DE-SC0010576). We thank the Robert A. Welch Foundation (Grants: RMC, F-0032, and GH, F-1841) for sustained support of our research.

GLOSSARY

ATR-IR = attenuated total reflectance infrared
BEP = Brønsted–Evans–Polanyi
CO_2RR = carbon dioxide reduction reaction
CHE = computational hydrogen electrode
CV = cyclic voltammetry
DEMS = differential electrochemical mass spectrometry
DENs = dendrimer-encapsulated nanoparticles
DFT = density functional theory
E_B = binding energy
ECSA = electrochemically active surface area
EDX = energy dispersive X-ray spectroscopy
EM = electron microscopy
EXAFS = extended X-ray absorption fine structure
FCC = face-centered cubic
FCT = face-centered tetragonal
HAADF = high-angle annular dark-field
HER = hydrogen evolution reaction
HE-XRD = high-energy X-ray diffraction
HR-TEM = high-resolution transmission electron microscopy
IL-TEM = identical-location transmission electron microscopy
IR = infrared spectroscopy
LH = Langmuir–Hinshelwood
MPC(s) = monolayer-protected cluster(s)
NHC = N-heterocycle
NHE = normal hydrogen electrode
NP(s) = nanoparticle(s)
ORR = oxygen reduction reaction
OTECCM = optically targeted electrochemical cell microscopy
PAMAM = poly(amidoamine) dendrimer
PDF = pair distribution function
PEMFC(s) = proton-exchange membrane fuel cell(s)
PPI = poly(propyleneimine)
PVP = poly(vinyl)pyrrolidone
QM/MM = quantum mechanics/molecular mechanics
RDV = rotating disk voltammetry
RHE = reversible hydrogen electrode
RMC = reverse Monte Carlo
RRDV = rotating ring disk voltammetry
SECCM = scanning electrochemical cell microscopy
SEM = scanning electron microscopy
SHE = standard hydrogen electrode
SMCR = seed-mediated co-reduction
SML = supervised machine learning
STEM = scanning transmission electron microscopy
TM(s) = transition metal(s)
TOF = turnover frequency
UPD = underpotential deposition
U_{rlp} = rate-limiting potential
XAFS = X-ray absorption fine structure
XANES = X-ray absorption near-edge structure
XAS = X-ray absorption spectroscopy
XPS = X-ray photoelectron spectroscopy
XRD = X-ray diffraction

REFERENCES

(1) Ferrando, R.; Jellinek, J.; Johnston, R. L. Nanoalloys: From Theory to Applications of Alloy Clusters and Nanoparticles. *Chem. Rev.* **2008**, *108*, 845–910.
(2) Cao, S.; Tao, F.; Tang, Y.; Li, Y.; Yu, J. Size- and Shape-Dependent Catalytic Performances of Oxidation and Reduction Reactions on Nanocatalysts. *Chem. Soc. Rev.* **2016**, *45*, 4747–4765.

DOI: 10.1021/acs.chemrev.9b00246
Chem. Rev. XXXX, XXX, XXX–XXX

(3) Mistry, H.; Varela, A. S.; Kühl, S.; Strasser, P.; Cuenya, B. R. Nanostructured Electrocatalysts with Tunable Activity and Selectivity. *Nat. Rev. Mater.* **2016**, *1*, 1−14.
(4) Anderson, R. M.; Yancey, D. F.; Zhang, L.; Chill, S. T.; Henkelman, G.; Crooks, R. M. A Theoretical and Experimental Approach for Correlating Nanoparticle Structure and Electrocatalytic Activity. *Acc. Chem. Res.* **2015**, *48*, 1351−1357.
(5) Roduner, E. Size Matters: Why Nanomaterials Are Different. *Chem. Soc. Rev.* **2006**, *35*, 583−592.
(6) Li, H.; Luo, L.; Kunal, P.; Bonifacio, C. S. S.; Duan, Z.; Yang, J. C. C.; Humphrey, S. M.; Crooks, R. M.; Henkelman, G. Oxygen Reduction Reaction on Classically Immiscible Bimetallics: A Case Study of RhAu. *J. Phys. Chem. C* **2018**, *122*, 2712−2716.
(7) Gawande, M. B.; Goswami, A.; Asefa, T.; Guo, H.; Biradar, A. V.; Peng, D.-L.; Zboril, R.; Varma, R. S. Core−Shell Nanoparticles: Synthesis and Applications in Catalysis and Electrocatalysis. *Chem. Soc. Rev.* **2015**, *44*, 7540−7590.
(8) Cui, C.; Gan, L.; Heggen, M.; Rudi, S.; Strasser, P. Compositional Segregation in Shaped Pt Alloy Nanoparticles and Their Structural Behaviour during Electrocatalysis. *Nat. Mater.* **2013**, *12*, 765−771.
(9) Duan, Z.; Zhong, J.; Wang, G. Modeling Surface Segregation Phenomena in the (111) Surface of Ordered Pt_3Ti Crystal. *J. Chem. Phys.* **2010**, *133*, 114701−114711.
(10) Zhang, L.; Iyyamperumal, R.; Yancey, D. F.; Crooks, R. M.; Henkelman, G. Design of Pt-Shell Nanoparticles with Alloy Cores for the Oxygen Reduction Reaction. *ACS Nano* **2013**, *7*, 9168−9172.
(11) Rossmeisl, J.; Skúlason, E.; Björketun, M. E.; Tripkovic, V.; Nørskov, J. K. Modeling the Electrified Solid−Liquid Interface. *Chem. Phys. Lett.* **2008**, *466*, 68−71.
(12) Nielsen, M.; Björketun, M. E.; Hansen, M. H.; Rossmeisl, J. Towards First Principles Modeling of Electrochemical Electrode-Electrolyte Interfaces. *Surf. Sci.* **2015**, *631*, 2−7.
(13) Rossmeisl, J.; Chan, K.; Ahmed, R.; Tripković, V.; Björketun, M. E. PH in Atomic Scale Simulations of Electrochemical Interfaces. *Phys. Chem. Chem. Phys.* **2013**, *15*, 10321−10325.
(14) Filhol, J. S.; Neurock, M. Elucidation of the Electrochemical Activation of Water over Pd by First Principles. *Angew. Chem., Int. Ed.* **2006**, *45*, 402−406.
(15) Fang, Y. H.; Wei, G. F.; Liu, Z. P. Theoretical Modeling of Electrode/Electrolyte Interface from First-Principles Periodic Continuum Solvation Method. *Catal. Today* **2013**, *202*, 98−104.
(16) Gilroy, K. D.; Ruditskiy, A.; Peng, H. C.; Qin, D.; Xia, Y. Bimetallic Nanocrystals: Syntheses, Properties, and Applications. *Chem. Rev.* **2016**, *116*, 10414−10472.
(17) Shan, S.; Luo, J.; Yang, L.; Zhong, C.-J. Nanoalloy Catalysts: Structural and Catalytic Properties. *Catal. Sci. Technol.* **2014**, *4*, 3570−3588.
(18) Liao, H.; Fisher, A.; Xu, Z. J. Surface Segregation in Bimetallic Nanoparticles: A Critical Issue in Electrocatalyst Engineering. *Small* **2015**, *11*, 3221−3246.
(19) Liu, S.; Huang, S. Size Effects and Active Sites of Cu Nanoparticle Catalysts for CO2 Electroreduction. *Appl. Surf. Sci.* **2019**, *475*, 20−27.
(20) Austin, N.; Zhao, S.; McKone, J. R.; Jin, R.; Mpourmpakis, G. Elucidating the Active Sites for CO2 Electroreduction on Ligand-Protected Au25 Nanoclusters. *Catal. Sci. Technol.* **2018**, *8*, 3795−3805.
(21) Trindell, J. A.; Clausmeyer, J.; Crooks, R. M. Size Stability and H2/CO Selectivity for Au Nanoparticles during Electrocatalytic CO2 Reduction. *J. Am. Chem. Soc.* **2017**, *139*, 16161−16167.
(22) Manthiram, K.; Surendranath, Y.; Alivisatos, A. P. Dendritic Assembly of Gold Nanoparticles during Fuel-Forming Electrocatalysis. *J. Am. Chem. Soc.* **2014**, *136*, 7237−7240.
(23) Wang, J.; Mcentee, M.; Tang, W.; Neurock, M.; Baddorf, A. P.; Maksymovych, P.; Yates, J. T. Formation, Migration, and Reactivity of Au−CO Complexes on Gold Surfaces. *J. Am. Chem. Soc.* **2016**, *138*, 1518−1526.
(24) Kim, H. Y.; Henkelman, G. CO Adsorption-Driven Surface Segregation of Pd on Au/Pd Bimetallic Surfaces: Role of Defects and Effect on CO Oxidation. *ACS Catal.* **2013**, *3*, 2541−2546.
(25) Timoshenko, J.; Duan, Z.; Henkelman, G.; Crooks, R. M.; Frenkel, A. I. Solving the Structure and Dynamics of Metal Nanoparticles by Combining X-Ray Absorption Fine Structure Spectroscopy and Atomistic Structure Simulations. *Annu. Rev. Anal. Chem.* **2019**, *12*, 501−522.
(26) Nørskov, J. K.; Abild-Pedersen, F.; Studt, F.; Bligaard, T. Density Functional Theory in Surface Chemistry and Catalysis. *Proc. Natl. Acad. Sci. U. S. A.* **2011**, *108*, 937−943.
(27) Nørskov, J. K.; Bligaard, T.; Rossmeisl, J.; Christensen, C. H. Towards the Computational Design of Solid Catalysts. *Nat. Chem.* **2009**, *1*, 37−46.
(28) Wang, G.; Van Hove, M. A.; Ross, P. N.; Baskes, M. I. Quantitative Prediction of Surface Segregation in Bimetallic Pt−M Alloy Nanoparticles. *Prog. Surf. Sci.* **2005**, *79*, 28−45.
(29) Williams, F. L.; Nason, D. Binary Alloy Surface Compositions from Bulk Alloy Thermodynamic Data. *Surf. Sci.* **1974**, *45*, 377−408.
(30) Tréglia, G.; Legrand, B.; Ducastelle, F.; Saúl, A.; Gallis, C.; Meunier, I.; Mottet, C.; Senhaji, A. Alloy Surfaces: Segregation, Reconstruction and Phase Transitions. *Comput. Mater. Sci.* **1999**, *15*, 196−235.
(31) Foiles, S. M. Calculation of the Surface Segregation of Ni-Cu Alloys with the Use of the Embedded-Atom Method. *Phys. Rev. B: Condens. Matter Mater. Phys.* **1985**, *32*, 7685−7693.
(32) Ouyang, R.; Xie, Y.; Jiang, D. Global Minimization of Gold Clusters by Combining Neural Network Potentials and the Basin-Hopping Method. *Nanoscale* **2015**, *7*, 14817−14821.
(33) Wales, D. J.; Doye, J. P. K. Global Optimization by Basin-Hopping and the Lowest Energy Structures of Lennard-Jones Clusters Containing up to 110 Atoms. *J. Phys. Chem. A* **1997**, *101*, 5111−5116.
(34) Doye, J. P. K.; Wales, D. J. Thermodynamics of Global Optimization. *Phys. Rev. Lett.* **1998**, *80*, 1357−1360.
(35) Goedecker, S. Minima Hopping: An Efficient Search Method for the Global Minimum of the Potential Energy Surface of Complex Molecular Systems. *J. Chem. Phys.* **2004**, *120*, 9911−9917.
(36) Wolf, M. D.; Landman, U. Genetic Algorithms for Structural Cluster Optimization. *J. Phys. Chem. A* **1998**, *102*, 6129−6137.
(37) Vilhelmsen, L. B.; Hammer, B. A Genetic Algorithm for First Principles Global Structure Optimization of Supported Nano Structures. *J. Chem. Phys.* **2014**, *141*, 044711.
(38) Jørgensen, M. S.; Groves, M. N.; Hammer, B. Combining Evolutionary Algorithms with Clustering toward Rational Global Structure Optimization at the Atomic Scale. *J. Chem. Theory Comput.* **2017**, *13*, 1486−1493.
(39) McGreevy, R. L.; Pusztai, L. Reverse Monte Carlo Simulation: A New Technique for the Determination of Disordered Structures. *Mol. Simul.* **1988**, *1*, 359−367.
(40) Mcgreevy, R. L. Reverse Monte Carlo Modelling. *J. Phys.: Condens. Matter* **2001**, *13*, R877−R913.
(41) Gurman, S. J.; McGreevy, R. L. Reverse Monte Carlo Simulation for the Analysis of EXAFS Data. *J. Phys.: Condens. Matter* **1990**, *2*, 9463−9473.
(42) Yancey, D. F.; Chill, S. T.; Zhang, L.; Frenkel, A. I.; Henkelman, G.; Crooks, R. M. A Theoretical and Experimental Examination of Systematic Ligand-Induced Disorder in Au Dendrimer-Encapsulated Nanoparticles. *Chem. Sci.* **2013**, *4*, 2912−2921.
(43) Duan, Z.; Li, Y.; Timoshenko, J.; Chill, S. T.; Anderson, R. M.; Yancey, D. F.; Frenkel, A. I.; Crooks, R. M.; Henkelman, G. A Combined Theoretical and Experimental EXAFS Study of the Structure and Dynamics of Au147 Nanoparticles. *Catal. Sci. Technol.* **2016**, *6*, 6879−6885.
(44) Timoshenko, J.; Frenkel, A. I. Probing Structural Relaxation in Nanosized Catalysts by Combining EXAFS and Reverse Monte Carlo Methods. *Catal. Today* **2017**, *280*, 274−282.
(45) Timoshenko, J.; Lu, D.; Lin, Y.; Frenkel, A. I. Supervised Machine-Learning-Based Determination of Three-Dimensional Struc-

DOI: 10.1021/acs.chemrev.9b00246
Chem. Rev. XXXX, XXX, XXX−XXX

ture of Metallic Nanoparticles. *J. Phys. Chem. Lett.* **2017**, *8*, 5091−5098.
(46) Nørskov, J. K.; Rossmeisl, J.; Logadottir, A.; Lindqvist, L.; Kitchin, J. R.; Bligaard, T.; Jónsson, H. Origin of the Overpotential for Oxygen Reduction at a Fuel-Cell Cathode. *J. Phys. Chem. B* **2004**, *108*, 17886−17892.
(47) Hyman, M. P.; Medlin, J. W. Theoretical Study of the Adsorption and Dissociation of Oxygen on Pt(111) in the Presence of Homogeneous Electric Fields. *J. Phys. Chem. B* **2005**, *109*, 6304−6310.
(48) Taylor, C. D.; Wasileski, S. A.; Filhol, J. S.; Neurock, M. First Principles Reaction Modeling of the Electrochemical Interface: Consideration and Calculation of a Tunable Surface Potential from Atomic and Electronic Structure. *Phys. Rev. B: Condens. Matter Mater. Phys.* **2006**, *73*, 165402.
(49) Zhao, J.; Chan, C. T.; Che, J. G. Effects of an Electric Field on a Water Bilayer on Ag(111). *Phys. Rev. B: Condens. Matter Mater. Phys.* **2007**, *75*, 085435.
(50) Otani, M.; Sugino, O. First-Principles Calculations of Charged Surfaces and Interfaces: A Plane-Wave Nonrepeated Slab Approach. *Phys. Rev. B: Condens. Matter Mater. Phys.* **2006**, *73*, 115407.
(51) Jinnouchi, R.; Anderson, A. B. Electronic Structure Calculations of Liquid-Solid Interfaces: Combination of Density Functional Theory and Modified Poisson-Boltzmann Theory. *Phys. Rev. B: Condens. Matter Mater. Phys.* **2008**, *77*, 245417.
(52) Sundararaman, R.; Goddard, W. A.; Arias, T. A. Grand Canonical Electronic Density-Functional Theory: Algorithms and Applications to Electrochemistry. *J. Chem. Phys.* **2017**, *146*, 114104.
(53) Goodpaster, J. D.; Bell, A. T.; Head-Gordon, M. Identification of Possible Pathways for C-C Bond Formation during Electrochemical Reduction of CO2: New Theoretical Insights from an Improved Electrochemical Model. *J. Phys. Chem. Lett.* **2016**, *7*, 1471−1477.
(54) Skúlason, E.; Karlberg, G. S.; Rossmeisl, J.; Bligaard, T.; Greeley, J. P.; Jónsson, H.; Nørskov, J. K. Density Functional Theory Calculations for the Hydrogen Evolution Reaction in an Electrochemical Double Layer on the Pt(111) Electrode. *Phys. Chem. Chem. Phys.* **2007**, *9*, 3241−3250.
(55) Chan, K.; Nørskov, J. K. Electrochemical Barriers Made Simple. *J. Phys. Chem. Lett.* **2015**, *6*, 2663−2668.
(56) Viswanathan, V.; Hansen, H. A.; Rossmeisl, J.; Nørskov, J. K. Universality in Oxygen Reduction Electrocatalysis on Metal Surfaces. *ACS Catal.* **2012**, *2*, 1654−1660.
(57) Akhade, S. A.; Nidzyn, R. M.; Rostamikia, G.; Janik, M. J. Using Brønsted-Evans-Polanyi Relations to Predict Electrode Potential-Dependent Activation Energies. *Catal. Today* **2018**, *312*, 82−91.
(58) Greeley, J. Theoretical Heterogeneous Catalysis: Scaling Relationships and Computational Catalyst Design. *Annu. Rev. Chem. Biomol. Eng.* **2016**, *7*, 605−635.
(59) Abild-Pedersen, F.; Greeley, J.; Studt, F.; Rossmeisl, J.; Munter, T. R.; Moses, P. G.; Skúlason, E.; Bligaard, T.; Nørskov, J. K. Scaling Properties of Adsorption Energies for Hydrogen-Containing Molecules on Transition-Metal Surfaces. *Phys. Rev. Lett.* **2007**, *99*, 4−7.
(60) Bligaard, T.; Nørskov, J. K.; Dahl, S.; Matthiesen, J.; Christensen, C. H.; Sehested, J. The Brønsted−Evans−Polanyi Relation and the Volcano Curve in Heterogeneous Catalysis. *J. Catal.* **2004**, *224*, 206−217.
(61) Gokhale, A. A.; Kandoi, S.; Greeley, J. P.; Mavrikakis, M.; Dumesic, J. A. Molecular-Level Descriptions of Surface Chemistry in Kinetic Models Using Density Functional Theory. *Chem. Eng. Sci.* **2004**, *59*, 4679−4691.
(62) Huang, K.; Clausmeyer, J.; Luo, L.; Jarvis, K.; Crooks, R. M. Shape-Controlled Electrodeposition of Single Pt Nanocrystals onto Carbon Nanoelectrodes. *Faraday Discuss.* **2018**, *210*, 267−280.
(63) Bohn, P. W. Science and Technology of Electrochemistry at Nano-Interfaces: Concluding Remarks. *Faraday Discuss.* **2018**, *210*, 481−493.
(64) Glasscott, M. W.; Dick, J. E. Direct Electrochemical Observation of Single Platinum Cluster Electrocatalysis on Ultramicroelectrodes. *Anal. Chem.* **2018**, *90*, 7804−7808.
(65) Liu, S.; Tian, N.; Xie, A. Y.; Du, J. H.; Xiao, J.; Liu, L.; Sun, H. Y.; Cheng, Z. Y.; Zhou, Z. Y.; Sun, S. G. Electrochemically Seed-Mediated Synthesis of Sub-10 Nm Tetrahexahedral Pt Nanocrystals Supported on Graphene with Improved Catalytic Performance. *J. Am. Chem. Soc.* **2016**, *138*, 5753−5756.
(66) Kim, J.; Bard, A. J. Electrodeposition of Single Nanometer-Size Pt Nanoparticles at a Tunneling Ultramicroelectrode and Determination of Fast Heterogeneous Kinetics for $Ru(NH_3)_6^{3+}$ Reduction. *J. Am. Chem. Soc.* **2016**, *138*, 975−979.
(67) Ustarroz, J.; Hammons, J. A.; Altantzis, T.; Hubin, A.; Bals, S.; Terryn, H. A Generalized Electrochemical Aggregative Growth Mechanism. *J. Am. Chem. Soc.* **2013**, *135*, 11550−11561.
(68) Hussein, H. E. M.; Maurer, R. J.; Amari, H.; Peters, J. J. P.; Meng, L.; Beanland, R.; Newton, M. E.; Macpherson, J. V. Tracking Metal Electrodeposition Dynamics from Nucleation and Growth of a Single Atom to a Crystalline Nanoparticle. *ACS Nano* **2018**, *12*, 7388−7396.
(69) Altimari, P.; Greco, F.; Pagnanelli, F. Nucleation and Growth of Metal Nanoparticles on a Planar Electrode: A New Model Based on Iso-Nucleation-Time Classes of Particles. *Electrochim. Acta* **2019**, *296*, 82−93.
(70) Yang, J.; Andrei, C. M.; Chan, Y.; Mehdi, B. L.; Browning, N. D.; Botton, G. A.; Soleymani, L. Liquid Cell Transmission Electron Microscopy Sheds Light on The Mechanism of Palladium Electrodeposition. *Langmuir* **2019**, *35*, 862−869.
(71) O'Mullane, A. P. From Single Crystal Surfaces to Single Atoms: Investigating Active Sites in Electrocatalysis. *Nanoscale* **2014**, *6*, 4012−4026.
(72) Zhou, M.; Dick, J. E.; Bard, A. J. Electrodeposition of Isolated Platinum Atoms and Clusters on Bismuth - Characterization and Electrocatalysis. *J. Am. Chem. Soc.* **2017**, *139*, 17677−17682.
(73) Yu, Y.; Sundaresan, V.; Bandyopadhyay, S.; Zhang, Y.; Edwards, M. A.; Mckelvey, K.; White, H. S.; Willets, K. A. Three-Dimensional Super-Resolution Imaging of Single Nanoparticles Delivered by Pipettes. *ACS Nano* **2017**, *11*, 10529−10538.
(74) Li, Y.; Cox, J. T.; Zhang, B. Electrochemical Responses and Electrocatalysis at Single Au Nanoparticles. *J. Am. Chem. Soc.* **2010**, *132*, 3047−3054.
(75) Hao, R.; Fan, Y.; Zhang, B. Imaging Dynamic Collision and Oxidation of Single Silver Nanoparticles at the Electrode/Solution Interface. *J. Am. Chem. Soc.* **2017**, *139*, 12274−12282.
(76) Kai, T.; Zoski, C. G.; Bard, A. J. Scanning Electrochemical Microscopy at the Nanometer Level. *Chem. Commun.* **2018**, *54*, 1934−1947.
(77) Saha, P.; Hill, J. W.; Walmsley, J. D.; Hill, C. M. Probing Electrocatalysis at Individual Au Nanorods via Correlated Optical and Electrochemical Measurements. *Anal. Chem.* **2018**, *90*, 12832−12839.
(78) Sambur, J. B.; Chen, P. Approaches to Single-Nanoparticle Catalysis. *Annu. Rev. Phys. Chem.* **2014**, *65*, 395−422.
(79) Mirkin, M. V.; Sun, T.; Yu, Y.; Zhou, M. Electrochemistry at One Nanoparticle. *Acc. Chem. Res.* **2016**, *49*, 2328−2335.
(80) Wang, Y.; Shan, X.; Tao, N. Emerging Tools for Studying Single Entity Electrochemistry. *Faraday Discuss.* **2016**, *193*, 9−39.
(81) Baker, L. A. Perspective and Prospectus on Single-Entity Electrochemistry. *J. Am. Chem. Soc.* **2018**, *140*, 15549−15559.
(82) Duan, Z.; Timoshenko, J.; Kunal, P.; House, S. D.; Wan, H.; Jarvis, K.; Bonifacio, C.; Yang, J. C.; Crooks, R. M.; Frenkel, A. I.; et al. Structural Characterization of Heterogeneous RhAu Nanoparticles from a Microwave-Assisted Synthesis. *Nanoscale* **2018**, *10*, 22520−22532.
(83) Bao, Y.; An, W.; Heath Turner, C.; Krishnan, K. M. The Critical Role of Surfactants in the Growth of Cobalt Nanoparticles. *Langmuir* **2010**, *26*, 478−483.
(84) Ortiz, N.; Skrabalak, S. E. On the Dual Roles of Ligands in the Synthesis of Colloidal Metal Nanostructures. *Langmuir* **2014**, *30*, 6649−6659.
(85) Kluenker, M.; Connolly, B. M.; Marolf, D. M.; Tahir, M. N.; Korschelt, K.; Simon, P.; Ko, U.; Plana-ruiz, S.; Barton, B.; Pantho, M.; et al. Controlling the Morphology of Au−Pd Heterodimer

DOI: 10.1021/acs.chemrev.9b00246
Chem. Rev. XXXX, XXX, XXX−XXX

Nanoparticles by Surface Ligands. *Inorg. Chem.* **2018**, *57*, 13640−13652.
(86) Huang, L.; Zhang, X.; Wang, Q.; Han, Y.; Fang, Y.; Dong, S. Shape-Control of Pt-Ru Nanocrystals: Tuning Surface Structure for Enhanced Electrocatalytic Methanol Oxidation. *J. Am. Chem. Soc.* **2018**, *140*, 1142−1147.
(87) Zhou, Z. Y.; Kang, X.; Song, Y.; Chen, S. Ligand-Mediated Electrocatalytic Activity of Pt Nanoparticles for Oxygen Reduction Reactions. *J. Phys. Chem. C* **2012**, *116*, 10592−10598.
(88) Kunz, S. Supported, Ligand-Functionalized Nanoparticles: An Attempt to Rationalize the Application and Potential of Ligands in Heterogeneous Catalysis. *Top. Catal.* **2016**, *59*, 1671−1685.
(89) Guo, Y.; Wu, Y.; Cao, R.; Zheng, S.; Yang, Y.; Chen, M. Platinum Nanoparticles Functionalized with Acetylene Derivatives and the Influence of Ligand Length on Their Electrocatalytic Activity. *J. Electroanal. Chem.* **2017**, *785*, 159−165.
(90) Hu, P.; Chen, L.; Deming, C. P.; Lu, J. E.; Bonny, L. W.; Chen, S. Effects of Para-Substituents of Styrene Derivatives on Their Chemical Reactivity on Platinum Nanoparticle Surfaces. *Nanoscale* **2016**, *8*, 12013−12021.
(91) Schrader, I.; Neumann, S.; Anda, S.; Schmidt, F.; Azov, V.; Kunz, S. Asymmetric Heterogeneous Catalysis: Transfer of Molecular Principles to Nanoparticles by Ligand Functionalization. *ACS Catal.* **2017**, *7*, 3979−3987.
(92) Rossi, L. M.; Fiorio, J. L.; Garcia, M. A. S. S.; Ferraz, C. P. The Role and Fate of Capping Ligands in Colloidally Prepared Metal Nanoparticle Catalysts. *Dalt. Trans.* **2018**, *47*, 5889−5915.
(93) Lim, B.; Xia, Y. Metal Nanocrystals with Highly Branched Morphologies. *Angew. Chem., Int. Ed.* **2011**, *50*, 76−85.
(94) Peng, Z.; Yang, H. Designer Platinum Nanoparticles: Control of Shape, Composition in Alloy, Nanostructure and Electrocatalytic Property. *Nano Today* **2009**, *4*, 143−164.
(95) Song, L.; Liang, Z.; Vukmirovic, M. B.; Adzic, R. R. Enhanced Oxygen Reduction Reaction Activity on Pt-Monolayer-Shell PdIr/Ni-Core Catalysts. *J. Electrochem. Soc.* **2018**, *165*, J3288−J3294.
(96) Xia, Y.; Xia, X.; Peng, H. C. Shape-Controlled Synthesis of Colloidal Metal Nanocrystals: Thermodynamic versus Kinetic Products. *J. Am. Chem. Soc.* **2015**, *137*, 7947−7966.
(97) Chakraborty, S.; Ansar, S. M.; Stroud, J. G.; Kitchens, C. L. Comparison of Colloidal versus Supported Gold Nanoparticle Catalysis. *J. Phys. Chem. C* **2018**, *122*, 7749−7758.
(98) Inoue, M.Solvothermal Synthesis of Metal Oxides. In *Handbook of Advanced Ceramics: Materials, Applications, Processing, and Properties*; Elsevier: St. Louis, 2013; pp 927−948.
(99) Biacchi, A. J.; Schaak, R. E. Ligand-Induced Fate of Embryonic Species in the Shape-Controlled Synthesis of Rhodium Nanoparticles. *ACS Nano* **2015**, *9*, 1707−1720.
(100) Yin, Z.; Gao, D.; Yao, S.; Zhao, B.; Cai, F.; Lin, L.; Tang, P.; Zhai, P.; Wang, G.; Ma, D.; et al. Highly Selective Palladium-Copper Bimetallic Electrocatalysts for the Electrochemical Reduction of CO2 to CO. *Nano Energy* **2016**, *27*, 35−43.
(101) Zhang, L. M.; Wang, Z. B.; Zhang, J. J.; Sui, X. L.; Zhao, L.; Han, J. C. Investigation on Electrocatalytic Activity and Stability of Pt/C Catalyst Prepared by Facile Solvothermal Synthesis for Direct Methanol Fuel Cell. *Fuel Cells* **2015**, *15*, 619−627.
(102) Kwon, S. G. U.; Hyeon, T. Colloidal Chemical Synthesis and Formation Kinetics of Uniformly Sized Nanocrystals of Metals, Oxides and Chalcogenides. *Acc. Chem. Res.* **2008**, *41*, 1696−1709.
(103) Rao, B. G.; Mukherjee, D.; Reddy, B. M. Novel Approaches for Preparation of Nanoparticles. In *Nanostructures for Novel Therapy*; Elsevier: St. Louis, 2017; pp 1−36.
(104) Zheng, X.; Liu, S.; Cheng, X.; Cheng, J.; Si, C.; Pan, Z.; Marcelli, A.; Chu, W.; Wu, Z. Synthesis and Characterization of Cu-Pt Bimetallic Nanoparticles. *J. Phys.: Conf. Ser.* **2013**, *430*, 012037.
(105) Wang, C.; Daimon, H.; Onodera, T.; Koda, T.; Sun, S. A General Approach to the Size- and Shape-Controlled Synthesis of Platinum Nanoparticles and Their Catalytic Reduction of Oxygen. *Angew. Chem., Int. Ed.* **2008**, *47*, 3588−3591.
(106) Vivien, A.; Guillaumont, M.; Meziane, L.; Salzemann, C.; Aubert, C.; Halbert, S.; Gérard, H.; Petit, M.; Petit, C. The Role of Oleylamine Revisited: An Original Disproportionation Route to Monodispersed Cobalt and Nickel Nanocrystals. *Chem. Mater.* **2019**, *31*, 960−968.
(107) Loukrakpam, R.; Shan, S.; Petkov, V.; Yang, L.; Luo, J.; Zhong, C.-J. Atomic Ordering Enhanced Electrocatalytic Activity of Nanoalloys for Oxygen Reduction Reaction. *J. Phys. Chem. C* **2013**, *117*, 20715−20721.
(108) Wanjala, B. N.; Loukrakpam, R.; Luo, J.; Njoki, P. N.; Mott, D.; Zhong, C.-J.; Shao, M.; Protsailo, L.; Kawamura, T. Thermal Treatment of PtNiCo Electrocatalysts: Effects of Nanoscale Strain and Structure on the Activity and Stability for the Oxygen Reduction Reaction. *J. Phys. Chem. C* **2010**, *114*, 17580−17590.
(109) Wu, J.; Shan, S.; Petkov, V.; Prasai, B.; Cronk, H.; Joseph, P.; Luo, J.; Zhong, C.-J. J. Composition-Structure-Activity Relationships for Palladium-Alloyed Nanocatalysts in Oxygen Reduction Reaction: An Ex-Situ/In-Situ High Energy X-Ray Diffraction Study. *ACS Catal.* **2015**, *5*, 5317−5327.
(110) Mourdikoudis, S.; Liz-marza, L. M. Oleylamine in Nanoparticle Synthesis. *Chem. Mater.* **2013**, *25*, 1465−1476.
(111) Humphrey, J. J. L.; Sadasivan, S.; Plana, D.; Celorrio, V.; Tooze, R. A.; Fermín, D. J. Surface Activation of Pt Nanoparticles Synthesised by "Hot Injection" in the Presence of Oleylamine. *Chem. - Eur. J.* **2015**, *21*, 12694−12701.
(112) Amiens, C.; Ciuculescu-pradines, D.; Philippot, K. Controlled Metal Nanostructures: Fertile Ground for Coordination Chemists. *Coord. Chem. Rev.* **2016**, *308*, 409−432.
(113) Wang, H.; Luo, W.; Zhu, L.; Zhao, Z.; Bin, E.; Tu, W.; Ke, X.; Sui, M.; Chen, C.; Chen, Q.; et al. Synergistically Enhanced Oxygen Reduction Electrocatalysis by Subsurface Atoms in Ternary PdCuNi Alloy Catalysts. *Adv. Funct. Mater.* **2018**, *28*, 1707219.
(114) Wang, D.; Li, Y. Bimetallic Nanocrystals: Liquid-Phase Synthesis and Catalytic Applications. *Adv. Mater.* **2011**, *23*, 1044−1060.
(115) Germano, L. D.; Marangoni, V. S.; Mogili, N. V. V.; Seixas, L.; Maroneze, C. M. Ultrasmall (<2 Nm) Au@Pt Nanostructures: Tuning the Surface Electronic States for Electrocatalysis. *ACS Appl. Mater. Interfaces* **2019**, *11*, 5661−5667.
(116) Murphy, C. J.; Sau, T. K.; Gole, A. M.; Orendorff, C. J.; Gao, J.; Gou, L.; Hunyadi, S. E.; Li, T. Anisotropic Metal Nanoparticles: Synthesis, Assembly, and Optical Applications. *J. Phys. Chem. B* **2005**, *109*, 13857−13870.
(117) Weiner, R. G.; Kunz, M. R.; Skrabalak, S. E. Seeding a New Kind of Garden: Synthesis of Architecturally Defined Multimetallic Nanostructures by Seed-Mediated Co-Reduction. *Acc. Chem. Res.* **2015**, *48*, 2688−2695.
(118) Samia, A. C. S.; Schlueter, J. A.; Jiang, J. S.; Bader, S. D.; Qin, C. J.; Lin, X. M. Effect of Ligand-Metal Interactions on the Growth of Transition-Metal and Alloy Nanoparticles. *Chem. Mater.* **2006**, *18*, 5203−5212.
(119) Meng, X.; Baride, A.; Jiang, C. Ligand Controlled Morphology Evolution of Active Intermediates for the Syntheses of Gold Nanostars. *Langmuir* **2016**, *32*, 6674−6681.
(120) Ortiz, N.; Weiner, R. G.; Skrabalak, S. E. Ligand-Controlled Co-Reduction versus Electroless Co-Deposition: Synthesis of Nanodendrites with Spatially Defined Bimetallic Distributions. *ACS Nano* **2014**, *8*, 12461−12467.
(121) Chen, D.; Yao, Q.; Cui, P.; Liu, H.; Xie, J.; Yang, J. Tailoring the Selectivity of Bimetallic Copper-Palladium Nanoalloys for Electrocatalytic Reduction of CO2 to CO. *ACS Appl. Energy Mater.* **2018**, *1*, 883−890.
(122) Yin, X.; Shi, M.; Wu, J.; Pan, Y. T.; Gray, D. L.; Bertke, J. A.; Yang, H. Quantitative Analysis of Different Formation Modes of Platinum Nanocrystals Controlled by Ligand Chemistry. *Nano Lett.* **2017**, *17*, 6146−6150.
(123) Lu, L.; Lou, B.; Zou, S.; Kobayashi, H.; Liu, J.; Xiao, L.; Fan, J. Robust Removal of Ligands from Noble Metal Nanoparticles by Electrochemical Strategies. *ACS Catal.* **2018**, *8*, 8484−8492.

DOI: 10.1021/acs.chemrev.9b00246
Chem. Rev. XXXX, XXX, XXX−XXX

(124) Alayoglu, S.; Nilekar, A. U.; Mavrikakis, M.; Eichhorn, B. Ru−Pt Core−Shell Nanoparticles for Preferential Oxidation of Carbon Monoxide in Hydrogen. *Nat. Mater.* **2008**, *7*, 333−338.
(125) Koczkur, K. M.; Mourdikoudis, S.; Polavarapu, L.; Skrabalak, S. E. Polyvinylpyrrolidone (PVP) in Nanoparticle Synthesis. *Dalt. Trans.* **2015**, *44*, 17883−17905.
(126) Liu, Z.; Hu, J. E.; Wang, Q.; Gaskell, K.; Frenkel, A. I.; Jackson, G. S.; Eichhorn, B. PtMo Alloy and MoOx@Pt Core-Shell Nanoparticles as Highly CO-Tolerant Electrocatalysts. *J. Am. Chem. Soc.* **2009**, *131*, 6924−6925.
(127) Masitas, R. A.; Zamborini, F. P. Oxidation of Highly Unstable < 4 Nm Diameter Gold Nanoparticles 850 MV Negative of the Bulk Oxidation Potential. *J. Am. Chem. Soc.* **2012**, *134*, 5014−5017.
(128) Munro, C. J.; Knecht, M. R. Applications and Advancements of Peptides in the Design of Metallic Nanomaterials. *Curr. Opin. Green Sustain. Chem.* **2018**, *12*, 63−68.
(129) Reske, R.; Mistry, H.; Behafarid, F.; Roldan Cuenya, B.; Strasser, P. Particle Size Effects in the Catalytic Electroreduction of CO2 on Cu Nanoparticles. *J. Am. Chem. Soc.* **2014**, *136*, 6978−6986.
(130) Mistry, H.; Reske, R.; Zeng, Z.; Zhao, Z. J.; Greeley, J. P.; Strasser, P.; Cuenya, B. R. Exceptional Size-Dependent Activity Enhancement in the Electroreduction of CO2 over Au Nanoparticles. *J. Am. Chem. Soc.* **2014**, *136*, 16473−16476.
(131) Smith, J. G.; Jain, P. K. The Ligand Shell as an Energy Barrier in Surface Reactions on Transition Metal Nanoparticles. *J. Am. Chem. Soc.* **2016**, *138*, 6765−6773.
(132) San, K. A.; Chen, V.; Shon, Y. S. Preparation of Partially Poisoned Alkanethiolate-Capped Platinum Nanoparticles for Hydrogenation of Activated Terminal Alkynes. *ACS Appl. Mater. Interfaces* **2017**, *9*, 9823−9832.
(133) Gevaerd, A.; Caetano, F. R.; Oliveira, P. R.; Zarbin, A. J. G.; Bergamini, M. F.; Marcolino-junior, L. H. Thiol-Capped Gold Nanoparticles: Influence of Capping Amount on Electrochemical Behavior and Potential Application as Voltammetric Sensor for Diltiazem. *Sens. Actuators, B* **2015**, *220*, 673−678.
(134) Li, J.; Nasaruddin, R.; Feng, Y.; Yang, J.; Yan, N.; Xie, J. Tuning the Accessibility and Activity of Au25(SR)18 Nanocluster Catalysts through Ligand Engineering. *Chem. - Eur. J.* **2016**, *22*, 14816−14820.
(135) Chakraborty, I.; Pradeep, T. Atomically Precise Clusters of Noble Metals: Emerging Link between Atoms and Nanoparticles. *Chem. Rev.* **2017**, *117*, 8208−8271.
(136) Kwak, K.; Choi, W.; Tang, Q.; Kim, M.; Lee, Y.; Jiang, D. E.; Lee, D. A Molecule-like $PtAu_{24}$ $(SC_6H_{13})_{18}$ Nanocluster as an Electrocatalyst for Hydrogen Production. *Nat. Commun.* **2017**, *8*, 1−8.
(137) Tang, Q.; Lee, Y.; Li, D. Y.; Choi, W.; Liu, C. W.; Lee, D.; Jiang, D. E. Lattice-Hydride Mechanism in Electrocatalytic CO2 Reduction by Structurally Precise Copper-Hydride Nanoclusters. *J. Am. Chem. Soc.* **2017**, *139*, 9728−9736.
(138) Kwak, K.; Lee, D. Electrochemistry of Atomically Precise Metal Nanoclusters. *Acc. Chem. Res.* **2019**, *52*, 12−22.
(139) Jin, R.; Zeng, C.; Zhou, M.; Chen, Y. Atomically Precise Colloidal Metal Nanoclusters and Nanoparticles: Fundamentals and Opportunities. *Chem. Rev.* **2016**, *116*, 10346−10413.
(140) Gallo, I. B. C.; Carbonio, E. A.; Villullas, H. M. What Determines Electrochemical Surface Processes on Carbon- Supported PdAu Nanoparticles? *ACS Catal.* **2018**, *8*, 1818−1827.
(141) Slanac, D. A.; Hardin, W. G.; Johnston, K. P.; Stevenson, K. J. Atomic Ensemble and Electronic Effects in Ag-Rich AgPd Nanoalloy Catalysts for Oxygen Reduction in Alkaline Media. *J. Am. Chem. Soc.* **2012**, *134*, 9812−9819.
(142) Alekseenko, A. A.; Moguchikh, E. A.; Safronenko, O. I.; Guterman, V. E. Durability of De-Alloyed PtCu/C Electrocatalysts. *Int. J. Hydrogen Energy* **2018**, *43*, 22885−22895.
(143) Torigoe, K.; Takahashi, M.; Tsuchiya, K.; Iwabata, K.; Ichihashi, T.; Sakaguchi, K.; Sugawara, F.; Abe, M. High-Power Abiotic Direct Glucose Fuel Cell Using a Gold−Platinum Bimetallic Anode Catalyst. *ACS Omega* **2018**, *3*, 18323−18333.
(144) Guo, S.; Zhang, X.; Zhu, W.; He, K.; Su, D.; Mendoza-Garcia, A.; Ho, S. F.; Lu, G.; Sun, S. Nanocatalyst Superior to Pt for Oxygen Reduction Reactions: The Case of Core/Shell Ag(Au)/CuPd Nanoparticles. *J. Am. Chem. Soc.* **2014**, *136*, 15026−15033.
(145) LaGrow, A. P.; Knudsen, K. R.; AlYami, N. M.; Anjum, D. H.; Bakr, O. M. Effect of Precursor Ligands and Oxidation State in the Synthesis of Bimetallic Nano-Alloys. *Chem. Mater.* **2015**, *27*, 4134−4141.
(146) Vykoukal, V.; Bursik, J.; Roupcova, P.; Cullen, D. A.; Pinkas, J. Solvothermal Hot Injection Synthesis of Core-Shell AgNi Nanoparticles. *J. Alloys Compd.* **2019**, *770*, 377−385.
(147) Zhang, S.; Guo, S.; Zhu, H.; Su, D.; Sun, S. Structure-Induced Enhancement in Electrooxidation of Trimetallic FePtAu Nanoparticles. *J. Am. Chem. Soc.* **2012**, *134*, 5060−5063.
(148) Desantis, C. J.; Sue, A. C.; Bower, M. M.; Skrabalak, S. E. Seed-Mediated Co-Reduction: A Versatile Route to Architecturally Controlled Bimetallic Nanostructures. *ACS Nano* **2012**, *6*, 2617−2628.
(149) Kunz, M. R.; McClain, S. M.; Chen, D. P.; Koczkur, K. M.; Weiner, R. G.; Skrabalak, S. E. Seed-Mediated Co-Reduction in a Large Lattice Mismatch System: Synthesis of Pd−Cu Nanostructures. *Nanoscale* **2017**, *9*, 7570−7576.
(150) Wang, C.; Chen, D. P.; Sang, X.; Unocic, R. R.; Skrabalak, S. E. Size-Dependent Disorder-Order Transformation in the Synthesis of Monodisperse Intermetallic PdCu Nanocatalysts. *ACS Nano* **2016**, *10*, 6345−6353.
(151) Chen, H.; Nishijima, M.; Wang, G.; Khene, S.; Zhu, M.; Deng, X.; Zhang, X.; Wen, W.; Luo, Y.; He, Q. The Ordered and Disordered Nano-Intermetallic AuCu/C Catalysts for the Oxygen Reduction Reaction: The Differences of the Electrochemical Performance. *J. Electrochem. Soc.* **2017**, *164*, F1654−F1661.
(152) Xiong, Y.; Xiao, L.; Yang, Y.; DiSalvo, F. J.; Abruña, H. D. High-Loading Intermetallic Pt3Co/C Core-Shell Nanoparticles as Enhanced Activity Electrocatalyst towards the Oxygen Reduction Reaction (ORR). *Chem. Mater.* **2018**, *30*, 1532−1539.
(153) Mohanraju, K.; Cindrella, L. Impact of Alloying and Lattice Strain on ORR Activity of Pt and Pd Based Ternary Alloys with Fe and Co for Proton Exchange Membrane Fuel Cell Applications. *RSC Adv.* **2014**, *4*, 11939.
(154) Ostojic, N.; Crooks, R. M. Electrocatalytic Reduction of Oxygen on Platinum Nanoparticles in the Presence and Absence of Interactions with the Electrode Surface. *Langmuir* **2016**, *32*, 9727−9735.
(155) Ostojic, N.; Duan, Z.; Galyamova, A.; Henkelman, G.; Crooks, R. M. Electrocatalytic Study of the Oxygen Reduction Reaction at Gold Nanoparticles in the Absence and Presence of Interactions with SnOx Supports. *J. Am. Chem. Soc.* **2018**, *140*, 13775−13785.
(156) Yang, L.; Shan, S.; Loukrakpam, R.; Petkov, V.; Ren, Y.; Wanjala, B. N.; Engelhard, M. H.; Luo, J.; Yin, J.; Chen, Y.; et al. Role of Support-Nanoalloy Interactions in the Atomic-Scale Structural and Chemical Ordering for Tuning Catalytic Sites. *J. Am. Chem. Soc.* **2012**, *134*, 15048−15060.
(157) Celorrio, V.; Montes De Oca, M. G.; Plana, D.; Moliner, R.; Lázaro, M. J.; Fermín, D. J. Effect of Carbon Supports on Electrocatalytic Reactivity of Au-Pd Core-Shell Nanoparticles. *J. Phys. Chem. C* **2012**, *116*, 6275−6282.
(158) Shahgaldi, S.; Hamelin, J. Improved Carbon Nanostructures as a Novel Catalyst Support in the Cathode Side of PEMFC: A Critical Review. *Carbon* **2015**, *94*, 705−728.
(159) Murthy, A. P.; Madhavan, J.; Murugan, K. Recent Advances in Hydrogen Evolution Reaction Catalysts on Carbon/Carbon- Based Supports in Acid Media. *J. Power Sources* **2018**, *398*, 9−26.
(160) Kumar, G.; Nikolla, E.; Linic, S.; Medlin, J. W.; Janik, M. J. Multicomponent Catalysts: Limitations and Prospects. *ACS Catal.* **2018**, *8*, 3202−3208.
(161) Song, H.; Luo, M.; Qiu, X.; Cao, G. Insights into the Endurance Promotion of PtSn/CNT Catalysts by Thermal Annealing for Ethanol Electro-Oxidation. *Electrochim. Acta* **2016**, *213*, 578−586.

DOI: 10.1021/acs.chemrev.9b00246
Chem. Rev. XXXX, XXX, XXX−XXX

(162) Zhu, L.; Zheng, J.; Yu, C.; Zhang, N.; Shu, Q.; Zhou, H.; Li, Y.; Chen, B. H. Effect of the Thermal Treatment Temperature of RuNi Bimetallic Nanocatalysts on Their Catalytic Performance for Benzene Hydrogenation. *RSC Adv.* **2016**, *6*, 13110−13119.
(163) Singh, P.; Buttry, D. A. Comparison of Oxygen Reduction Reaction at Silver Nanoparticles and Polycrystalline Silver Electrodes in Alkaline Solution. *J. Phys. Chem. C* **2012**, *116*, 10656−10663.
(164) Piccolo, L.; Li, Z. Y.; Demiroglu, I.; Moyon, F.; Konuspayeva, Z.; Berhault, G.; Afanasiev, P.; Lefebvre, W.; Yuan, J.; Johnston, R. L. Understanding and Controlling the Structure and Segregation Behaviour of AuRh Nanocatalysts. *Sci. Rep.* **2016**, *6*, 1−8.
(165) Hansen, T. W.; Delariva, A. T.; Challa, S. R.; Datye, A. K. Sintering of Catalytic Nanoparticles: Particle Migration or Ostwald Ripening ? *Acc. Chem. Res.* **2013**, *46*, 1720−1730.
(166) Behafarid, F.; Roldan Cuenya, B. Towards the Understanding of Sintering Phenomena at the Nanoscale: Geometric and Environmental Effects. *Top. Catal.* **2013**, *56*, 1542−1559.
(167) Wang, H.; Rempel, G. L. Bimetallic Dendrimer-Encapsulated Nanoparticle Catalysts. *Polym. Rev.* **2016**, *56*, 486−511.
(168) Myers, V. S.; Weir, M. G.; Carino, E. V.; Yancey, D. F.; Pande, S.; Crooks, R. M. Dendrimer-Encapsulated Nanoparticles: New Synthetic and Characterization Methods and Catalytic Applications. *Chem. Sci.* **2011**, *2*, 1632−1646.
(169) Luo, L.; Duan, Z.; Li, H.; Kim, J.; Henkelman, G.; Crooks, R. M. Tunability of the Adsorbate Binding on Bimetallic Alloy Nanoparticles for the Optimization of Catalytic Hydrogenation. *J. Am. Chem. Soc.* **2017**, *139*, 5538−5546.
(170) Gatard, S.; Deraedt, C.; Rapakousiou, A.; Sonet, D.; Salmon, L.; Ruiz, J.; Astruc, D. New Polysilyl Dendritic Precursors of Triazolylferrocenyl and Triazolylcobalticenium Dendrimers-Comparative Electrochemical Study and Stabilization of Small, Catalytically Active Pd Nanoparticles. *Organometallics* **2015**, *34*, 1643−1650.
(171) Inomata, Y.; Albrecht, K.; Yamamoto, K. Size-Dependent Oxidation State and CO Oxidation Activity of Tin Oxide Clusters. *ACS Catal.* **2018**, *8*, 451−456.
(172) Yamamoto, K.; Imaoka, T. Precision Synthesis of Subnanoparticles Using Dendrimers as a Superatom Synthesizer. *Acc. Chem. Res.* **2014**, *47*, 1127−1136.
(173) Kambe, T.; Hosono, R.; Imaoka, T.; Yamamoto, K. Ultra-Small Bismuth Particle in Dendrimer Protected by Polyvinylpyrrolidone. *J. Photopolym. Sci. Technol.* **2018**, *31*, 311−314.
(174) Yancey, D. F.; Zhang, L.; Crooks, R. M.; Henkelman, G. Au@Pt Dendrimer Encapsulated Nanoparticles as Model Electrocatalysts for Comparison of Experiment and Theory. *Chem. Sci.* **2012**, *3*, 1033−1040.
(175) Luo, L.; Zhang, L.; Henkelman, G.; Crooks, R. M. Unusual Activity Trend for CO Oxidation on Pd_xAu_{140-x}@Pt Core@Shell Nanoparticle Electrocatalysts. *J. Phys. Chem. Lett.* **2015**, *6*, 2562−2568.
(176) Weir, M. G.; Knecht, M. R.; Frenkel, A. I.; Crooks, R. M. Structural Analysis of PdAu Dendrimer-Encapsulated Bimetallic Nanoparticles. *Langmuir* **2010**, *26*, 1137−1146.
(177) Gomez, M. V.; Guerra, J.; Velders, A. H.; Crooks, R. M. NMR Characterization of Fourth-Generation PAMAM Dendrimers in the Presence and Absence of Palladium Dendrimer-Encapsulated Nanoparticles. *J. Am. Chem. Soc.* **2009**, *131*, 341−350.
(178) Gröhn, F.; Bauer, B. J.; Akpalu, Y. A.; Jackson, C. L.; Amis, E. J. Dendrimer Templates for the Formation of Gold Nanoclusters. *Macromolecules* **2000**, *33*, 6042−6050.
(179) Wang, H.; Rempel, G. L. Bimetallic Dendrimer-Encapsulated Nanoparticle Catalysts. *Polym. Rev.* **2016**, *56*, 486−511.
(180) Gates, A. T.; Nettleton, E. G.; Myers, V. S.; Crooks, R. M. Synthesis and Characterization of NiSn Dendrimer-Encapsulated Nanoparticles. *Langmuir* **2010**, *26*, 12994−12999.
(181) Carino, E. V.; Crooks, R. M. Characterization of Pt @ Cu Core @ Shell Dendrimer-Encapsulated Nanoparticles Synthesized by Cu Underpotential Deposition. *Langmuir* **2011**, *27*, 4227−4235.
(182) Luo, L.; Timoshenko, J.; Lapp, A. S.; Frenkel, A. I.; Crooks, R. M. Structural Characterization of Rh and RhAu Dendrimer-Encapsulated Nanoparticles. *Langmuir* **2017**, *33*, 12434−12442.
(183) Knecht, M. R.; Weir, M. G.; Frenkel, A. I.; Crooks, R. M. Structural Rearrangement of Bimetallic Alloy PdAu Nanoparticles within Dendrimer Templates to Yield Core/Shell Configuration. *Chem. Mater.* **2008**, *20*, 1019−1028.
(184) Anderson, R. M.; Zhang, L.; Loussaert, J. A.; Frenkel, A. I.; Henkelman, G.; Crooks, R. M. An Experimental and Theoretical Investigation of the Inversion of Pd@Pt. *ACS Nano* **2013**, *7*, 9345−9353.
(185) Yancey, D. F.; Carino, E. V.; Crooks, R. M. Electrochemical Synthesis and Electrocatalytic Properties of Au@Pt Dendrimer-Encapsulated Nanoparticles. *J. Am. Chem. Soc.* **2010**, *132*, 10988−10989.
(186) Bernechea, M.; García-Rodríguez, S.; Terreros, P.; De Jesús, E.; Fierro, J. L. G.; Rojas, S. Synthesis of Core-Shell PtRu Dendrimer-Encapsulated Nanoparticles. Relevance as Electrocatalysts for CO Oxidation. *J. Phys. Chem. C* **2011**, *115*, 1287−1294.
(187) Iyyamperumal, R.; Zhang, L.; Henkelman, G.; Crooks, R. M. Efficient Electrocatalytic Oxidation of Formic Acid Using Au@Pt. *J. Am. Chem. Soc.* **2013**, *135*, 5521−5524.
(188) Yin, C.; Tyo, E. C.; Kuchta, K.; von Issendorff, B.; Vajda, S. Atomically Precise (Catalytic) Particles Synthesized by a Novel Cluster Deposition Instrument. *J. Chem. Phys.* **2014**, *140*, 174201.
(189) Von Weber, A.; Anderson, S. L. Electrocatalysis by Mass-Selected Ptn Clusters. *Acc. Chem. Res.* **2016**, *49*, 2632−2639.
(190) Halder, A.; Curtiss, L. A.; Fortunelli, A.; Vajda, S. Perspective: Size Selected Clusters for Catalysis and Electrochemistry. *J. Chem. Phys.* **2018**, *148*, 110901.
(191) Vajda, S.; White, M. G. Catalysis Applications of Size-Selected Cluster Deposition. *ACS Catal.* **2015**, *5*, 7152−7176.
(192) Halder, A.; Liu, C.; Liu, Z.; Emery, J. D.; Pellin, M. J.; Curtiss, L. A.; Zapol, P.; Vajda, S.; Martinson, A. B. F. Water Oxidation Catalysis via Size-Selected Iridium Clusters. *J. Phys. Chem. C* **2018**, *122*, 9965−9972.
(193) Yang, B.; Liu, C.; Halder, A.; Tyo, E. C.; Martinson, A. B. F.; Seifert, S.; Zapol, P.; Curtiss, L. A.; Vajda, S. Copper Cluster Size Effect in Methanol Synthesis from CO2. *J. Phys. Chem. C* **2017**, *121*, 10406−10412.
(194) Ustarroz, J.; Ornelas, I. M.; Zhang, G.; Perry, D.; Kang, M.; Bentley, C. L.; Walker, M.; Unwin, P. R. Mobility and Poisoning of Mass-Selected Platinum Nanoclusters during the Oxygen Reduction Reaction. *ACS Catal.* **2018**, *8*, 6775−6790.
(195) Papaefthimiou, V.; Tournus, F.; Hillion, A.; Khadra, G.; Teschner, D.; Knop-Gericke, A.; Dupuis, V.; Zafeiratos, S. Mixing Patterns and Redox Properties of Iron-Based Alloy Nanoparticles under Oxidation and Reduction Conditions. *Chem. Mater.* **2014**, *26*, 1553−1560.
(196) Velázquez-Palenzuela, A.; Masini, F.; Pedersen, A. F.; Escudero-Escribano, M.; Deiana, D.; Malacrida, P.; Hansen, T. W.; Friebel, D.; Nilsson, A.; Stephens, I. E. L.; et al. The Enhanced Activity of Mass-Selected PtxGd Nanoparticles for Oxygen Electroreduction. *J. Catal.* **2015**, *328*, 297−307.
(197) Lapp, A. S.; Duan, Z.; Marcella, N.; Luo, L.; Henkelman, G.; Ringnalda, J.; Frenkel, A. I.; Crooks, R. M. Experimental and Theoretical Structural Investigation of AuPt Nanoparticles Synthesized Using a Direct Electrochemical Method. *J. Am. Chem. Soc.* **2018**, *140*, 6249−6259.
(198) He, X.; Wang, Y.; Zhang, X.; Dong, M.; Wang, G.; Zhang, B.; Niu, Y.; Yao, S.; He, X.; Liu, H. Controllable in Situ Surface Restructuring of Cu Catalysts and Remarkable Enhancement of Their Catalytic Activity. *ACS Catal.* **2019**, *9*, 2213−2221.
(199) Epp, J. X-Ray Diffraction (XRD) Techniques for Materials Characterization. In *Materials Characterization Using Nondestructive Evaluation (NDE) Methods*; Elsevier: St. Louis, 2016; pp 81−124.
(200) Dinnebier, R. E.; Billinge, S. J. L. Principles of Powder Diffraction. *Powder Diffraction: Theory and Practice*; RSC Publishing: Cambridge, 2008; pp 1−19.

DOI: 10.1021/acs.chemrev.9b00246
Chem. Rev. XXXX, XXX, XXX−XXX

(201) Celorrio, V.; Montes de Oca, M. G.; Plana, D.; Moliner, R.; Lazaro, M. J.; Fermín, D. J. Effect of Carbon Supports on Electrocatalytic Reactivity of Au−Pd Core−Shell Nanoparticles. *J. Phys. Chem. C* **2012**, *116*, 6275−6282.
(202) Ren, Y. High-Energy Synchrotron x-Ray Diffraction and Its Application to in Situ Structural Phase-Transition Studies in Complex Sample Environments. *JOM* **2012**, *64*, 140−149.
(203) Billinge, S. Local Structure from Total Scattering and Atomic Pair Distribution Function (PDF) Analysis. *Powder Diffraction: Theory and Practice*; RSC Publishing: Cambridge, 2008; pp 464−493.
(204) Banerjee, S.; Liu, C. H.; Lee, J. D.; Kovyakh, A.; Grasmik, V.; Prymak, O.; Koenigsmann, C.; Liu, H.; Wang, L.; Abeykoon, A. M. M.; et al. Improved Models for Metallic Nanoparticle Cores from Atomic Pair Distribution Function (PDF) Analysis. *J. Phys. Chem. C* **2018**, *122*, 29498−29506.
(205) Wu, J.; Shan, S.; Cronk, H.; Chang, F.; Kareem, H.; Zhao, Y.; Luo, J.; Petkov, V.; Zhong, C. J. Understanding Composition-Dependent Synergy of PtPd Alloy Nanoparticles in Electrocatalytic Oxygen Reduction Reaction. *J. Phys. Chem. C* **2017**, *121*, 14128−14136.
(206) Knecht, M. R.; Weir, M. G.; Myers, V. S.; Pyrz, W. D.; Ye, H.; Petkov, V.; Buttrey, D. J.; Frenkel, A. I.; Crooks, R. M. Synthesis and Characterization of Pt Dendrimer-Encapsulated Nanoparticles: Effect of the Template on Nanoparticle Formation. *Chem. Mater.* **2008**, *20*, 5218−5228.
(207) Petkov, V.; Prasai, B.; Shan, S.; Ren, Y.; Wu, J.; Cronk, H.; Luo, J.; Zhong, C.-J. Structural Dynamics and Activity of Nano-catalysts inside Fuel Cells by in Operando Atomic Pair Distribution Studies. *Nanoscale* **2016**, *8*, 10749−10767.
(208) Schmies, H.; Wang, G.; Kühl, S.; Bergmann, A.; Strasser, P.; Hornberger, E.; Drnec, J.; Sandbeck, D. J. S.; Cherevko, S.; Mayrhofer, K. J. J.; et al. In Situ Stability Studies of Platinum Nanoparticles Supported on Ruthenium−Titanium Mixed Oxide (RTO) for Fuel Cell Cathodes. *ACS Catal.* **2018**, *8*, 9675−9683.
(209) LiBretto, N. J.; Ren, Y.; Zhang, G.; Miller, J. T.; Yang, C. Identification of Surface Structures in Pt3Cr Intermetallic Nano-catalysts. *Chem. Mater.* **2019**, *31*, 1597−1609.
(210) Tuaev, X.; Rudi, S.; Petkov, V.; Hoell, A.; Strasser, P. In Situ Study of Atomic Structure Transformations of Pt-Ni Nanoparticle Catalysts during Electrochemical Potential Cycling. *ACS Nano* **2013**, *7*, 5666−5674.
(211) Li, T.; Senesi, A. J.; Lee, B. Small Angle X-Ray Scattering for Nanoparticle Research. *Chem. Rev.* **2016**, *116*, 11128−11180.
(212) Gilbert, J. A.; Kariuki, N. N.; Wang, X.; Kropf, A. J.; Yu, K.; Groom, D. J.; Ferreira, P. J.; Morgan, D.; Myers, D. J. Pt Catalyst Degradation in Aqueous and Fuel Cell Environments Studied via In-Operando Anomalous Small-Angle X-Ray Acattering. *Electrochim. Acta* **2015**, *173*, 223−234.
(213) Ingham, B.; Lim, T. H.; Dotzler, C. J.; Henning, A.; Toney, M. F.; Tilley, R. D. How Nanoparticles Coalesce: An in Situ Study of Au Nanoparticle Aggregation and Grain Growth. *Chem. Mater.* **2011**, *23*, 3312−3317.
(214) Binninger, T.; Garganourakis, M.; Han, J.; Patru, A.; Fabbri, E.; Sereda, O.; Kötz, R.; Menzel, A.; Schmidt, T. J. Particle-Support Interferences in Small-Angle X-Ray Scattering from Supported-Catalyst Materials. *Phys. Rev. Appl.* **2015**, *3*, 1−6.
(215) Yu, C.; Koh, S.; Leisch, J. E.; Toney, M. F.; Strasser, P. Size and Composition Distribution Dynamics of Alloy Nanoparticle Electrocatalysts Probed by Anomalous Small Angle X-Ray Scattering (ASAXS). *Faraday Discuss.* **2009**, *140*, 283−296.
(216) Watts, J. F.; Wolstenholme, J. *An Introduction to Surface Analysis by XPS and AES*; John Wiley & Sons, Ltd.: Hoboken, 2003; Vol. 3.
(217) Doh, W. H.; Papaefthimiou, V.; Dintzer, T.; Dupuis, V.; Zafeiratos, S. Synchrotron Radiation X-Ray Photoelectron Spectroscopy as a Tool to Resolve the Dimensions of Spherical Core/Shell Nanoparticles. *J. Phys. Chem. C* **2014**, *118*, 26621−26628.
(218) Powell, C. J.; Werner, W. S. M.; Shard, A. G.; Castner, D. G. Evaluation of Two Methods for Determining Shell Thicknesses of Core-Shell Nanoparticles by X-Ray Photoelectron Spectroscopy. *J. Phys. Chem. C* **2016**, *120*, 22730−22738.
(219) Chudzicki, M.; Werner, W. S. M.; Shard, A. G.; Wang, Y. C.; Castner, D. G.; Powell, C. J. Evaluating the Internal Structure of Core-Shell Nanoparticles Using X-Ray Photoelectron Intensities and Simulated Spectra. *J. Phys. Chem. C* **2015**, *119*, 17687−17696.
(220) Powell, C. J.; Werner, W. S. M.; Kalbe, H.; Shard, A. G.; Castner, D. G. Comparisons of Analytical Approaches for Determining Shell Thicknesses of Core-Shell Nanoparticles by X-Ray Photoelectron Spectroscopy. *J. Phys. Chem. C* **2018**, *122*, 4073−4082.
(221) Alayoglu, S.; Somorjai, G. A. Ambient Pressure X-Ray Photoelectron Spectroscopy for Probing Monometallic, Bimetallic and Oxide-Metal Catalysts under Reactive Atmospheres and Catalytic Reaction Conditions. *Top. Catal.* **2016**, *59*, 420−438.
(222) Arble, C.; Jia, M.; Newberg, J. T. Lab-Based Ambient Pressure X-Ray Photoelectron Spectroscopy from Past to Present. *Surf. Sci. Rep.* **2018**, *73*, 37−57.
(223) Salmeron, M. From Surfaces to Interfaces: Ambient Pressure XPS and Beyond. *Top. Catal.* **2018**, *61*, 2044−2051.
(224) Tsyshevsky, R.; Fears, K.; Kuklja, M. M.; Head, A. R.; Eichhorn, B.; Trotochaud, L.; Bluhm, H. Coupling Ambient Pressure X-Ray Photoelectron Spectroscopy with Density Functional Theory to Study Complex Surface Chemistry and Catalysis. *Top. Catal.* **2018**, *61*, 2175−2184.
(225) Knop-Gericke, A.; Stotz, E.; Arrigo, R.; Hävecker, M.; Velasco Vélez, J. J.; Streibel, V.; Schlögl, R.; Yi, Y.; Skorupska, K. In Situ Electrochemical Cells to Study the Oxygen Evolution Reaction by Near Ambient Pressure X-Ray Photoelectron Spectroscopy. *Top. Catal.* **2018**, *61*, 2064−2084.
(226) Booth, S. G.; Tripathi, A. M.; Strashnov, I.; Dryfe, R. A. W.; Walton, A. S. The Offset Droplet: A New Methodology for Studying the Solid/Water Interface Using x-Ray Photoelectron Spectroscopy. *J. Phys.: Condens. Matter* **2017**, *29*, 454001.
(227) Penner-Hahn, J. E. X-Ray Absorption Spectroscopy. *Comprehensive Coordination Chemistry II*; Elsevier: St. Louis, 2011; pp 159−186.
(228) Liu, H.; An, W.; Li, Y.; Frenkel, A. I.; Sasaki, K.; Koenigsmann, C.; Su, D.; Anderson, R. M.; Crooks, R. M.; Adzic, R. R.; et al. In Situ Probing of the Active Site Geometry of Ultrathin Nanowires for the Oxygen Reduction Reaction. *J. Am. Chem. Soc.* **2015**, *137*, 12597−12609.
(229) Yang, Y.; Wang, Y.; Xiong, Y.; Huang, X.; Shen, L.; Huang, R.; Wang, H.; Pastore, J. P.; Yu, S.; Xiao, L.; et al. In Situ X-ray Absorption Spectroscopy of a Synergistic Co−Mn Oxide Catalyst for the Oxygen Reduction Reaction. *J. Am. Chem. Soc.* **2019**, *141*, 1463−1466.
(230) Myers, V. S.; Frenkel, A. I.; Crooks, R. M. In Situ Structural Characterization of Platinum Dendrimer-Encapsulated Oxygen Reduction Electrocatalysts. *Langmuir* **2012**, *28*, 1596−1603.
(231) Kim, D.; Xie, C.; Becknell, N.; Yu, Y.; Karamad, M.; Chan, K.; Crumlin, E. J.; Nørskov, J. K.; Yang, P. Electrochemical Activation of CO2 through Atomic Ordering Transformations of AuCu Nano-particles. *J. Am. Chem. Soc.* **2017**, *139*, 8329−8336.
(232) Su, J.; Ge, R.; Dong, Y.; Hao, F.; Chen, L. Recent Progress in Single-Atom Electrocatalysts: Concept, Synthesis, and Applications in Clean Energy Conversion. *J. Mater. Chem. A* **2018**, *6*, 14025−14042.
(233) Peng, Y.; Lu, B.; Chen, S. Carbon-Supported Single Atom Catalysts for Electrochemical Energy Conversion and Storage. *Adv. Mater.* **2018**, *30*, 1801995.
(234) Su, X.; Yang, X.; Huang, Y.; Liu, B.; Zhang, T. Single-Atom Catalysis toward Efficient CO2 Conversion to CO and Formate Products. *Acc. Chem. Res.* **2019**, *52*, 656−664.
(235) O'Mullane, A. P. From Single Crystal Surfaces to Single Atoms: Investigating Active Sites in Electrocatalysis. *Nanoscale* **2014**, *6*, 4012−4026.
(236) Meier, J. C.; Katsounaros, I.; Galeano, C.; Bongard, H. J.; Topalov, A. A.; Kostka, A.; Karschin, A.; Schüth, F.; Mayrhofer, K. J. J.

DOI: 10.1021/acs.chemrev.9b00246
Chem. Rev. XXXX, XXX, XXX−XXX

Stability Investigations of Electrocatalysts on the Nanoscale. *Energy Environ. Sci.* **2012**, *5*, 9319−9330.
(237) Zana, A.; Arenz, M.; Altmann, L.; Speder, J.; Bäumer, M.; Roefzaad, M. Probing Degradation by IL-TEM: The Influence of Stress Test Conditions on the Degradation Mechanism. *J. Electrochem. Soc.* **2013**, *160*, F608−F615.
(238) Lafforgue, C.; Zadick, A.; Dubau, L.; Maillard, F.; Chatenet, M. Selected Review of the Degradation of Pt and Pd-Based Carbon-Supported Electrocatalysts for Alkaline Fuel Cells: Towards Mechanisms of Degradation. *Fuel Cells* **2018**, *18*, 229−238.
(239) Teixeira-Neto, E.; Souza, N. E.; Ticianelli, E. A.; Rocha, T. A.; da Silva, G. C.; Gonzalez, E. R.; Bott-Neto, J. L. Support Modification in Pt/C Electrocatalysts for Durability Increase: A Degradation Study Assisted by Identical Location Transmission Electron Microscopy. *Electrochim. Acta* **2018**, *265*, 523−531.
(240) Sytwu, K.; Hayee, F.; Narayan, T. C.; Koh, A. L.; Sinclair, R.; Dionne, J. A. Visualizing Facet-Dependent Hydrogenation Dynamics in Individual Palladium Nanoparticles. *Nano Lett.* **2018**, *18*, 5357−5363.
(241) Beermann, V.; Gocyla, M.; Kühl, S.; Padgett, E.; Schmies, H.; Goerlin, M.; Erini, N.; Shviro, M.; Heggen, M.; Dunin-Borkowski, R. E.; et al. Tuning the Electrocatalytic Oxygen Reduction Reaction Activity and Stability of Shape-Controlled Pt-Ni Nanoparticles by Thermal Annealing -Elucidating the Surface Atomic Structural and Compositional Changes. *J. Am. Chem. Soc.* **2017**, *139*, 16536−16547.
(242) Rodríguez, P.; Plana, D.; Fermín, D. J.; Koper, M. T. M. New Insights into the Catalytic Activity of Gold Nanoparticles for CO Oxidation in Electrochemical Media. *J. Catal.* **2014**, *311*, 182−189.
(243) Peng, Y.; Lu, B.; Wang, N.; Li, L.; Chen, S. Impacts of Interfacial Charge Transfer on Nanoparticle Electrocatalytic Activity towards Oxygen Reduction. *Phys. Chem. Chem. Phys.* **2017**, *19*, 9336−9348.
(244) Min, X.; Kanan, M. W. Pd-Catalyzed Electrohydrogenation of Carbon Dioxide to Formate: High Mass Activity at Low Overpotential and Identification of the Deactivation Pathway. *J. Am. Chem. Soc.* **2015**, *137*, 4701−4708.
(245) Park, H.; Choi, J.; Kim, H.; Hwang, E.; Ha, D. H.; Ahn, S. H.; Kim, S. K. AgIn Dendrite Catalysts for Electrochemical Reduction of CO2 to CO. *Appl. Catal., B* **2017**, *219*, 123−131.
(246) Arán-Ais, R. M.; Yu, Y.; Hovden, R.; Solla-Gullón, J.; Herrero, E.; Feliu, J. M.; Abruña, H. D. Identical Location Transmission Electron Microscopy Imaging of Site-Selective Pt Nanocatalysts: Electrochemical Activation and Surface Disordering. *J. Am. Chem. Soc.* **2015**, *137*, 14992−14998.
(247) Fowler, B.; Lucas, C. A.; Omer, A.; Wang, G.; Stamenković, V. R.; Marković, N. M. Segregation and Stability at Pt3Ni(111) Surfaces and Pt75Ni25 Nanoparticles. *Electrochim. Acta* **2008**, *53*, 6076−6080.
(248) Grgur, B. N.; Marković, N. M.; Ross, P. N. Electrooxidation of H2, CO, and H2/CO Mixtures on a Well-Characterized Pt70Mo30 Bulk Alloy Electrode. *J. Phys. Chem. B* **1998**, *102*, 2494−2501.
(249) Zhang, S.; Zhang, X.; Jiang, G.; Zhu, H.; Guo, S.; Su, D.; Lu, G.; Sun, S. Tuning Nanoparticle Structure and Surface Strain for Catalysis Optimization. *J. Am. Chem. Soc.* **2014**, *136*, 7734−7739.
(250) Sharma, M.; Jung, N.; Yoo, S. J. Toward High-Performance Pt-Based Nanocatalysts for Oxygen Reduction Reaction through Organic−Inorganic Hybrid Concepts. *Chem. Mater.* **2018**, *30*, 2−24.
(251) Farias, M. J. S.; Cheuquepán, W.; Tanaka, A. A.; Feliu, J. M. Nonuniform Synergistic Effect of Sn and Ru in Site-Specific Catalytic Activity of Pt at Bimetallic Surfaces toward CO Electro-Oxidation. *ACS Catal.* **2017**, *7*, 3434−3445.
(252) Koper, M. T. M. Structure Sensitivity and Nanoscale Effects in Electrocatalysis. *Nanoscale* **2011**, *3*, 2054−2073.
(253) Zhang, L.; Anderson, R. M.; Crooks, R. M.; Henkelman, G. Correlating Structure and Function of Metal Nanoparticles for Catalysis. *Surf. Sci.* **2015**, *640*, 65−72.
(254) Feng, X.; Jiang, K.; Fan, S.; Kanan, M. W. A Direct Grain-Boundary-Activity Correlation for CO Electroreduction on Cu Nanoparticles. *ACS Cent. Sci.* **2016**, *2*, 169−174.
(255) Monzó, J.; Malewski, Y.; Kortlever, R.; Vidal-Iglesias, F. J.; Solla-Gullón, J.; Koper, M. T. M.; Rodríguez, P. Enhanced Electrocatalytic Activity of Au@Cu Core@shell Nanoparticles towards CO2 Reduction. *J. Mater. Chem. A* **2015**, *3*, 23690−23698.
(256) Kim, C.; Jeon, H. S.; Eom, T.; Jee, M. S.; Kim, H.; Friend, C. M.; Min, B. K.; Hwang, Y. J. Achieving Selective and Efficient Electrocatalytic Activity for CO2 Reduction Using Immobilized Silver Nanoparticles. *J. Am. Chem. Soc.* **2015**, *137*, 13844−13850.
(257) Cao, Z.; Zacate, S. B.; Sun, X.; Liu, J.; Hale, E. M.; Carson, W. P.; Tyndall, S. B.; Xu, J.; Liu, X.; Liu, X.; et al. Tuning Gold Nanoparticles with Chelating Ligands for Highly Efficient Electrocatalytic CO2 Reduction. *Angew. Chem., Int. Ed.* **2018**, *57*, 12675−12679.
(258) Wang, Z.; Wu, L.; Sun, K.; Chen, T.; Jiang, Z.; Cheng, T.; Goddard, W. A., III Surface Ligand Promotion of Carbon Dioxide Reduction through Stabilizing Chemisorbed Reactive Intermediates. *J. Phys. Chem. Lett.* **2018**, *9*, 3057−3061.
(259) Mayrhofer, K. J. J.; Juhart, V.; Hartl, K.; Hanzlik, M.; Arenz, M. Adsorbate-Induced Surface Segregation for Core-Shell Nanocatalysts. *Angew. Chem., Int. Ed.* **2009**, *48*, 3529−3531.
(260) Yu, L.; Akolkar, R. Lead Underpotential Deposition for the Surface Characterization of Silver Ad-Atom Modified Gold Electrocatalysts for Glucose Oxidation. *J. Electroanal. Chem.* **2017**, *792*, 61−65.
(261) Baturina, O. A.; Lu, Q.; Padilla, M. A.; Xin, L.; Li, W.; Serov, A.; Artyushkova, K.; Atanassov, P.; Xu, F.; Epshteyn, A.; et al. CO2 Electroreduction to Hydrocarbons on Carbon-Supported Cu Nanoparticles. *ACS Catal.* **2014**, *4*, 3682−3695.
(262) Kumar, A.; Buttry, D. A. Size-Dependent Underpotential Deposition of Copper on Palladium Nanoparticles. *J. Phys. Chem. C* **2015**, *119*, 16927−16933.
(263) Hernández, J.; Herrero, E.; Feliu, J. M.; Aldaz, A. In Situ Surface Characterization and Oxygen Reduction Reaction on Shape-Controlled Gold Nanoparticles. *J. Nanosci. Nanotechnol.* **2009**, *9*, 2256−2273.
(264) Hebié, S.; Napporn, T. W.; Morais, C.; Kokoh, K. B. Size-Dependent Electrocatalytic Activity of Free Gold Nanoparticles for the Glucose Oxidation Reaction. *ChemPhysChem* **2016**, *17*, 1454−1462.
(265) Oviedo, O. A.; Vélez, P.; Macagno, V. A.; Leiva, E. P. M. Surface Science Underpotential Deposition: From Planar Surfaces to Nanoparticles. *Surf. Sci.* **2015**, *631*, 23−34.
(266) Carino, E. V.; Kim, H. Y.; Henkelman, G.; Crooks, R. M. Site-Selective Cu Deposition on Pt Dendrimer-Encapsulated Nanoparticles: Correlation of Theory and Experiment. *J. Am. Chem. Soc.* **2012**, *134*, 4153−4162.
(267) Luo, L.; Zhang, L.; Duan, Z.; Lapp, A. S.; Henkelman, G.; Crooks, R. M. Efficient CO Oxidation Using Dendrimer-Encapsulated Pt Nanoparticles Activated with < 2% Cu Surface Atoms. *ACS Nano* **2016**, *10*, 8760−8769.
(268) Busch, M.; Halck, N. B.; Kramm, U. I.; Siahrostami, S.; Krtil, P.; Rossmeisl, J. Beyond the Top of the Volcano? − A Unified Approach to Electrocatalytic Oxygen Reduction and Oxygen Evolution. *Nano Energy* **2016**, *29*, 126−135.
(269) Janik, M. J.; Taylor, C. D.; Neurock, M. First-Principles Analysis of the Initial Electroreduction Steps of Oxygen over Pt(111). *J. Electrochem. Soc.* **2009**, *156*, B126−B135.
(270) Mavrikakis, M.; Hammer, B.; Nørskov, J. K. Effect of Strain on the Reactivity of Metal Surfaces. *Phys. Rev. Lett.* **1998**, *81*, 2819−2822.
(271) Kitchin, J. R.; Nørskov, J. K.; Barteau, M. A.; Chen, J. G. Modification of the Surface Electronic and Chemical Properties of Pt(111) by Subsurface 3d Transition Metals. *J. Chem. Phys.* **2004**, *120*, 10240−10246.
(272) Duan, Z.; Wang, G. A First Principles Study of Oxygen Reduction Reaction on a Pt(111) Surface Modified by a Subsurface Transition Metal M (M = Ni, Co, or Fe). *Phys. Chem. Chem. Phys.* **2011**, *13*, 20178−20187.
(273) Zhang, J.; Vukmirovic, M. B.; Sasaki, K.; Nilekar, A. U.; Mavrikakis, M.; Adzic, R. R. Mixed-Metal Pt Monolayer Electro-

DOI: 10.1021/acs.chemrev.9b00246
Chem. Rev. XXXX, XXX, XXX−XXX

catalysts for Enhanced Oxygen Reduction Kinetics. *J. Am. Chem. Soc.* **2005**, *127*, 12480−12481.
(274) Nilekar, A. U.; Mavrikakis, M. Improved Oxygen Reduction Reactivity of Platinum Monolayers on Transition Metal Surfaces. *Surf. Sci.* **2008**, *602*, L89−L94.
(275) Wang, L.; Zeng, Z.; Ma, C.; Liu, Y.; Giroux, M.; Chi, M.; Jin, J.; Greeley, J. P.; Wang, C. Plating Precious Metals on Nonprecious Metal Nanoparticles for Sustainable Electrocatalysts. *Nano Lett.* **2017**, *17*, 3391−3395.
(276) Wang, L.; Gao, W.; Liu, Z.; Zeng, Z.; Liu, Y.; Giroux, M.; Chi, M.; Wang, G.; Greeley, J. P.; Pan, X.; et al. Core-Shell Nanostructured Cobalt-Platinum Electrocatalysts with Enhanced Durability. *ACS Catal.* **2018**, *8*, 35−42.
(277) Nair, A. S.; Pathak, B. Computational Screening for ORR Activity of 3d Transition Metal Based M@Pt Core−Shell Clusters. *J. Phys. Chem. C* **2019**, *123*, 3634−3644.
(278) Yang, L.; Vukmirovic, M. B.; Su, D.; Sasaki, K.; Herron, J. A.; Mavrikakis, M.; Liao, S.; Adzic, R. R. Tuning the Catalytic Activity of Ru@Pt Core-Shell Nanoparticles for the Oxygen Reduction Reaction by Varying the Shell Thickness. *J. Phys. Chem. C* **2013**, *117*, 1748−1753.
(279) Brankovic, S. R.; Wang, J. X.; Adžić, R. R. Metal Monolayer Deposition by Replacement of Metal Adlayers on Electrode Surfaces. *Surf. Sci.* **2001**, *474*, L173−L179.
(280) Todoroki, N.; Watanabe, H.; Kondo, T.; Kaneko, S.; Wadayama, T. Highly Enhanced Oxygen Reduction Reaction Activity and Electrochemical Stability of Pt/Ir(111) Bimetallic Surfaces. *Electrochim. Acta* **2016**, *222*, 1616−1621.
(281) Friebel, D.; Viswanathan, V.; Miller, D. J.; Anniyev, T.; Ogasawara, H.; Larsen, A. H.; O'Grady, C. P.; Nørskov, J. K.; Nilsson, A. Balance of Nanostructure and Bimetallic Interactions in Pt Model Fuel Cell Catalysts: In Situ XAS and DFT Study. *J. Am. Chem. Soc.* **2012**, *134*, 9664−9671.
(282) Strasser, P.; Koh, S.; Anniyev, T.; Greeley, J. P.; More, K.; Yu, C.; Liu, Z.; Kaya, S.; Nordlund, D.; Ogasawara, H.; et al. Lattice-Strain Control of the Activity in Dealloyed Core-Shell Fuel Cell Catalysts. *Nat. Chem.* **2010**, *2*, 454−460.
(283) Fu, T.; Huang, J.; Lai, S.; Zhang, S.; Fang, J.; Zhao, J. Pt Skin Coated Hollow Ag-Pt Bimetallic Nanoparticles with High Catalytic Activity for Oxygen Reduction Reaction. *J. Power Sources* **2017**, *365*, 17−25.
(284) Li, J.; Xi, Z.; Pan, Y.-T.; Spendelow, J. S.; Duchesne, P. N.; Su, D.; Li, Q.; Yu, C.; Yin, Z.; Shen, B.; et al. Fe Stabilization by Intermetallic $L1_0$-FePt and Pt Catalysis Enhancement in $L1_0$-FePt/Pt Nanoparticles for Efficient Oxygen Reduction Reaction in Fuel Cells. *J. Am. Chem. Soc.* **2018**, *140*, 2926−2932.
(285) Corona, B.; Howard, M.; Zhang, L.; Henkelman, G. Computational Screening of Core@shell Nanoparticles for the Hydrogen Evolution and Oxygen Reduction Reactions. *J. Chem. Phys.* **2016**, *145*, 244708.
(286) Bing, Y.; Liu, H.; Zhang, L.; Ghosh, D.; Zhang, J. Nanostructured Pt-Alloy Electrocatalysts for PEM Fuel Cell Oxygen Reduction Reaction. *Chem. Soc. Rev.* **2010**, *39*, 2184−2202.
(287) Kim, C.; Dionigi, F.; Beermann, V.; Wang, X.; Möller, T.; Strasser, P. Alloy Nanocatalysts for the Electrochemical Oxygen Reduction (ORR) and the Direct Electrochemical Carbon Dioxide Reduction Reaction (CO2RR). *Adv. Mater.* **2019**, *31*, 1805617.
(288) He, Y.; Wu, Y. L.; Zhu, X. X.; Wang, J. N. Remarkable Improvement of the Catalytic Performance of PtFe Nanoparticles by Structural Ordering and Doping. *ACS Appl. Mater. Interfaces* **2019**, *11*, 11527−11536.
(289) Stamenkovic, V. R.; Fowler, B.; Mun, B. S.; Wang, G.; Ross, P. N.; Lucas, C. A.; Marković, N. M. Improved Oxygen Reduction Activity on Pt3Ni(111) via Increased Surface Site Availability. *Science* **2007**, *315*, 493−497.
(290) Wang, G.; Van Hove, M. A.; Ross, P. N.; Baskes, M. I. Monte Carlo Simulations of Segregation in Pt-Ni Catalyst Nanoparticles. *J. Chem. Phys.* **2005**, *122*, 024706.
(291) Shviro, M.; Gocyla, M.; Polani, S.; Heggen, M.; Zitoun, D.; Dunin-Borkowski, R. E. Morphological, Structural, and Compositional Evolution of Pt−Ni Octahedral Electrocatalysts with Pt-Rich Edges and Ni-Rich Core: Toward the Rational Design of Electrocatalysts for the Oxygen Reduction Reaction. *Part. Part. Syst. Charact.* **2019**, *36*, 1800442.
(292) Chen, C.; Kang, Y.; Huo, Z.; Zhu, Z.; Huang, W.; Xin, H. L.; Snyder, J. D.; Li, D.; Herron, J. A.; Mavrikakis, M.; et al. Highly Crystalline Multimetallic Nanoframes with Three-Dimensional Electrocatalytic Surfaces. *Science* **2014**, *343*, 1339−1343.
(293) Wu, J.; Qi, L.; You, H.; Gross, A.; Li, J.; Yang, H. Icosahedral Platinum Alloy Nanocrystals with Enhanced Electrocatalytic Activities. *J. Am. Chem. Soc.* **2012**, *134*, 11880−11883.
(294) Wu, J.; Zhang, J.; Peng, Z.; Yang, S.; Wagner, F. T.; Yang, H. Truncated Octahedral Pt3Ni Oxygen Reduction Reaction Electrocatalysts. *J. Am. Chem. Soc.* **2010**, *132*, 4984−4985.
(295) Choi, S.-I.; Xie, S.; Shao, M.; Odell, J. H.; Lu, N.; Peng, H.-C.; Protsailo, L.; Guerrero, S.; Park, J.; Xia, X.; et al. Synthesis and Characterization of 9 Nm Pt−Ni Octahedra with a Record High Activity of 3.3 A/Mg Pt for the Oxygen Reduction Reaction. *Nano Lett.* **2013**, *13*, 3420−3425.
(296) Zhang, J.; Yang, H.; Fang, J.; Zou, S. Synthesis and Oxygen Reduction Activity of Shape-Controlled Pt3Ni Nanopolyhedra. *Nano Lett.* **2010**, *10*, 638−644.
(297) Wu, J.; Gross, A.; Yang, H. Shape and Composition-Controlled Platinum Alloy Nanocrystals Using Carbon Monoxide as Reducing Agent. *Nano Lett.* **2011**, *11*, 798−802.
(298) Chaudhari, N. K.; Joo, J.; Kim, B.; Ruqia, B.; Choi, S. Il; Lee, K. Recent Advances in Electrocatalysts toward the Oxygen Reduction Reaction: The Case of PtNi Octahedra. *Nanoscale* **2018**, *10*, 20073−20088.
(299) Kühl, S.; Gocyla, M.; Heyen, H.; Selve, S.; Heggen, M.; Dunin-Borkowski, R. E.; Strasser, P. Concave Curvature Facets Benefit Oxygen Electroreduction Catalysis on Octahedral Shaped PtNi Nanocatalysts. *J. Mater. Chem. A* **2019**, *7*, 1149−1159.
(300) Cui, C.; Gan, L.; Li, H.-H.; Yu, S.-H.; Heggen, M.; Strasser, P. Octahedral PtNi Nanoparticle Catalysts: Exceptional Oxygen Reduction Activity by Tuning the Alloy Particle Surface Composition. *Nano Lett.* **2012**, *12*, 5885−5889.
(301) Mani, P.; Srivastava, R.; Strasser, P. Dealloyed Binary PtM3 (M = Cu, Co, Ni) and Ternary PtNi3M (M = Cu, Co, Fe, Cr) Electrocatalysts for the Oxygen Reduction Reaction: Performance in Polymer Electrolyte Membrane Fuel Cells. *J. Power Sources* **2011**, *196*, 666−673.
(302) Lokanathan, M.; Patil, I. M.; Navaneethan, M.; Parey, V.; Thapa, R.; Kakade, B. Designing of Stable and Highly Efficient Ordered Pt2CoNi Ternary Alloy Electrocatalyst: The Origin of Dioxygen Reduction Activity. *Nano Energy* **2018**, *43*, 219−227.
(303) Lokanathan, M.; Patil, I. M.; Kakade, B. Trimetallic PtNiCo Nanoflowers as Efficient Electrocatalysts towards Oxygen Reduction Reaction. *Int. J. Hydrogen Energy* **2018**, *43*, 8983−8990.
(304) Leteba, G.; Mitchell, D.; Levecque, P.; Lang, C. Solution-Grown Dendritic Pt-Based Ternary Nanostructures for Enhanced Oxygen Reduction Reaction Functionality. *Nanomaterials* **2018**, *8*, 462.
(305) Kühl, S.; Heyen, H.; Strasser, P. Mo-Doped Shaped Nanoparticles Based on PtNi-Alloys - A Promising ORR Catalyst? *ECS Trans.* **2016**, *75*, 723−730.
(306) Luo, L.; Abbo, H. S.; Titinchi, S. J. J.; Tsiakaras, P.; Yin, S. Highly Efficient Electrocatalysts for Oxygen Reduction Reaction: Nitrogen-Doped PtNiMo Ternary Alloys. *Int. J. Hydrogen Energy* **2019**, *44*, 6582−6591.
(307) Huang, X.; Zhao, Z.; Cao, L.; Chen, Y.; Zhu, E.; Lin, Z.; Li, M.; Yan, A.; Zettl, A.; Wang, Y. M.; et al. High-Performance Transition Metal−Doped Pt3Ni Octahedra for Oxygen Reduction Reaction. *Science* **2015**, *348*, 1230−1234.
(308) Dai, Y.; Ou, L.; Liang, W.; Yang, F.; Liu, Y.; Chen, S. Efficient and Superiorly Durable Pt-Lean Electrocatalysts of Pt−W Alloys for

DOI: 10.1021/acs.chemrev.9b00246
Chem. Rev. XXXX, XXX, XXX−XXX

the Oxygen Reduction Reaction. *J. Phys. Chem. C* **2011**, *115*, 2162−2168.
(309) Wang, Y. Y.; Chen, D. J.; Tong, Y. Y. J. Mechanistic Insight into Sulfide-Enhanced Oxygen Reduction Reaction Activity and Stability of Commercial Pt Black: An in Situ Raman Spectroscopic Study. *ACS Catal.* **2016**, *6*, 5000−5004.
(310) Wang, Y. Y.; Chen, D. J.; Allison, T. C.; Tong, Y. J. Effect of Surface-Bound Sulfide on Oxygen Reduction Reaction on Pt: Breaking the Scaling Relationship and Mechanistic Insights. *J. Chem. Phys.* **2019**, *150*, 041728.
(311) Greeley, J.; Stephens, I. E. L.; Bondarenko, A. S.; Johansson, T. P.; Hansen, H. A.; Jaramillo, T. F.; Rossmeisl, J.; Chorkendorff, I.; Nørskov, J. K. Alloys of Platinum and Early Transition Metals as Oxygen Reduction Electrocatalysts. *Nat. Chem.* **2009**, *1*, 552−556.
(312) Kibler, L. A.; El-Aziz, A. M.; Hoyer, R.; Kolb, D. M. Tuning Reaction Rates by Lateral Strain in a Palladium Monolayer. *Angew. Chem., Int. Ed.* **2005**, *44*, 2080−2084.
(313) Wu, J.; Shan, S.; Luo, J.; Joseph, P.; Petkov, V.; Zhong, C. J. PdCu Nanoalloy Electrocatalysts in Oxygen Reduction Reaction: Role of Composition and Phase State in Catalytic Synergy. *ACS Appl. Mater. Interfaces* **2015**, *7*, 25906−25913.
(314) Liu, S.; Zhang, Q.; Li, Y.; Han, M.; Gu, L.; Nan, C.; Bao, J.; Dai, Z. Five-Fold Twinned Pd2NiAg Nanocrystals with Increased Surface Ni Site Availability to Improve Oxygen Reduction Activity. *J. Am. Chem. Soc.* **2015**, *137*, 2820−2823.
(315) Tang, W.; Zhang, L.; Henkelman, G. Catalytic Activity of Pd/Cu Random Alloy Nanoparticles for Oxygen Reduction. *J. Phys. Chem. Lett.* **2011**, *2*, 1328−1331.
(316) Zhang, L.; Henkelman, G. Tuning the Oxygen Reduction Activity of Pd Shell Nanoparticles with Random Alloy Cores. *J. Phys. Chem. C* **2012**, *116*, 20860−20865.
(317) Wang, G.; Guan, J.; Xiao, L.; Huang, B.; Wu, N.; Lu, J.; Zhuang, L. Pd Skin on AuCu Intermetallic Nanoparticles: A Highly Active Electrocatalyst for Oxygen Reduction Reaction in Alkaline Media. *Nano Energy* **2016**, *29*, 268−274.
(318) Jiang, G.; Zhu, H.; Zhang, X.; Shen, B.; Wu, L.; Zhang, S.; Lu, G.; Wu, Z.; Sun, S. Core/Shell Face-Centered Tetragonal FePd/Pd Nanoparticles as an Efficient Non-Pt Catalyst for the Oxygen Reduction Reaction. *ACS Nano* **2015**, *9*, 11014−11022.
(319) Vojvodic, A.; Nørskov, J. K. New Design Paradigm for Heterogeneous Catalysts. *Natl. Sci. Rev.* **2015**, *2*, 140−149.
(320) Beden, B.; Lamy, C.; de Tacconi, N. R.; Arvia, A. J. The Electrooxidation of CO: A Test Reaction in Electrocatalysis. *Electrochim. Acta* **1990**, *35*, 691−704.
(321) Lee, J. G.; An, K. Catalytic CO Oxidation on Nanocatalysts. *Top. Catal.* **2018**, *61*, 986−1001.
(322) Rioux, R. M.; Komor, R.; Song, H.; Hoefelmeyer, J. D.; Grass, M.; Niesz, K.; Yang, P.; Somorjai, G. A. Kinetics and Mechanism of Ethylene Hydrogenation Poisoned by CO on Silica-Supported Monodisperse Pt Nanoparticles. *J. Catal.* **2008**, *254*, 1−11.
(323) Zinola, C. F. A Method for the Synthesis of Platinum Nanoparticles with Defined Crystalline Orientations and Their Catalytic Activity towards Nitrogen and Carbon Monoxide Oxidations. *J. Electrochem. Soc.* **2017**, *164*, H170−H182.
(324) Leng, Y.-J.; Wang, X.; Hsing, I.-M. Assessment of CO-Tolerance for Different Pt-Alloy Anode Catalysts in a Polymer Electrolyte Fuel Cell Using Ac Impedance Spectroscopy. *J. Electroanal. Chem.* **2002**, *528*, 145−152.
(325) Waszczuk, P.; Wieckowski, A.; Zelenay, P.; Gottesfeld, S.; Coutanceau, C.; Léger, J. M.; Lamy, C. Adsorption of CO Poison on Fuel Cell Nanoparticle Electrodes from Methanol Solutions: A Radioactive Labeling Study. *J. Electroanal. Chem.* **2001**, *511*, 55−64.
(326) Kim, G.; Jhi, S. H. Carbon Monoxide-Tolerant Platinum Nanoparticle Catalysts on Defect-Engineered Graphene. *ACS Nano* **2011**, *5*, 805−810.
(327) Matin, M. A.; Lee, E.; Kim, H.; Yoon, W. S.; Kwon, Y. U. Rational Syntheses of Core-Shell Fe@(PtRu) Nanoparticle Electrocatalysts for the Methanol Oxidation Reaction with Complete Suppression of CO-Poisoning and Highly Enhanced Activity. *J. Mater. Chem. A* **2015**, *3*, 17154−17164.
(328) Zhang, Z. C.; Tian, X. C.; Zhang, B. W.; Huang, L.; Zhu, F. C.; Qu, X. M.; Liu, L.; Liu, S.; Jiang, Y. X.; Sun, S. G. Engineering Phase and Surface Composition of Pt3Co Nanocatalysts: A Strategy for Enhancing CO Tolerance. *Nano Energy* **2017**, *34*, 224−232.
(329) Spendelow, J. S.; Goodpaster, J. D.; Kenis, P. J. A.; Wieckowski, A. Mechanism of CO Oxidation on Pt(111) in Alkaline Media. *J. Phys. Chem. B* **2006**, *110*, 9545−9555.
(330) Maillard, F.; Savinova, E. R.; Stimming, U. CO Monolayer Oxidation on Pt Nanoparticles: Further Insights into the Particle Size Effects. *J. Electroanal. Chem.* **2007**, *599*, 221−232.
(331) Koper, M. T. M. Structure Sensitivity and Nanoscale Effects in Electrocatalysis. *Nanoscale* **2011**, *3*, 2054−2073.
(332) Koper, M. T. M.; Jansen, A. P. J.; Van Santen, R. A.; Lukkien, J. J.; Hilbers, P. A. J. Monte Carlo Simulations of a Simple Model for the Electrocatalytic CO Oxidation on Platinum. *J. Chem. Phys.* **1998**, *109*, 6051−6062.
(333) Lebedeva, N. P.; Koper, M. T. M.; Feliu, J. M.; van Santen, R. A. Mechanism and Kinetics of the Electrochemical CO Adlayer Oxidation on Pt(111). *J. Electroanal. Chem.* **2002**, *524*−*525*, 242−251.
(334) Wang, H.; Jusys, Z.; Behm, R. J.; Abruña, H. D. New Insights into the Mechanism and Kinetics of Adsorbed CO Electrooxidation on Platinum: Online Mass Spectrometry and Kinetic Monte Carlo Simulation Studies. *J. Phys. Chem. C* **2012**, *116*, 11040−11053.
(335) Lebedeva, N. P.; Koper, M. T. M.; Feliu, J. M.; van Santen, R. A. Role of Crystalline Defects in Electrocatalysis: Mechanism and Kinetics of CO Adlayer Oxidation on Stepped Platinum Electrodes. *J. Phys. Chem. B* **2002**, *106*, 12938−12947.
(336) Gómez-Marín, A. M.; Hernández-Ortíz, J. P. Mean Field Approximation of Langmuir-Hinshelwood CO-Surface Reactions Considering Lateral Interactions. *J. Phys. Chem. C* **2013**, *117*, 15716−15727.
(337) McCallum, C.; Pletcher, D. An Investigation of the Mechanism of the Oxidation of Carbon Monoxide Adsorbed onto a Smooth Pt Electrode in Aqueous Acid. *J. Electroanal. Chem. Interfacial Electrochem.* **1976**, *70*, 277−290.
(338) Korzeniewski, C.; Kardash, D. Use of a Dynamic Monte Carlo Simulation in the Study of Nucleation-and-Growth Models for CO Electrochemical Oxidation. *J. Phys. Chem. B* **2001**, *105*, 8663−8671.
(339) Farias, M. J. S.; Camara, G. A.; Feliu, J. M. Understanding the CO Preoxidation and the Intrinsic Catalytic Activity of Step Sites in Stepped Pt Surfaces in Acidic Medium. *J. Phys. Chem. C* **2015**, *119*, 20272−20282.
(340) Chung, D. Y.; Lee, M. J.; Kim, M.; Shin, H.; Kim, M. J.; Yoo, J. M.; Park, S.; Sung, Y. E. CO Electro-Oxidation Reaction on Pt Nanoparticles: Understanding Peak Multiplicity through Thiol Derivative Molecule Adsorption. *Catal. Today* **2017**, *293*−*294*, 2−7.
(341) Ciapina, E. G.; Santos, S. F.; Gonzalez, E. R. Electrochemical CO Stripping on Nanosized Pt Surfaces in Acid Media: A Review on the Issue of Peak Multiplicity. *J. Electroanal. Chem.* **2018**, *815*, 47−60.
(342) Wang, W.; Zhang, J.; Wang, F.; Mao, B. W.; Zhan, D.; Tian, Z. Q. Mobility and Reactivity of Oxygen Adspecies on Platinum Surface. *J. Am. Chem. Soc.* **2016**, *138*, 9057−9060.
(343) Farias, M. J. S.; Vidal-Iglesias, F. J.; Solla-Gullón, J.; Herrero, E.; Feliu, J. M. On the Behavior of CO Oxidation on Shape-Controlled Pt Nanoparticles in Alkaline Medium. *J. Electroanal. Chem.* **2014**, *716*, 16−22.
(344) Farias, M. J. S.; Busó-Rogero, C.; Vidal-Iglesias, F. J.; Solla-Gullón, J.; Camara, G. A.; Feliu, J. M. Mobility and Oxidation of Adsorbed CO on Shape-Controlled Pt Nanoparticles in Acidic Medium. *Langmuir* **2017**, *33*, 865−871.
(345) McPherson, I. J.; Ash, P. A.; Jones, L.; Varambhia, A.; Jacobs, R. M. J.; Vincent, K. A. Electrochemical CO Oxidation at Platinum on Carbon Studied through Analysis of Anomalous in Situ IR Spectra. *J. Phys. Chem. C* **2017**, *121*, 17176−17187.
(346) Liu, S.; Arce, A. S.; Nilsson, S.; Albinsson, D.; Hellberg, L.; Alekseeva, S.; Langhammer, C. In Situ Plasmonic Nanospectroscopy

DOI: 10.1021/acs.chemrev.9b00246
Chem. Rev. XXXX, XXX, XXX−XXX

of the CO Oxidation Reaction over Single Pt Nanoparticles. *ACS Nano* **2019**, *13*, 6090−6100.
(347) Rodríguez, P.; Koverga, A. A.; Koper, M. T. M. Carbon Monoxide as a Promoter for Its Own Oxidation on a Gold Electrode. *Angew. Chem., Int. Ed.* **2010**, *49*, 1241−1243.
(348) Rodríguez, P.; Garcia-Araez, N.; Koper, M. T. M. Self-Promotion Mechanism for CO Electrooxidation on Gold. *Phys. Chem. Chem. Phys.* **2010**, *12*, 9373.
(349) Rodríguez, P.; Feliu, J. M.; Koper, M. T. M. Unusual Adsorption State of Carbon Monoxide on Single-Crystalline Gold Electrodes in Alkaline Media. *Electrochem. Commun.* **2009**, *11*, 1105−1108.
(350) Rodríguez, P.; Garcia-Araez, N.; Koverga, A.; Frank, S.; Koper, M. T. M. CO Electroxidation on Gold in Alkaline Media: A Combined Electrochemical, Spectroscopic, and DFT Study. *Langmuir* **2010**, *26*, 12425−12432.
(351) Kumar, S.; Zou, S. Electrooxidation of CO on Uniform Arrays of Au Nanoparticles: Effects of Particle Size and Interparticle Spacing. *Langmuir* **2009**, *25*, 574−581.
(352) Falsig, H.; Hvolbæk, B.; Kristensen, I. S.; Jiang, T.; Bligaard, T.; Christensen, C. H.; Nørskov, J. K. Trends in the Catalytic CO Oxidation Activity of Nanoparticles. *Angew. Chem., Int. Ed.* **2008**, *47*, 4835−4839.
(353) Gallo, I. B. C.; Carbonio, E. A.; Villullas, H. M. What Determines Electrochemical Surface Processes on Carbon-Supported PdAu Nanoparticles? *ACS Catal.* **2018**, *8*, 1818−1827.
(354) Shin, K.; Zhang, L.; An, H.; Ha, H.; Yoo, M.; Lee, H. M.; Henkelman, G.; Kim, H. Y. Interface Engineering for a Rational Design of Poison-Free Bimetallic CO Oxidation Catalysts. *Nanoscale* **2017**, *9*, 5244−5253.
(355) Saravanan, G.; Jayasree, K. P.; Divya, Y.; Pallavi, M.; Nitin, L. Ordered Intermetallic Pt-Fe Nano-Catalysts for Carbon Monoxide and Benzene Oxidation. *Intermetallics* **2018**, *94*, 179−185.
(356) Chen, W.; Gao, W.; Tu, P.; Robert, T.; Ma, Y.; Shan, H.; Gu, X.; Shang, W.; Tao, P.; Song, C.; et al. Neighboring Pt Atom Sites in an Ultrathin FePt Nanosheet for the Efficient and Highly CO-Tolerant Oxygen Reduction Reaction. *Nano Lett.* **2018**, *18*, 5905−5912.
(357) Buatier de Mongeot, F.; Scherer, M.; Gleich, B.; Kopatzki, E.; Behm, R. J. CO Adsorption and Oxidation on Bimetallic Pt/Ru(0001) Surfaces − a Combined STM and TPD/TPR Study. *Surf. Sci.* **1998**, *411*, 249−262.
(358) Ianniello, R.; Schmidt, V. M.; Stimming, U.; Stumper, J.; Wallau, A. CO Adsorption and Oxidation on Pt and PtRu Alloys: Dependence on Substrate Composition. *Electrochim. Acta* **1994**, *39*, 1863−1869.
(359) Liu, P.; Logadottir, A.; Nørskov, J. K. Modeling the Electro-Oxidation of CO and H2/CO on Pt, Ru, PtRu and Pt3Sn. *Electrochim. Acta* **2003**, *48*, 3731−3742.
(360) Koper, M. T. M.; Shubina, T. E.; van Santen, R. A. Periodic Density Functional Study of CO and OH Adsorption on Pt−Ru Alloy Surfaces: Implications for CO Tolerant Fuel Cell Catalysts. *J. Phys. Chem. B* **2002**, *106*, 686−692.
(361) Liu, Z.; Ma, L.; Zhang, J.; Hongsirikarn, K.; Goodwin, J. G. Pt Alloy Electrocatalysts for Proton Exchange Membrane Fuel Cells: A Review. *Catal. Rev.: Sci. Eng.* **2013**, *55*, 255−288.
(362) Liu, Z.; Jackson, G. S.; Eichhorn, B. W. Tuning the CO-Tolerance of Pt-Fe Bimetallic Nanoparticle Electrocatalysts through Architectural Control. *Energy Environ. Sci.* **2011**, *4*, 1900.
(363) Liu, Z.; Jackson, G. S.; Eichhorn, B. W. PtSn Intermetallic, Core-Shell, and Alloy Nanoparticles as CO-Tolerant Electrocatalysts for H2 Oxidation. *Angew. Chem., Int. Ed.* **2010**, *49*, 3173−3176.
(364) Shi, G.; Yano, H.; Tryk, D. A.; Iiyama, A.; Uchida, H. Highly Active, CO-Tolerant, and Robust Hydrogen Anode Catalysts: Pt-M (M = Fe, Co, Ni) Alloys with Stabilized Pt-Skin Layers. *ACS Catal.* **2017**, *7*, 267−274.
(365) Zhang, L.; Henkelman, G. Computational Design of Alloy-Core@shell Metal Nanoparticle Catalysts. *ACS Catal.* **2015**, *5*, 655−660.
(366) Chen, D.-J.; Tong, Y. Y. J. *The Bifunctional Electrocatalysis of Carbon Monoxide Oxidation Reaction*; Elsevier: 2018.
(367) Gisbert, R.; García, G.; Koper, M. T. M. Oxidation of Carbon Monoxide on Poly-Oriented and Single-Crystalline Platinum Electrodes over a Wide Range of PH. *Electrochim. Acta* **2011**, *56*, 2443−2449.
(368) Duan, Z.; Henkelman, G. Calculations of the PH-Dependent Onset Potential for CO Electrooxidation on Au(111). *Langmuir* **2018**, *34*, 15268−15275.
(369) Duan, Z.; Henkelman, G. Theoretical Resolution of the Exceptional Oxygen Reduction Activity of Au(100) in Alkaline Media. *ACS Catal.* **2019**, *9*, 5567−5573.
(370) Stoffelsma, C.; Rodriguez, P.; Garcia, G.; Garcia-Araez, N.; Strmcnik, D.; Marković, N. M.; Koper, M. T. M. Promotion of the Oxidation of Carbon Monoxide at Stepped Platinum Single-Crystal Electrodes in Alkaline Media by Lithium and Beryllium Cations. *J. Am. Chem. Soc.* **2010**, *132*, 16127−16133.
(371) Zhu, D. D.; Liu, J. L.; Qiao, S. Z. Recent Advances in Inorganic Heterogeneous Electrocatalysts for Reduction of Carbon Dioxide. *Adv. Mater.* **2016**, *28*, 3423−3452.
(372) Wang, Z. L.; Li, C.; Yamauchi, Y. Nanostructured Nonprecious Metal Catalysts for Electrochemical Reduction of Carbon Dioxide. *Nano Today* **2016**, *11*, 373−391.
(373) Zhang, Q.; Xu, W.; Xu, J.; Liu, Y.; Zhang, J. High Performing and Cost-Effective Metal/Metal Oxide/Metal Alloy Catalysts/Electrodes for Low Temperature CO2 Electroreduction. *Catal. Today* **2018**, *318*, 15−22.
(374) Huang, J.; Buonsanti, R. Colloidal Nanocrystals as Heterogeneous Catalysts for Electrochemical CO2 Conversion. *Chem. Mater.* **2019**, *31*, 13−25.
(375) Back, S.; Yeom, M. S.; Jung, Y. Active Sites of Au and Ag Nanoparticle Catalysts for CO2 Electroreduction to CO. *ACS Catal.* **2015**, *5*, 5089−5096.
(376) Gao, D.; Wang, J.; Wu, H.; Jiang, X.; Miao, S.; Wang, G.; Bao, X. PH Effect on Electrocatalytic Reduction of CO2 over Pd and Pt Nanoparticles. *Electrochem. Commun.* **2015**, *55*, 1−5.
(377) Shin, H.; Ha, Y.; Kim, H. 2D Covalent Metals: A New Materials Domain of Electrochemical CO2 Conversion with Broken Scaling Relationship. *J. Phys. Chem. Lett.* **2016**, *7*, 4124−4129.
(378) Tornow, C. E.; Thorson, M. R.; Ma, S.; Gewirth, A. A.; Kenis, P. J. a. Nitrogen-Based Catalysts for Electrochemical Reduction of CO_2 to CO. *J. Am. Chem. Soc.* **2012**, *134*, 19520−19523.
(379) Bagherzadeh, S.; Mankad, N. P. Catalyst Control of Selectivity in CO2 Reduction Using a Tunable Heterobimetallic Effect. *J. Am. Chem. Soc.* **2015**, *137*, 10898−10901.
(380) Lu, Q.; Rosen, J.; Zhou, Y.; Hutchings, G. S.; Kimmel, Y. C.; Chen, J. G.; Jiao, F. A Selective and Efficient Electrocatalyst for Carbon Dioxide Reduction. *Nat. Commun.* **2014**, *5*, 3242.
(381) Lates, V.; Falch, A.; Jordaan, A.; Peach, R.; Kriek, R. J. An Electrochemical Study of Carbon Dioxide Electroreduction on Gold-Based Nanoparticle Catalysts. *Electrochim. Acta* **2014**, *128*, 75−84.
(382) Xie, H.; Wang, T.; Liang, J.; Li, Q.; Sun, S. Cu-Based Nanocatalysts for Electrochemical Reduction of CO2. *Nano Today* **2018**, *21*, 41−54.
(383) Raciti, D.; Wang, C. Recent Advances in CO2 Reduction Electrocatalysis on Copper. *ACS Energy Lett.* **2018**, *3*, 1545−1556.
(384) Ma, T.; Fan, Q.; Li, X.; Qiu, J.; Wu, T.; Sun, Z. Graphene-Based Materials for Electrochemical CO2 Reduction. *J. CO2 Util.* **2019**, *30*, 168−182.
(385) Schouten, K. J. P.; Kwon, Y.; Van Der Ham, C. J. M.; Qin, Z.; Koper, M. T. M. A New Mechanism for the Selectivity to C1 and C2 Species in the Electrochemical Reduction of Carbon Dioxide on Copper Electrodes. *Chem. Sci.* **2011**, *2*, 1902−1909.
(386) Kortlever, R.; Shen, J.; Schouten, K. J. P.; Calle-Vallejo, F.; Koper, M. T. M. Catalysts and Reaction Pathways for the Electrochemical Reduction of Carbon Dioxide. *J. Phys. Chem. Lett.* **2015**, *6*, 4073−4082.

DOI: 10.1021/acs.chemrev.9b00246
Chem. Rev. XXXX, XXX, XXX−XXX

(387) Zhang, X.; Liu, J. X.; Zijlstra, B.; Filot, I. A. W.; Zhou, Z.; Sun, S.; Hensen, E. J. M. Optimum Cu Nanoparticle Catalysts for CO2 Hydrogenation towards Methanol. *Nano Energy* **2018**, *43*, 200−209.
(388) Klinkova, A.; De Luna, P.; Dinh, C.-T.; Voznyy, O.; Larin, E. M.; Kumacheva, E.; Sargent, E. H. Rational Design of Efficient Palladium Catalysts for Electroreduction of Carbon Dioxide to Formate. *ACS Catal.* **2016**, *6*, 8115−8120.
(389) Feaster, J. J.; Shi, C.; Cave, E. R.; Hatsukade, T.; Abram, D. N.; Kuhl, K. P.; Hahn, C.; Nørskov, J. K.; Jaramillo, T. F. Understanding Selectivity for the Electrochemical Reduction of Carbon Dioxide to Formic Acid and Carbon Monoxide on Metal Electrodes. *ACS Catal.* **2017**, *7*, 4822−4827.
(390) Sheng, W.; Kattel, S.; Yao, S.; Yan, B.; Liang, Z.; Hawxhurst, C. J.; Wu, Q.; Chen, J. G. Electrochemical Reduction of CO2 to Synthesis Gas with Controlled CO/H2 Ratios. *Energy Environ. Sci.* **2017**, *10*, 1180−1185.
(391) Andrews, E.; Katla, S.; Kumar, C.; Patterson, M.; Sprunger, P.; Flake, J. C. Electrocatalytic Reduction of CO2 at Au Nanoparticle Electrodes: Effects of Interfacial Chemistry on Reduction Behavior. *J. Electrochem. Soc.* **2015**, *162*, F1373−F1378.
(392) Andrews, E.; Flake, J. C.; Fang, Y. CO2 Electrocatalytic Reduction of Gold and Copper Electrodes: Role of Particle Size and Surface Chemistry. *ECS Trans.* **2015**, *66*, 67−70.
(393) Gao, D.; Zhou, H.; Wang, J.; Miao, S.; Yang, F.; Wang, G.; Wang, J.; Bao, X. Size-Dependent Electrocatalytic Reduction of CO2 over Pd Nanoparticles. *J. Am. Chem. Soc.* **2015**, *137*, 4288−4291.
(394) Zhu, W.; Michalsky, R.; Metin, Ö.; Lv, H.; Guo, S.; Wright, C. J.; Sun, X.; Peterson, A. A.; Sun, S. Monodisperse Au Nanoparticles for Selective Electrocatalytic Reduction of CO_2 to CO. *J. Am. Chem. Soc.* **2013**, *135*, 16833−16836.
(395) Wang, H.; Han, Z.; Zhang, L.; Cui, C.; Zhu, X.; Liu, X.; Han, J.; Ge, Q. Enhanced CO Selectivity and Stability for Electrocatalytic Reduction of CO2 on Electrodeposited Nanostructured Porous Ag Electrode. *J. CO2 Util.* **2016**, *15*, 41−49.
(396) Zhang, Y.; Ji, L.; Qiu, W.; Shi, X.; Asiri, A. M.; Sun, X. Iodide-Derived Nanostructured Silver Promotes Selective and Efficient Carbon Dioxide Conversion into Carbon Monoxide. *Chem. Commun.* **2018**, *54*, 2666−2669.
(397) Guo, S. X.; Li, F.; Chen, L.; Macfarlane, D. R.; Zhang, J. Polyoxometalate-Promoted Electrocatalytic CO2 Reduction at Nanostructured Silver in Dimethylformamide. *ACS Appl. Mater. Interfaces* **2018**, *10*, 12690−12697.
(398) Sun, K.; Wu, L.; Qin, W.; Zhou, J.; Hu, Y.; Jiang, Z.; Shen, B.; Wang, Z. Enhanced Electrochemical Reduction of CO2 to CO on Ag Electrocatalysts with Increased Unoccupied Density of States. *J. Mater. Chem. A* **2016**, *4*, 12616−12623.
(399) Hsieh, Y. C.; Senanayake, S. D.; Zhang, Y.; Xu, W.; Polyansky, D. E. Effect of Chloride Anions on the Synthesis and Enhanced Catalytic Activity of Silver Nanocoral Electrodes for CO2 Electroreduction. *ACS Catal.* **2015**, *5*, 5349−5356.
(400) Jiang, K.; Kharel, P.; Peng, Y.; Gangishetty, M. K.; Lin, H. Y. G.; Stavitski, E.; Attenkofer, K.; Wang, H. Silver Nanoparticles with Surface-Bonded Oxygen for Highly Selective CO2 Reduction. *ACS Sustainable Chem. Eng.* **2017**, *5*, 8529−8534.
(401) Peng, X.; Karakalos, S. G.; Mustain, W. E. Preferentially Oriented Ag Nanocrystals with Extremely High Activity and Faradaic Efficiency for CO2 Electrochemical Reduction to CO. *ACS Appl. Mater. Interfaces* **2018**, *10*, 1734−1742.
(402) Ma, M.; Liu, K.; Shen, J.; Kas, R.; Smith, W. A. In Situ Fabrication and Reactivation of Highly Selective and Stable Ag Catalysts for Electrochemical CO2 Conversion. *ACS Energy Lett.* **2018**, *3*, 1301−1306.
(403) Wu, J.; Yadav, R. M.; Liu, M.; Sharma, P. P.; Tiwary, C. S.; Ma, L.; Zou, X.; Zhou, X. D.; Yakobson, B. I.; Lou, J.; et al. Achieving Highly Efficient, Selective, and Stable CO2 Reduction on Nitrogen-Doped Carbon Nanotubes. *ACS Nano* **2015**, *9*, 5364−5371.
(404) Wu, J.; Sharifi, T.; Gao, Y.; Zhang, T.; Ajayan, P. M. Emerging Carbon-Based Heterogeneous Catalysts for Electrochemical Reduction of Carbon Dioxide into Value-Added Chemicals. *Adv. Mater.* **2019**, *31*, 1804257.
(405) Zhang, S.; Kang, P.; Ubnoske, S.; Brennaman, M. K.; Song, N.; House, R. L.; Glass, J. T.; Meyer, T. J. Polyethylenimine Enhanced Electrocatalytic Reduction of CO2 to Formate at Nitrogen Doped Carbon Nanomaterials. *J. Am. Chem. Soc.* **2014**, *136*, 7845−7848.
(406) Mazánek, V.; Luxa, J.; Matějková, S.; Kučera, J.; Sedmidubský, D.; Pumera, M.; Sofer, Z. Ultrapure Graphene Is a Poor Electrocatalyst: Definitive Proof of the Key Role of Metallic Impurities in Graphene-Based Electrocatalysis. *ACS Nano* **2019**, *13*, 1574−1582.
(407) Tan, S. M.; Pumera, M. Two-Dimensional Materials on the Rocks: Positive and Negative Role of Dopants and Impurities in Electrochemistry. *ACS Nano* **2019**, *13*, 2681−2728.
(408) Lum, Y.; Kwon, Y.; Lobaccaro, P.; Chen, L.; Clark, E. L.; Bell, A. T.; Ager, J. W. Trace Levels of Copper in Carbon Materials Show Significant Electrochemical CO2 Reduction Activity. *ACS Catal.* **2016**, *6*, 202−209.
(409) Tamura, J.; Ono, A.; Sugano, Y.; Huang, C.; Nishizawa, H.; Mikoshiba, S. Electrochemical Reduction of CO2 to Ethylene Glycol on Imidazolium Ion-Terminated Self-Assembly Monolayer-Modified Au Electrodes in an Aqueous Solution. *Phys. Chem. Chem. Phys.* **2015**, *17*, 26072−26078.
(410) Fang, Y.; Flake, J. C. Electrochemical Reduction of CO2 at Functionalized Au Electrodes. *J. Am. Chem. Soc.* **2017**, *139*, 3399−3405.
(411) Templeton, A. C.; Wuelfing, W. P.; Murray, R. W. Monolayer-Protected Cluster Molecules. *Acc. Chem. Res.* **2000**, *33*, 27−36.
(412) Kauffman, D. R.; Alfonso, D.; Matranga, C.; Qian, H.; Jin, R. Experimental and Computational Investigation of Au25 Clusters and CO2: A Unique Interaction and Enhanced Electrocatalytic Activity. *J. Am. Chem. Soc.* **2012**, *134*, 10237−10243.
(413) Kauffman, D. R.; Thakkar, J.; Siva, R.; Matranga, C.; Ohodnicki, P. R.; Zeng, C.; Jin, R. Efficient Electrochemical CO2 Conversion Powered by Renewable Energy. *ACS Appl. Mater. Interfaces* **2015**, *7*, 15626−15632.
(414) Wang, Z.; Sun, K.; Liang, C.; Wu, L.; Niu, Z.; Gao, J. Synergistic Chemisorbing and Electronic Effects for Efficient CO2 Reduction Using Cysteamine-Functionalized Gold Nanoparticles. *ACS Appl. Energy Mater.* **2019**, *2*, 192−195.
(415) Kim, C.; Eom, T.; Jee, M. S.; Jung, H.; Kim, H.; Min, B. K.; Hwang, Y. J. Insight into Electrochemical CO2 Reduction on Surface-Molecule-Mediated Ag Nanoparticles. *ACS Catal.* **2017**, *7*, 779−785.
(416) Lucio, A. J.; Shaw, S. K. Pyridine and Pyridinium Electrochemistry on Polycrystalline Gold Electrodes and Implications for CO2 Reduction. *J. Phys. Chem. C* **2015**, *119*, 12523−12530.
(417) Lu, H.; Zhou, Z.; Prezhdo, O. V.; Brutchey, R. L. Exposing the Dynamics and Energetics of the N-Heterocyclic Carbene-Nanocrystal Interface. *J. Am. Chem. Soc.* **2016**, *138*, 14844−14847.
(418) Tegeder, P.; Freitag, M.; Chepiga, K. M.; Muratsugu, S.; Möller, N.; Lamping, S.; Tada, M.; Glorius, F.; Ravoo, B. J. N-Heterocyclic Carbene-Modified Au−Pd Alloy Nanoparticles and Their Application as Biomimetic and Heterogeneous Catalysts. *Chem. - Eur. J.* **2018**, *24*, 18682−18688.
(419) Smith, C. A.; Narouz, M. R.; Lummis, P. A.; Singh, I.; Nazemi, A.; Li, C.-H.; Crudden, C. M. N-Heterocyclic Carbenes in Materials Chemistry. *Chem. Rev.* **2019**, *119*, 4986−5056.
(420) Han, Z.; Kortlever, R.; Chen, H. Y.; Peters, J. C.; Agapie, T. CO2 Reduction Selective for C ≥ 2 Products on Polycrystalline Copper with N-Substituted Pyridinium Additives. *ACS Cent. Sci.* **2017**, *3*, 853−859.
(421) Cao, Z.; Kim, D.; Hong, D.; Yu, Y.; Xu, J.; Lin, S.; Wen, X.; Nichols, E. M.; Jeong, K.; Reimer, J. A.; et al. A Molecular Surface Functionalization Approach to Tuning Nanoparticle Electrocatalysts for Carbon Dioxide Reduction. *J. Am. Chem. Soc.* **2016**, *138*, 8120−8125.
(422) Zhu, S.; Wang, Q.; Qin, X.; Gu, M.; Tao, R.; Lee, B. P.; Zhang, L.; Yao, Y.; Li, T.; Shao, M. Tuning Structural and Compositional Effects in Pd−Au Nanowires for Highly Selective

DOI: 10.1021/acs.chemrev.9b00246
Chem. Rev. XXXX, XXX, XXX−XXX

and Active CO2 Electrochemical Reduction Reaction. *Adv. Energy Mater.* **2018**, *8*, 1802238.
(423) Hahn, C.; Abram, D. N.; Hansen, H. A.; Hatsukade, T.; Jackson, A.; Johnson, N. C.; Hellstern, T. R.; Kuhl, K. P.; Cave, E. R.; Feaster, J. T.; et al. Synthesis of Thin Film AuPd Alloys and Their Investigation for Electrocatalytic CO2 Reduction. *J. Mater. Chem. A* **2015**, *3*, 20185−20194.
(424) Liu, P.; Nørskov, J. K. Ligand and Ensemble Effects in Adsorption on Alloy Surfaces. *Phys. Chem. Chem. Phys.* **2001**, *3*, 3814−3818.
(425) Kim, D.; Resasco, J.; Yu, Y.; Asiri, A. M.; Yang, P. Synergistic Geometric and Electronic Effects for Electrochemical Reduction of Carbon Dioxide Using Gold-Copper Bimetallic Nanoparticles. *Nat. Commun.* **2014**, *5*, 4948.
(426) Chen, K.; Zhang, X.; Williams, T.; Bourgeois, L.; MacFarlane, D. R. Electrochemical Reduction of CO2 on Core-Shell Cu/Au Nanostructure Arrays for Syngas Production. *Electrochim. Acta* **2017**, *239*, 84−89.
(427) Andrews, E.; Fang, Y.; Flake, J. C. Electrochemical Reduction of CO2 at CuAu Nanoparticles: Size and Alloy Effects. *J. Appl. Electrochem.* **2018**, *48*, 435−441.
(428) Zhu, W.; Zhang, L.; Yang, P.; Hu, C.; Dong, H.; Zhao, Z. J.; Mu, R.; Gong, J. Formation of Enriched Vacancies for Enhanced CO2 Electrocatalytic Reduction over AuCu Alloys. *ACS Energy Lett.* **2018**, *3*, 2144−2149.
(429) Plana, D.; Flórez-Montaño, J.; Celorrio, V.; Pastor, E.; Fermín, D. J. Tuning CO2 Electroreduction Efficiency at Pd Shells on Au Nanocores. *Chem. Commun.* **2013**, *49*, 10962−10964.
(430) Humphrey, J. J. L.; Plana, D.; Celorrio, V.; Sadasivan, S.; Tooze, R. P.; Rodríguez, P.; Fermín, D. J. Electrochemical Reduction of Carbon Dioxide at Gold-Palladium Core-Shell Nanoparticles: Product Distribution versus Shell Thickness. *ChemCatChem* **2016**, *8*, 952−960.
(431) Kortlever, R.; Peters, I.; Balemans, C.; Kas, R.; Kwon, Y.; Mul, G.; Koper, M. T. M. Palladium−Gold Catalyst for the Electrochemical Reduction of CO2 to C1−C5 Hydrocarbons. *Chem. Commun.* **2016**, *52*, 10229−10232.
(432) Kauffman, D. R.; Alfonso, D. R.; Tafen, D. N.; Wang, C.; Zhou, Y.; Yu, Y.; Lekse, J. W.; Deng, X.; Espinoza, V.; Trindell, J. A.; et al. Selective Electrocatalytic Reduction of CO2 into CO at Small, Thiol-Capped Au/Cu Nanoparticles. *J. Phys. Chem. C* **2018**, *122*, 27991−28000.
(433) Choi, J.; Kim, M. J.; Ahn, S. H.; Choi, I.; Jang, J. H.; Ham, Y. S.; Kim, J. J.; Kim, S. K. Electrochemical CO2 Reduction to CO on Dendritic Ag-Cu Electrocatalysts Prepared by Electrodeposition. *Chem. Eng. J.* **2016**, *299*, 37−44.
(434) Lee, S.; Park, G.; Lee, J. Importance of Ag-Cu Biphasic Boundaries for Selective Electrochemical Reduction of CO2 to Ethanol. *ACS Catal.* **2017**, *7*, 8594−8604.
(435) Wang, Y.; Wang, D.; Dares, C. J.; Marquard, S. L.; Sheridan, M. V.; Meyer, T. J. CO2 Reduction to Acetate in Mixtures of Ultrasmall (Cu)n, (Ag)m Bimetallic Nanoparticles. *Proc. Natl. Acad. Sci. U. S. A.* **2018**, *115*, 278−283.
(436) Ma, S.; Sadakiyo, M.; Heim, M.; Luo, R.; Haasch, R. T.; Gold, J. I.; Yamauchi, M.; Kenis, P. J. A. Electroreduction of Carbon Dioxide to Hydrocarbons Using Bimetallic Cu-Pd Catalysts with Different Mixing Patterns. *J. Am. Chem. Soc.* **2017**, *139*, 47−50.
(437) Takashima, T.; Suzuki, T.; Irie, H. Electrochemical Carbon Dioxide Reduction on Copper-Modified Palladium Nanoparticles Synthesized by Underpotential Deposition. *Electrochim. Acta* **2017**, *229*, 415−421.
(438) Clark, E. L.; Hahn, C.; Jaramillo, T. F.; Bell, A. T. Electrochemical CO2 Reduction over Compressively Strained CuAg Surface Alloys with Enhanced Multi-Carbon Oxygenate Selectivity. *J. Am. Chem. Soc.* **2017**, *139*, 15848−15857.
(439) Higgins, D. C.; Landers, A. T.; Ji, Y.; Nitopi, S.; Morales-Guio, C. G.; Wang, L.; Chan, K.; Hahn, C.; Jaramillo, T. F. Guiding Electrochemical Carbon Dioxide Reduction toward Carbonyls Using Copper Silver Thin Films with Interphase Miscibility. *ACS Energy Lett.* **2018**, *3*, 2947−2955.
(440) Huang, J.; Mensi, M.; Oveisi, E.; Mantella, V.; Buonsanti, R. Structural Sensitivities in Bimetallic Catalysts for Electrochemical CO2 Reduction Revealed by Ag-Cu Nanodimers. *J. Am. Chem. Soc.* **2019**, *141*, 2490−2499.

DOI: 10.1021/acs.chemrev.9b00246
Chem. Rev. XXXX, XXX, XXX−XXX